Title
Improved Asphalt Bases and Slab-Base Engineered Interlayers for Rigid Pavements

Authors
Mateos, Angel
Millan, Miguel Angel
Harvey, John
et al.

Publication Date
2026-07-01

DOI
10.7922/G27P8WSG

RESEARCH REPORT

Improved Asphalt Bases and Slab-Base Engineered Interlayers for Rigid Pavements

AUTHORS

Angel Mateos, Miguel Angel Millan, John Harvey, Fabian Paniagua, Justin Yu, Somayeh Nassiri, Jeff Buscheck, and Julian Brotschi

Report No: UCPRC-RR-2025-04 | July 2026

Partnered Pavement Research Center Strategic Plan Element (PPRC SPE) 4.99 (TO-020) (DRISI Task 4226): Piloting of Cold Recycling and New Asphalt Base Designs and Interlayers for Concrete Pavements

PREPARED FOR

California Department of Transportation
Division of Research, Innovation and System Information
Office of Materials and Infrastructure

PREPARED BY

University of California Pavement Research Center
UC Davis and UC Berkeley

TECHNICAL REPORT DOCUMENTATION PAGE

1. REPORT NUMBER UCPRC-RR-2025-04	**2. GOVERNMENT ASSOCIATION NUMBER**	**3. RECIPIENT'S CATALOG NUMBER**
4. TITLE AND SUBTITLE Improved Asphalt Bases and Slab-Base Engineered Interlayers for Rigid Pavements		**5. REPORT PUBLICATION DATE** July 2026 **6. PERFORMING ORGANIZATION CODE**
7. AUTHOR(S) Angel Mateos (ORCID: 0000-0002-3614-2858); Miguel Angel Millan (ORCID: 0000-0002-9116-9076); John Harvey (ORCID: 0000-0002-8924-6212); Fabian Paniagua (ORCID: 0000-0002-2385-4899); Justin Yu (ORCID: 0009-0001-1068-3090); Somayeh Nassiri (ORCID 0000-0001-5367-2167); Jeff Buscheck (ORCID: 0000-0002-0930-6861); Julian Brotschi (ORCID: 0000-0002-1752-2898)		**8. PERFORMING ORGANIZATION REPORT NUMBER** UCPRC-RR-2025-04 UCD-ITS-RR-26-53
9. PERFORMING ORGANIZATION NAME AND ADDRESS University of California Pavement Research Center Department of Civil and Environmental Engineering, UC Davis 1 Shields Avenue Davis, CA 95616		**10. WORK UNIT NUMBER** **11. CONTRACT OR GRANT NUMBER** 65A1056
12. SPONSORING AGENCY AND ADDRESS California Department of Transportation Division of Research, Innovation, and System Information P.O. Box 942873 Sacramento, CA 94273-0001		**13. TYPE OF REPORT AND PERIOD COVERED** Research Report September 2023 to September 2025 **14. SPONSORING AGENCY CODE**
15. SUPPLEMENTAL NOTES doi:10.7922/G27P8WSG		
16. ABSTRACT The goal of the research presented in this report is to develop recommendations for improving the design of asphalt concrete as a base for rigid pavement and engineered interlayers (or "bond breakers") between jointed plain concrete pavement (JPCP) slabs and lean concrete base (LCB). A full-scale test track was built and monitored to study JPCP slab-base interaction under various environmental conditions. The test track consisted of four independent slabs: one slab with a rubberized hot mix asphalt–gap-graded (RHMA-G) base and three slabs with an LCB and one interlayer (curing compound, geotextile, or microsurfacing). Monitoring measurements from the test track included concrete hygrothermal strains, such as horizontal expansion/contraction and curling/warping of the slabs, as well as falling weight deflectometer (FWD) deflections. The overall ranking of slab support from best to worst was as follows: RHMA-G and microsurfacing performed similarly, curing compound, and geotextile. The FWD corner deflection for the LCB with curing compound was up to three times larger than that for the RHMA-G base. Test track materials were sampled during construction for laboratory testing, and an additional RHMA-G and two hot mix asphalts (HMAs) were tested for comparison. Based on the laboratory testing and finite element method modeling, the RHMA-G is expected to perform similarly to HMA as a rigid pavement base. However, both HMA and RHMA-G performance can be improved for this use by enhancing their capacity to deform under slow loading and resist long-term moisture damage. This report includes recommendations for specifications for base layers for rigid pavement, which can be applied to Caltrans specifications.		
17. KEYWORDS jointed plain concrete pavement (JPCP), lean concrete base (LCB), engineered interlayer, rubberized hot mix asphalt–gap-graded (RHMA-G), drying shrinkage, warping, thermal deformation, thermal curling, microsurfacing, geotextile	**18. DISTRIBUTION STATEMENT** No restrictions.	
19. SECURITY CLASSIFICATION (of this report) Unclassified	**20. NUMBER OF PAGES** 98	**21. PRICE** None

Reproduction of completed page authorized.

UCPRC ADDITIONAL INFORMATION

1. DRAFT STAGE Final	**2. VERSION NUMBER** 1
3. UCPRC STRATEGIC PLAN ELEMENT NUMBER 4.99 (TO-020)	**4. CALTRANS TASK NUMBER** 4214
5. CALTRANS TECHNICAL LEAD AND REVIEWER(S) Deepak Maskey	**6. FHWA NUMBER** CA264214a

7. PROPOSALS FOR IMPLEMENTATION

It is recommended that rubberized hot mix asphalt–gap-graded (RHMA-G) be allowed for use in the bases of rigid pavements in addition to hot mix asphalt (HMA). The same thickness should be prescribed for both materials. Caltrans may consider extending the rubber use mandate to the bases of rigid pavements.

It is recommended that the use of lean concrete base (LCB) with a microsurfacing interlayer be evaluated in a pilot project before including microsurfacing as an alternative in Caltrans Standard Specifications Section 36-2, “Base Bond Breaker.” Additionally, it is recommended that Caltrans Std. Specs. Section 36-2, be updated to not allow the use of geotextile as a slab-LCB bond breaker.

8. RELATED DOCUMENTS

9. VERSION UPDATES

10. LABORATORY ACCREDITATION

The UCPRC laboratory is accredited by AASHTO re:source and CCRL for the laboratory testing discussed in this report.

11. SIGNATURES

A. Mateos **FIRST AUTHOR**	J.T. Harvey **TECHNICAL REVIEW**	C. Fink **EDITOR**	J.T. Harvey **PRINCIPAL INVESTIGATOR**	D. Maskey **CALTRANS TECHNICAL LEAD(S)**	S. Mafi **CALTRANS CONTRACT MANAGER**

DISCLAIMER

This document is disseminated in the interest of information exchange. The contents of this report reflect the views of the authors, who are responsible for the facts and accuracy of the data presented herein. The contents do not necessarily reflect the official views or policies of the State of California or the Federal Highway Administration. This publication does not constitute a standard, specification, or regulation. This report does not constitute an endorsement by the Department of any product described herein.

ACKNOWLEDGMENTS

The University of California Pavement Research Center acknowledges the following individuals and organizations who contributed to the project: Caltrans Office of Concrete Pavement for the support and technical lead of the project, in particular: Allen King, Deepak Maskey, and Dulce R. Feldman; Caltrans DRISI project manager Somayeh Mafi; Teichert Aggregates (Pete Conlin), Vanguard Construction (Greg Bridges), VSS International (Rick Cross), CEMEX (Mark Hill), and UC Davis Transportation and Parking Services (Wayne Morris) for the support of the construction of the test sections; the Southwest Concrete Pavement Association (Charles Stuart) and Ergon Asphalt & Emulsions (Mo Rahman and Todd Vargason) for the advice in designing the experiment; the UCPRC laboratory and field staff; and UCPRC publications manager Camille Fink.

PROJECT OBJECTIVES

The objective of TO-020 is to develop recommendations for designing new hot mix asphalt (HMA) bases for jointed plain concrete pavement (JPCP) and continuously reinforced concrete pavement (CRCP), and interlayers (bond breakers) to be used between the JPCP slabs and the lean concrete bases (LCB). The new HMA may include high recycled asphalt pavement (RAP) content and/or recycled tire rubber. This will be achieved through the following tasks:

- Task 1: Monitoring of concrete slab test track.
- Task 2: Laboratory testing of standard concrete pavement bases.
- Task 3: Design and testing of improved base materials and interlayers.
- Task 4: Pilot implementation in the field.

The research summarized in this report completes the work of Task 1 and Task 2 by presenting the results of the monitoring of the concrete slab test track and the results of the laboratory testing of standard concrete pavement base materials.

EXECUTIVE SUMMARY

The Caltrans Rigid Pavement Design Catalog considers two types of bases for jointed plain concrete pavement (JPCP): hot mix asphalt (HMA) and lean concrete base (LCB). The HMA typically used for concrete pavement bases is the conventional mix used for asphalt pavements. The use of the conventional mix has limitations since the HMA design and construction focus is on maximizing rutting and fatigue resistance over a wide temperature range. However, the requirements that the asphalt mix must fulfill as a base for concrete pavement are considerably different, particularly regarding its ability to deform under slow loading and to maintain adhesion to the concrete slab. In addition to HMA, the Rigid Pavement Design Catalog allows the use of LCB for JPCP. However, research conducted by the UCPRC and others has strongly indicated that JPCP performs better with an asphalt base rather than with LCB.

The goal of the research presented in this report is to develop recommendations for improving the design of the asphalt concrete for use as the base of rigid pavements and engineered interlayers for use between the JPCP slabs and the LCB. The study was designed to address the following questions:

(1) How should asphalt concrete design be adapted to optimize its performance as a rigid pavement base?

(2) Can rubberized hot mix asphalt–gap-graded (RHMA-G) be used as a rigid pavement base instead of HMA?

(3) Why does JPCP perform considerably worse, in terms of cracking, with LCB than with HMA base?

(4) Can the performance of JPCP with LCB be improved by using an engineered interlayer? If yes, which interlayer?

The research is based on three main pillars: full-scale test track monitoring, laboratory testing, and finite element method (FEM) modeling. This research project included the following sampling and testing activities:

- A full-scale test track was built and monitored to study JPCP slab-base interaction mechanisms. The test track includes four independent slabs—one slab with an RHMA-G base and three slabs with an LCB and one interlayer (curing compound, geotextile, or microsurfacing). The curing compound interlayer represents the current practice of JPCP construction in California. The geotextile is a nonwoven polypropylene geosynthetic, 14.7 oz./yd^2 (500 g/m^2), meeting AASHTO M288 specifications. The microsurfacing is a Type II gradation meeting Caltrans Standard Specifications, Section 37-3, “Slurry Seals and Micro-Surfacings,” with a thickness around 0.2 in. (5 mm). c (PLCC) was used for building the slabs, which measure 12 × 12 ft. (3.6 × 3.6 m) and are 7 in. (178 mm) thick. The slabs were instrumented with thermocouples and vibrating wire strain gauges to measure concrete strain due to the hygrothermal actions (drying shrinkage and thermal actions). The measured strains were used to calculate the curling/warping (curvature) of the slabs.

- In addition to monitoring the concrete hygrothermal strains, the test track was periodically evaluated using the falling weight deflectometer (FWD). In each of the evaluations, each slab was tested at the center and corners twice a day (morning and afternoon). The goal of the FWD evaluations was to determine how the corner deflection changes versus the curvature of the slab and how this change varies from section to section.

- The different materials—RHMA-G, LCB, and PLCC—were sampled during the test track construction and used for specimen preparation and laboratory testing.
- In addition to the RHMA-G, a standard HMA was sampled and tested in the laboratory. The HMA represents current practice for JPCP and continuously reinforced concrete pavement (CRCP) base construction in California. The two asphalt concrete mixes (RHMA-G and HMA) were tested following a protocol that was developed in this research project for the evaluation of asphalt concrete mixes for use as JPCP bases. The testing protocol includes standardized asphalt concrete tests as well as new tests that were developed as part of this research project, the hanging test and the Universal Testing Machine (UTM) ramp test. These two tests measure the capacity of the asphalt concrete to absorb hygrothermal movements of the concrete slabs while imposing minimum slab restraint and preventing slab-base separation, a capacity referred to in this report as the "cushion effect."
- The interlayers were not tested in the laboratory.
- Two FEM models were developed and used in this research, both employing *Abaqus* software. The first models the structural response of the slabs under FWD or traffic loading. The second models the slab-base debonding that occurs due to the slab curling/warping created by the hygrothermal actions.

The conclusions are summarized in the following discussion and grouped to address the main questions this research intended to answer:

(1) How should asphalt concrete design be adapted to optimize its performance as a base for rigid pavement?

  - The experimental data collected in this research indicates that there is room for improving the performance of asphalt concrete as a JPCP base. Enhancements should focus on increasing the capacity to deform under slow loading and resisting long-term moisture damage.
  - Most likely, increasing the capacity to deform under slow loading and enhancing long-term moisture resistance will result in softer asphalt concrete and increased susceptibility to rutting. However, rutting is not an issue as the base will be protected by the JPCP slabs. Additionally, FEM modeling indicates that the softening of the asphalt concrete base is not a concern for JPCP performance.
  - The directions for improving asphalt concrete for JPCP bases are also applicable to CRCP bases.

(2) Can RHMA-G be used as a rigid pavement base instead of HMA?

  - No reason was found to not use RHMA-G, instead of HMA, as a rigid pavement base, indicated by the two mixtures tested in this project. The lower stiffness of the RHMA-G compared with the HMA is expected to have a minor effect on the rigid pavement performance.

- The results of the laboratory testing of two HMA and two RHMA-G mixes used regularly in Caltrans projects indicate that RHMA-G should perform similarly to HMA as a rigid pavement base.

(3) Why does JPCP perform considerably worse, in terms of cracking, with LCB than with HMA base?

- The experimental data collected in this research indicate that the RHMA-G base provides much better support to the slab than the LCB with the typical curing compound interlayer when the slab curvature is high. In the summer evaluations, when slab curvature was particularly high, the corner deflection in the section with LCB and curing compound was up to three times the corner deflection in the section with the RHMA-G base.
- The experimental data collected from the sections and the FEM modeling confirm that the use of a LCB, together with the curing compound interlayer, results in a rigid contact between the slabs and base that is not desirable. Because of the rigid contact, the slabs lose support from the base as they curl/warp due to temperature changes and drying shrinkage. Because of this loss of support, the traffic loading applied close to or at the joints produces considerable tensile stresses at the top of the slabs, which may result in top-down cracking.

(4) Can the performance of JPCP with LCB be improved by using an engineered interlayer? If yes, which interlayer?

- Yes. Despite its small thickness of 0.2 in. (5 mm), the microsurfacing interlayer considerably improved the performance of the curing compound interlayer. In fact, the corner deflection in the section with the LCB and the microsurfacing interlayer was similar to the corner deflection in the section with the RHMA-G base.
- The geotextile did not improve the performance of the curing compound interlayer. This outcome confirms the initial expectation that the geotextile would not be able to provide the "cushion effect" required to prevent the rigid contact between the slabs and the LCB.

The following are recommendations based on the findings of this research:

- It is recommended that RHMA-G be allowed as the base layer of rigid pavements in addition to HMA. The same thickness should be prescribed for both materials. Caltrans may consider extending the rubber use mandate to the base layer of rigid pavements.
- It is also recommended that the use of a slab-LCB microsurfacing interlayer be evaluated in a pilot project before including microsurfacing as an alternative in Caltrans Std. Specs. Section 36-2, "Base Bond Breaker." On the other hand, it is recommended that Caltrans Std. Specs. Section 36-2 be updated to not allow the use of geotextile as a slab-LCB bond breaker.
- Further research is needed to optimize the design of asphalt concrete mixes, including HMA and RHMA-G, for their performance as a rigid pavement base. This research and optimization will be conducted in ongoing Caltrans PPRC Project 4.99, "Piloting New Asphalt Base Designs and Interlayers for Concrete Pavements." The same applies to optimizing cold recycling materials for use as a rigid pavement base, which is the focus of ongoing Caltrans PPRC Project 4.98, "Use of Cold Recycling as Base for Concrete Pavements."
- Microsurfacing has shown excellent performance as a slab-LCB interlayer.

TABLE OF CONTENTS

LIST OF FIGURES

LIST OF TABLES

LIST OF ABBREVIATIONS

AMPT	Asphalt Mixture Performance Tester
ATPB	Asphalt-treated permeable base
CC	Curing compound
CRCP	Continuously reinforced concrete pavement
CRM	Crumb rubber modifier
CTE	Coefficient of thermal expansion
DB	Debonding
DGAB	Dense-graded aggregate base
FEM	Finite element method
FWD	Falling weight deflectometer
GEO	Geotextile
HDM	Highway Design Manual
HMA	Hot mix asphalt
IDEAL-CT	IDEAL cracking tolerance
ITS	Indirect tensile strength
JPCP	Jointed plain concrete pavement
LCB	Lean concrete base
LTE	Load transfer efficiency
LTPP	Long-term pavement performance
LVDT	Linear variable differential transformer
MIC	Microsurfacing
MiST	Moisture-Induced Stress Tester
NMAS	Nominal maxim aggregate size
PATB	Permeable asphalt-treated base
PCS	Pavement condition survey
PG	Performance grade
PLC	Portland limestone cement
PLCC	Portland limestone cement concrete
RAP	Recycled asphalt pavement
RHMA-G	Rubberized hot mix asphalt–gap-graded
SDEG	Stiffness degradation
TWM	Total weight of mix

UTM	Universal testing machine
VWSG	Vibrating wire strain gauge
WIM	Weigh-in-motion

LIST OF TEST METHODS AND SPECIFICATIONS

ASTM C31-21	Making and Curing Concrete Test Specimens in the Field
ASTM C39-21	Compressive Strength of Cylindrical Concrete Specimens
ASTM C78-22	Flexural Strength of Concrete (Using Simple Beam with Third-Point Loading)
ASTM C150-07	Standard Specification for Portland Cement
ASTM C157-17	Length Change of Hardened Hydraulic Cement Mortar and Concrete
ASTM C171-20	Standard Specification for Sheet Materials for Curing Concrete
ASTM C309-19	Standard Specification for Liquid Membrane-Forming Compounds for Curing Concrete
ASTM C403-08	Standard Test Method for Time of Setting of Concrete Mixtures by Penetration Resistance
ASTM C469-02	Static Modulus of Elasticity and Poisson's Ratio of Concrete in Compression
ASTM C494-17	Standard Specification for Chemical Admixtures for Concrete
ASTM C595-08a	Standard Specification for Blended Hydraulic Cements
ASTM C989-10	Standard Specification for Slag Cement for Use in Concrete and Mortars
ASTM D7196-18	Raveling Test of Cold-Mixed Emulsified Asphalt Samples
ASTM D7870-20	Moisture Conditioning Compacted Asphalt Mixture Specimens by Using Hydrostatic Pore Pressure
ASTM D8225-19	Determination of Cracking Tolerance Index of Asphalt Mixture Using the Indirect Tensile Cracking Test at Intermediate Temperature
AASHTO M 288-21	Standard Specification for Geosynthetic Specification for Highway Applications
AASHTO M 320-21	Standard Specification for Performance-Graded Asphalt Binder
AASHTO T 283-14	Resistance of Compacted Asphalt Mixtures to Moisture-Induced Damage
AASHTO T 336-15	Coefficient of Thermal Expansion of Hydraulic Cement Concrete
AASHTO T 378-22	Determining the Dynamic Modulus and Flow Number for Asphalt Mixtures Using the Asphalt Mixture Performance Tester (AMPT)

CONVERSION FACTORS

APPROXIMATE CONVERSIONS TO SI UNITS				
Symbol	**When You Know**	**Multiply By**	**To Find**	**Symbol**
		LENGTH		
in.	inches	25.40	millimeters	mm
ft.	feet	0.3048	meters	m
yd.	yards	0.9144	meters	m
mi.	miles	1.609	kilometers	km
		AREA		
in^2	square inches	645.2	square millimeters	mm^2
ft^2	square feet	0.09290	square meters	m^2
yd^2	square yards	0.8361	square meters	m^2
ac.	acres	0.4047	hectares	ha
mi^2	square miles	2.590	square kilometers	km^2
		VOLUME		
fl. oz.	fluid ounces	29.57	milliliters	mL
gal.	gallons	3.785	liters	L
ft^3	cubic feet	0.02832	cubic meters	m^3
yd^3	cubic yards	0.7646	cubic meters	m^3
		MASS		
oz.	ounces	28.35	grams	g
lb.	pounds	0.4536	kilograms	kg
T	short tons (2000 pounds)	0.9072	metric tons	t
		TEMPERATURE (exact degrees)		
°F	Fahrenheit	(F-32)/1.8	Celsius	°C
		FORCE and PRESSURE or STRESS		
lbf	pound-force	4.448	newtons	N
lbf/in^2	pound-force per square inch	6.895	kilopascals	kPa
APPROXIMATE CONVERSIONS FROM SI UNITS				
Symbol	**When You Know**	**Multiply By**	**To Find**	**Symbol**
		LENGTH		
mm	millimeters	0.03937	inches	in.
m	meters	3.281	feet	ft.
m	meters	1.094	yards	yd.
km	kilometers	0.6214	miles	mi.
		AREA		
mm^2	square millimeters	0.001550	square inches	in^2
m^2	square meters	10.76	square feet	ft^2
m^2	square meters	1.196	square yards	yd^2
ha	hectares	2.471	acres	ac.
km^2	square kilometers	0.3861	square miles	mi^2
		VOLUME		
mL	milliliters	0.03381	fluid ounces	fl. oz.
L	liters	0.2642	gallons	gal.
m^3	cubic meters	35.31	cubic feet	ft^3
m^3	cubic meters	1.308	cubic yards	yd^3
		MASS		
g	grams	0.03527	ounces	oz.
kg	kilograms	2.205	pounds	lb.
t	metric tons	1.102	short tons (2000 pounds)	T
		TEMPERATURE (exact degrees)		
°C	Celsius	1.8C + 32	Fahrenheit	°F
		FORCE and PRESSURE or STRESS		
N	newtons	0.2248	pound-force	lbf
kPa	kilopascals	0.1450	pound-force per square inch	lbf/in^2

*SI is the abbreviation for the International System of Units. Appropriate rounding should be made to comply with Section 4 of ASTM E380. (Revised April 2021)

1 INTRODUCTION

1.1 Background

Caltrans has implemented a new Rigid Pavement Design Catalog, supported by the University of California Pavement Research Center (UCPRC) through Partnered Pavement Research Center (PPRC) Project 3.53 *(1)*. The new design catalog considers two types of bases for jointed plain concrete pavement (JPCP): hot mix asphalt (HMA) and lean concrete base (LCB). For continuously reinforced concrete pavement (CRCP), only HMA is considered.

Currently, the Caltrans HMA base for JPCP and CRCP is designed and built following the Caltrans Standard Specifications, Section 39-2.02 (HMA Type A) *(2)*. Section 39 also includes other types of asphalt concrete mixes, including rubberized hot mix asphalt–gap-graded (RHMA-G), which is not allowed for use as a base layer for rigid pavement. RHMA-G is a gap-graded mix with at least 7.5% virgin asphalt rubber binder that has a minimum of 18% waste tire crumb rubber modifier.

While Caltrans does not allow the use of RHMA-G as a rigid pavement base, the evaluation of RHMA-G as the base of a thin concrete overlay in a full-scale test track, as part of PPRC Project 4.58B *(3)* and in a field pilot as part of PPRC Project 3.39 and Project 3.54 *(4)*, found no evidence that this mix would not perform properly as a rigid pavement base. Furthermore, RHMA-G is Caltrans' preferred surface mix for new construction, reconstruction, and rehabilitation of asphalt pavements and for asphalt overlays of rigid pavements. This preference aligns with the California State Legislature's rubber use mandate: "The Department of Transportation shall use, on an annual average, not less than 11.58 pounds of CRM [crumb rubber modifier] per metric ton of the total amount of asphalt paving materials used" (California Public Resources Code, Section 42703).

The HMA typically used for concrete pavement bases is the conventional mix used for asphalt pavements. In its conventional use, the HMA design and construction focus is on maximizing rutting and fatigue resistance over a wide temperature range. However, the requirements that the asphalt mix must fulfill as a base for concrete pavement are considerably different. Aging, one of the mechanisms that lead to asphalt cracking, is minimized due to the thermal insulation, protection from ultraviolet rays, and restriction of entry by air provided by the concrete pavement. Also, traffic-induced stress levels in an HMA base under concrete are lower than in asphalt-surfaced pavements; as a result, fatigue cracking is much less of a concern than it is in the conventional use of HMA. The same applies to rutting, due to the relatively low stress and low maximum temperatures resulting from the structural and thermal protection provided by the concrete pavement.

On the other hand, long-term moisture resistance is critical, as concrete pavements are typically designed for a 40-year life before minor rehabilitation (around 60 years before major reconstruction). Therefore, the asphalt base is expected to perform properly for much longer than conventional asphalt pavements, which are designed to last 20 years before minor rehabilitation. The moisture damage requirements for the asphalt base are similar to the requirements for asphalt pavements designed to last 40 years. Consequently, there is a need to optimize HMA design and construction to maximize performance as a concrete pavement base. This optimization will result in mixes that, when used as a concrete pavement base, will perform better and therefore be more cost-effective and environmentally beneficial than regular HMA due to improved performance.

One of the main challenges in developing optimized asphalt mixes for concrete pavement bases is that the vast majority of asphalt mix testing methods and specifications are conceived for the asphalt mix's conventional use as part of an asphalt pavement. One of the few examples of asphalt mix specifications for a concrete pavement base was developed in 2003 at the UCPRC as part of the Interstate 15 Devore long-life JPCP construction *(5)*.

In addition to HMA, the Caltrans Rigid Pavement Design Catalog allows the use of LCB for JPCP. However, research conducted by UCPRC and others has strongly indicated that JPCP performs better with an asphalt base than with LCB. Long-term pavement performance (LTPP) SPS-2 sections were designed to evaluate the effect of several structural factors on the performance of JPCP. One of these factors was the type of base material. The SPS-2 sections included three types of bases: dense-graded aggregate base (DGAB), lean concrete base (LCB), and permeable asphalt-treated base (PATB), referred to as asphalt-treated permeable base (ATPB) in Caltrans Standard Specifications. The longitudinal and transverse cracking performance were much worse for the sections with LCB compared with those with PATB, as shown in Figure 1.1 *(6)*.

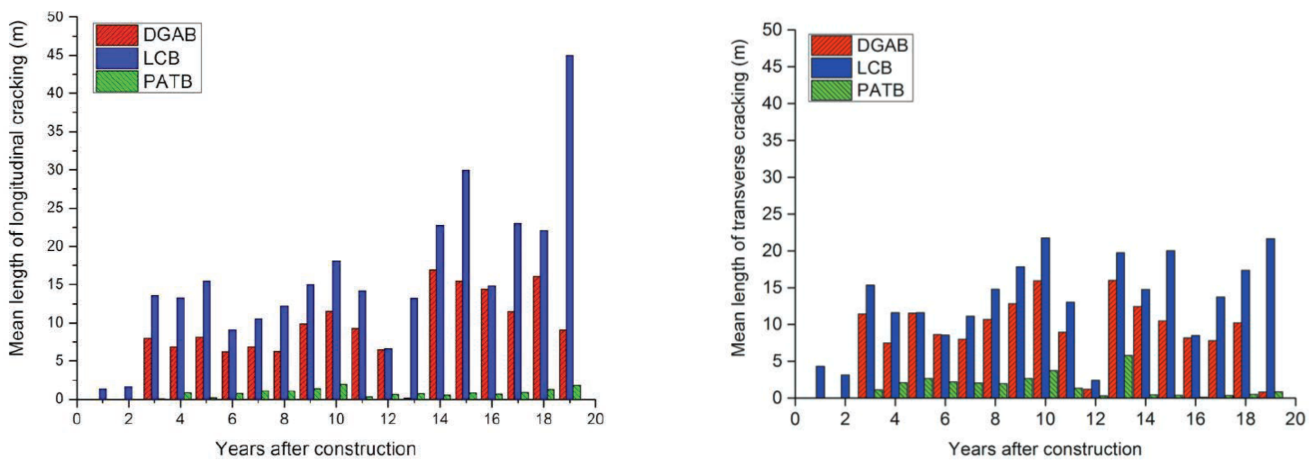

(a) (b)

Source: Xu and Cebon (2017) *(6)*.

Figure 1.1: (a) Longitudinal and (b) transverse cracking performance of the LTPP SPS-2 sections for three different bases.

The poor performance of the JPCP with LCB was also found in a recent UCPRC study that used multinomial logistic regression to analyze annual field measurement data from the Caltrans pavement condition survey (PCS) database *(7)*. It included manual (1978 to 2013) and automated (2010 to 2018) PCS data from 446 new construction and reconstruction JPCP projects, totaling approximately 4,380 lane miles (7,050 lane-km). The calibrated statistical model was used to quantify the effects of different factors on JPCP cracking performance. The factors included in the analysis were climate region; weigh-in-motion (WIM) class (1 to 5), which defines truck axle load intensity normalized by truck traffic volume as used by Caltrans for pavement design and management *(8)*; truck traffic volume; base material type; slab thickness; use of dowels; slab length; and shoulder type. The effect of base material type (LCB versus HMA) was statistically significant, and the calibrated model indicated that JPCP with LCB developed cracking much faster (180% faster) than JPCP with an HMA base (e.g., the same level of cracking may take 40 years with an HMA base and only 14.3 years [40 divided by 2.8] with LCB).

Past research at the UCPRC suggested that the combination of the dry climate (high drying shrinkage) present in many California regions, together with a stiff base material (such as lean concrete), increases the risk of JPCP cracking *(9)*. The hypothetical mechanism explaining why this combination of high drying shrinkage and stiff base is believed to increase the risk of JPCP cracking is outlined in Figure 1.2 and explained as follows:

- JPCP slabs are seldom flat; they curl and warp[1] due to temperature and drying shrinkage differentials across the slab depth.
- As the slabs curl and warp, they lose support if the base is not able to flow and adapt to the slab's new shape.
- Because the LCB is a stiff and elastic material with little capacity to adapt to the new shape of the pavement slabs as they curl and warp, a separation or gap results between the pavement slabs and the LCB, causing the corners and edges of the slabs to lose contact with the base. LCB is stiffer than HMA, so it elastically deforms less under the more transient environmental loading of day-to-night curling. LCB is also elastic and cannot creep to further adapt to longer-term slab shape changes, such as those occurring under seasonal drying shrinkage, while HMA is viscoelastic and can creep (meaning it can flow).
- Due to the lack of contact with the base, the slabs function as cantilever slabs rather than as slabs supported by a multilayer structure. Consequently, traffic loading applied close to or at the joints can produce considerable tensile stresses at the top of the slabs, potentially resulting in top-down cracking.
- In contrast, the HMA base has a large capacity to deform and flow, allowing it to accommodate the curling and warping deformations of the slabs without losing contact with them. This support enables the slabs to effectively resist traffic loading, functioning as parts of a multilayer structure rather than as cantilever slabs.

The mechanism outlined above is a hypothesis validated by the experimental data and analysis presented in this report. The bottom line is that a rigid (stiff and elastic) base, together with a rigid contact between the slab and the base, is not desirable.

[1] The term "curling" is typically used to refer to slab curvature due to thermal gradient (gradient versus depth), while the term "warping" is typically used to refer to slab curvature due to differential drying shrinkage (differential versus depth).

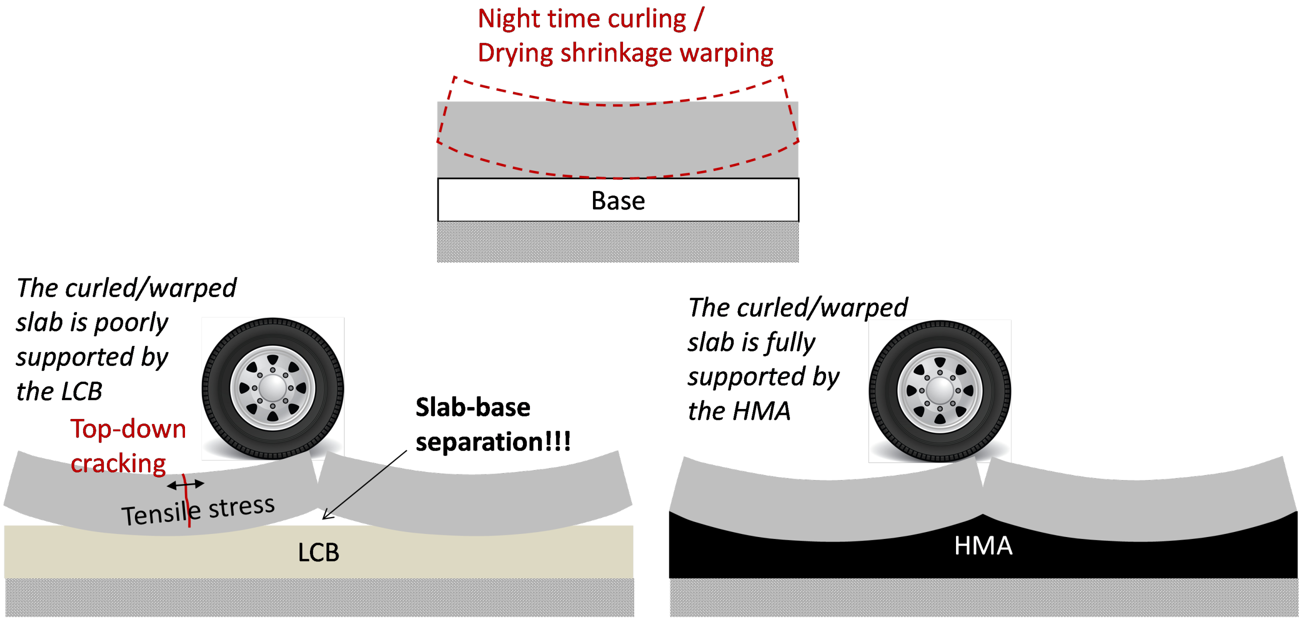

Figure 1.2: Interaction between curled/warped slab (concave upward) and base.

Despite the poor performance of JPCP with LCB, compared with the HMA base, the LCB offers advantages in terms of construction logistics (e.g., use of the same paving machine for the base and the pavement) and the possibility of using lower-quality aggregates, including greater percentages of recycled materials. For these reasons, there is interest in continuing to use LCB in JPCP. As previously explained, it is believed that the poor performance of JPCP with LCB is due to the low capacity of the lean concrete to flow/adapt to the curling/warping of the slabs. It is also believed that by using an appropriate interlayer between the concrete slabs and the LCB, the performance of JPCP with LCB should match or improve in comparison to the performance of JPCP with HMA base.

JPCP practice involves the use of a "bond breaker" between the concrete slabs and the rigid base. The corresponding Caltrans requirements are included in the Caltrans Std. Specs. Section 36-2, "Base Bond Breaker" *(2)*. For LCB, the specifications require the use of any of three bond breakers: sprayed PG 64-10 asphalt binder, curing compound, or geosynthetic. For new Caltrans JPCP construction and JPCP lane reconstruction projects, the curing compound is the most commonly used bond breaker. Polyethylene film and white curing paper, both following ASTM C171 specifications, are allowed with rapid-strength concrete bases and are frequently used in individual slab replacements that take place overnight.

The curing compound bond breaker prescribed by Caltrans specifications consists of one or more applications of ASTM C309 Type 2 (white pigmented) compound to achieve a total coverage rate of at least 0.12 gal./yd^2 (0.54 L/m^2). While the curing compound film is expected to break the bond between the concrete slabs and the LCB, it is too thin to provide any cushioning effect between the slabs and LCB, and, consequently, it may result in an undesirable rigid contact between them. This hypothesis is also validated by the experimental data and analysis presented later in this report. The LCB may also restrict concrete early-age deformation, leading to premature cracking.

A major limitation in developing an interlayer material between concrete slabs and LCB is the lack of understanding of slab-base interaction mechanisms. Current mechanistic-empirical modeling oversimplifies the slab-base interaction problem by considering, among other simplifications, that the slab and base are fully bonded in the vertical direction, while two extreme conditions—full bonding or full unbonding—are typically considered in the horizontal direction *(10)*. The bond is assumed to be broken after a certain period. This approach fails to reproduce the differences in performance between JPCP with LCB and JPCP with HMA base.

1.2 Problem Statement

The following problems were identified:

- The Caltrans HMA mixture design method was developed for its conventional use as an asphalt pavement layer. It has not been customized to perform as a concrete pavement base, which was a recommendation made in 2006 (*9*).
- The Caltrans *Highway Design Manual* (*HDM*) does not allow the use of RHMA-G for concrete pavement bases.
- The performance data from the Caltrans road network indicate that the cracking performance of JPCP is considerably worse with LCB than with the HMA base.
- An understanding of JPCP slab-base interaction mechanisms is lacking.
- A procedure for testing the suitability of an asphalt mix as a JPCP base and optimizing the performance is lacking. The same testing procedure issue applies to the interlayer to be used between the JPCP slabs and a rigid base like LCB.

1.3 Goal and Questions to Answer

The goal of the research presented in this report is to develop recommendations for improving the design of the asphalt concrete used as the base of rigid pavements and the design of engineered interlayers used between the JPCP slabs and the LCB. The study was designed to address the following questions:

(1) How should asphalt concrete design be adapted to optimize its performance as a base for rigid pavement?

(2) Can RHMA-G be used as a rigid pavement base instead of HMA?

(3) Why does JPCP perform considerably worse, in terms of cracking, with LCB than with an HMA base?

(4) Can the performance of JPCP with LCB be improved by using an engineered interlayer? If yes, which interlayer?

1.4 Experimental Approach

Answering the four questions formulated in Section 1.3 would be difficult, if not impossible, without a good understanding of the slab-base interaction mechanisms in JPCP. Studying these interaction mechanisms is the main reason for including the evaluation of a full-scale test track in this research project. The answers to the four questions formulated in Section 1.3 also require a laboratory testing methodology (collection of testing procedures) for evaluating the suitability of asphalt concrete, including both HMA and RHMA-G, as a JPCP base or the suitability of a material as an interlayer between the JPCP slabs and the LCB. For this research, a methodology for testing asphalt concrete as a JPCP base was developed and applied to several mixes.

Further, the need exists for criteria for assessing if the results of the different tests are acceptable. The criteria may be based on a comparison with a material with known good performance. However, pavement performance is not simple; rather, it is the outcome of a complex interaction between different material properties. Most frequently, modeling is required to evaluate how a collection of material properties impacts pavement performance. Unfortunately, the capabilities of the current practice of JPCP mechanistic-empirical modeling are limited when it comes to slab-base interactions. To overcome this limitation, this research project includes the development of a finite element method (FEM) model that can more accurately address slab-base interaction.

The research presented in this report is based on three main pillars: full-scale test track monitoring, laboratory testing, and FEM modeling. The approach used to address the research goals includes the following steps:

(1) Selection and sampling of asphalt concrete mixes for test track construction and laboratory characterization. The selection of the mixes is discussed in Section 2.1.

(2) Selection and sampling of JPCP slab-LCB interlayers for test track construction. The selection of the interlayers is discussed in Section 2.2.

(3) Designing, building, and monitoring of a full-scale test track to study JPCP slab-base interaction mechanisms. The test track includes an asphalt concrete base—in this case, RHMA-G—and LCB with different interlayers. The monitoring includes the concrete hygrothermal strains to measure expansion/contraction and curling/warping of the slabs and the deflection under falling weight deflectometer (FWD) loading, which also provides a means to identify the effects of curling and warping. The monitoring period presented in this report starts from the construction of the test track in June 2022 through September 2023. The design of the test track and its instrumentation are presented in Section 2.3. The test track construction is presented in Chapter 3 and the monitoring in Chapter 4.

(4) Identification of the relevant properties of the JPCP base and, for each property, the selection of the corresponding laboratory testing procedure applicable to asphalt concrete. The relevant properties of the JPCP base and the selected laboratory testing procedures are discussed in Section 2.4. The results of the laboratory testing of the asphalt concrete mixes are presented in Chapter 5, together with LCB and concrete laboratory testing results.

(5) Development of a JPCP FEM model that can better address slab-base interaction. The model has the following capabilities: (1) modeling of the structural response of curled/warped slabs under traffic and FWD loading for different scenarios of slab-base bonding, (2) modeling of the slab-base debonding under hygrothermal actions, and (3) development of model parameters obtained from laboratory testing of the base material and, for JPCP with LCB, the interlayer. The model was calibrated based on the test track monitoring results, including the measured curling/warping of the slabs and the deflections measured under FWD loading. The FEM model development and calibration are presented in Chapter 6.

(6) Identification of answers to each of the questions formulated in Section 1.3, based on the results of the laboratory testing, results of the test track monitoring, and FEM modeling. The answers to the questions are presented in Chapter 7.

1.5 Scope of the Report

The following are additional details about the scope of this research project:

- While this research focuses on JPCP, some of the conclusions and recommendations regarding JPCP asphalt bases have been extrapolated to CRCP.
- Thin concrete overlays on asphalt, also referred to as JPCP with thin and short slabs (short-jointed plain concrete pavements), are not specifically addressed in this research.
- This research does not intend to develop improved asphalt mixes for use as concrete pavement bases; the intent instead is to formulate guidelines and recommendations for developing those mixes. While the same applies to slab-rigid base interlayers, one of the interlayers evaluated in this research project performed very satisfactorily and its use is recommended for pilot implementation in the field.
- This report does not include any laboratory testing of JPCP slab-LCB interlayers. A methodology for laboratory testing of such interlayers is not available yet, and it will be developed as part of the ongoing PPRC Project 4.99.
- The use of cold recycling in JPCP bases is not addressed in this report, but it is the subject of the subsequent Caltrans PPRC Project 4.98, "Use of Cold Recycling as Base for Concrete Pavements."

1.6 Measurement Units

In this report, both US and metric units (provided in parentheses after the US units) are included in the general discussion. There is one exception: the performance grade of the asphalt binder is reported in metric units (°C) following AASHTO M 320-21. A conversion table (US versus metric) is provided on page xvii.

1.7 Terminology: Asphalt Concrete, Asphalt, and Concrete

In this report, the term "asphalt concrete" refers to the combination of stone, sand, and filler bound together by asphalt binder and other additives and produced at high temperatures, typically above 270°F (132°C). Two asphalt concrete mixes are referred to in this study: conventional HMA and rubberized hot mix asphalt–gap-graded (RHMA-G). The terms "asphalt" and "asphalt concrete" are used interchangeably in this report. The term "asphalt binder" refers to the binder in asphalt concrete. The term "concrete" (without "asphalt" preceding it) is exclusively used to refer to hydraulic cement (e.g., portland cement) concrete.

2 EXPERIMENTAL DESIGN

This chapter reviews the experimental design of this study, including the selection of materials, test track design, testing methodologies, and specimen preparation.

2.1 Selection of Asphalt Concrete Mixes and Lean Concrete Base for Laboratory Testing and Test Track Construction

Answering the questions that were formulated for this research (Section 1.3) requires the evaluation of standard base materials, as these questions refer to JPCP performance with a standard HMA base, standard LCB, or the potential performance with standard RHMA-G. The selection of a unique "standard" material is debatable due to the variety of HMA and LCB mixes used in Caltrans JPCP base construction; the same applies to RHMA-G used in asphalt overlays. However, budget and time limitations allowed for the evaluation of only one material per group (one HMA, one RHMA-G, and one LCB). Each example material was selected after consulting with Caltrans and respective industries to ensure the materials would represent, as much as possible, standard practice on the Caltrans road network.

While one material was selected for each of the three groups, only RHMA-G and LCB were used for the test track construction. Adding the HMA to the test track would have been desirable, but this was not possible due to budget limitations and because the differences between the mechanical properties of HMA and RHMA-G are not large enough to expect any measurable difference between the two potential test track sections (one with the HMA base versus another with the RHMA-G base). Therefore, a comparison of HMA versus RHMA-G performance as a JPCP base was conducted based on laboratory testing and FEM modeling.

The following are details of the selected materials:

- HMA (laboratory testing only):
    - Mix design by Teichert (Perkins drum mixer plant, Sacramento area, California)
    - Superpave design, 85 gyrations at 87 psi (600 kPa) pressure; HMA follows Caltrans Std. Specs. Section 39
    - 3/4 in. (19 mm) nominal maximum aggregate size
    - PG 64-10 virgin binder, supplied by Valero refinery at Benicia
    - 13% recycled asphalt pavement (RAP) content (percent refers to aggregate replacement); RAP passing 3/8 in. (9.5 mm); RAP binder content 4.5% by total weight of mix (TWM)
    - Asphalt binder content (virgin plus RAP) 4.8% TWM. Out of the 4.8% asphalt binder content, 1.12% comes from the RAP while 3.68% is virgin asphalt
    - Alluvial aggregates, mostly siliceous
    - This HMA is commonly used for bases and intermediate layers in Caltrans asphalt pavements and also used in JPCP and CRCP bases
    - Loose mix sampled from plant on March 16, 2023; mix sampled in 3.5-gallon (13 L) buckets and stored in a UCPRC laboratory at room temperature until used for laboratory specimen fabrication

- RHMA-G (laboratory testing and evaluation in test track):
  - Mix design by Teichert (Perkins drum mixer plant, Sacramento area, California)
  - Superpave design, 100 gyrations at 120 psi (825 kPa) pressure; RHMA-G follows Caltrans Std. Specs. Section 39
  - 3/4 in. (19 mm) nominal maximum aggregate size
  - Asphalt rubber binder, with 82% PG 64-16 base binder and extender oil, and 18% crumb rubber modifier (CRM)
  - PG 64-16 base virgin binder, supplied by Valero refinery at Benicia
  - 0% RAP content
  - Asphalt rubber binder content 7.5% TWM
  - Alluvial aggregates, mostly siliceous
  - This RHMA-G is commonly used for a 2.4 in. (60 mm) thick surface overlay in Caltrans asphalt pavements
  - Loose mix sampled from plant on May 26, 2022 (the same day it was used for the test track paving); mix sampled in 5-gallon (19 L) buckets and stored in a UCPRC laboratory at room temperature until used for laboratory specimen fabrication
- LCB (laboratory testing and evaluation in test track):
  - Mix design by Elite Ready Mix (Bradshaw Road plant, Sacramento area, California)
  - Designed to provide 530 psi (3.65 MPa) compressive strength at 7 days; LCB follows Caltrans Std. Specs. Section 28
  - 1 in. (25 mm) nominal maximum aggregate size
  - 271 lb. portland cement/yd^3 (161 kg/m^3)
  - Portland cement Type II (ASTM C150), supplied by CEMEX (Victorville plant, California)
  - No supplementary cementitious material
  - Water to cement ratio: 1.29
  - Admixtures: ASTM C494 Type A Water Reducer, used at 3 to 6 oz./cwt (oz./100 lb. of cement) (2 to 4 mL per cement kg)
  - Design slump: 2±1 in. (50±25 mm) (low slump, compatible with slip-form paving)
  - Alluvial aggregates, mostly siliceous
  - This LCB is commonly used for the construction of Caltrans JPCP bases
  - Specimens for laboratory testing were prepared using fresh mixture sampled during the test track construction on May 6, 2022

2.2 Selection of Interlayers for Test Track Construction

Three different JPCP slab-LCB interlayers were selected for evaluation on the test track: curing compound, geotextile, and microsurfacing. As discussed in Section 2.5, the interlayers were not tested in the laboratory. The curing compound interlayer was selected since it is the most commonly used bond breaker in new JPCP construction and JPCP lane reconstruction projects in California. The test track section with the curing compound interlayer is the control section that represents the current Caltrans practice of JPCP with LCB. The geotextile was selected since it had been recommended by the Concrete Pavement Technology Center as a "separation layer" for the unbonded concrete overlay of existing concrete pavements *(11)*. Another reason for selecting this application is that the geotextile is already included in the Caltrans repertory of bond breakers (Caltrans Std. Specs. Section 36-2, "Base Bond Breaker"). However, while these two interlayers are expected to effectively break the bond between the slabs and the LCB, neither was expected to reduce the gap between LCB and concrete pavement when the slabs curl/warp. Consequently, microsurfacing was selected as the third interlayer.

The reasons for selecting microsurfacing were the following: (1) it was believed that it was capable of providing the aforementioned "cushion effect," preventing the separation between the slabs and the LCB, (2) it would provide a number of constructability advantages (listed below), and (3) no technical, economic, or environmental reason was found that would discard the use of microsurfacing as a JPCP-LCB interlayer.

The following are constructability advantages that microsurfacing would provide if used as a JPCP-LCB interlayer:

- The cost is relatively low, comparable to geotextile, and much lower than HMA.
- The application is very fast (microsurfacing can be placed faster than walking speed).
- Microsurfacing can be opened to construction traffic in two hours.
- The microsurfacing paving operation requires minimal equipment and no compaction.

Microsurfacing can be regarded as a high-quality slurry; a slurry is a "homogenous mixture of emulsified asphalt, water, well-graded fine aggregate, and mineral filler that has a creamy fluid-like appearance when applied" *(12)*. Compared with the conventional slurry, the microsurfacing emulsified asphalt is polymer modified and the filler must include portland cement. Quality control/quality assurance requirements are somewhat stricter for microsurfacing than for a slurry. While a slurry must be placed as a monolayer, microsurfacing can be applied in several lifts (e.g., for filling ruts). Also, microsurfacing can be opened to traffic in two hours, around half the time that a slurry typically requires.

Microsurfacing is included in Caltrans Std. Specs. Section 37-3, "Slurry Seals and Micro-Surfacings," but it is not one of the alternatives that Caltrans currently allows for use as a JPCP slab-LCB bond breaker. Section 37-3 considers three microsurfacing gradations—I, II, and III—with nominal maximum aggregate sizes of No. 8 (2.38 mm), No. 4 (4.75 mm), and 3/8 in. (9.5 mm). The required amount of microsurfacing materials for standard paving applications is 8 to 12 lb./yd^2 (4.3 to 6.5 kg/m^2) for Type I, 10 to 18 lb./yd^2 (5.4 to 9.8 kg/m^2) for Type II, and 20 to 25 lb./yd^2 for Type III (10.8 to 13.6 kg/m^2). These amounts result in average microsurfacing layer thicknesses of around 0.1 in. (3 mm) for Type I, 0.2 in. (5 mm) for Type II, and 0.3 in. (8 mm) for Type III. The Type II gradation was selected for evaluation in this study since it was believed that a thickness of 0.2 in. (5 mm) would be enough to provide the cushion effect required to prevent the rigid contact between the slabs and the LCB.

While the three interlayers were used for the test track construction, they were not tested in the laboratory for different reasons. The research team was confident that the curing compound and the geotextile would provide the bond-breaking between the slab and the LCB with no cushioning effect (i.e., there would be hard contact between the slabs and the LCB with any of the two interlayers). The only mechanistic property to be determined for hard contact is the friction coefficient, which is not relevant to this research. The microsurfacing interlayer was not tested in the laboratory since the attempt to produce composite specimens (concrete-microsurfacing-LCB) in the laboratory was not successful. A second attempt will be conducted as part of ongoing PPRC Project 4.99, "Piloting New Asphalt Base Designs and Interlayers for Concrete Pavements."

The following are details of the selected interlayers:

- Curing compound:
  - Material and construction following Caltrans Std. Specs. Section 36-2, "Base Bond Breaker" and Section 90, "Concrete"
  - Coverage rate: 0.12 gal./yd^2 (0.54 L/m^2)
  - Type: ASTM C309 2B (white pigmented, resin-based)
- Geotextile:
  - Supplied by Propex GeoSolutions
  - Material and construction following Caltrans Std. Specs. Section 36-2, "Base Bond Breaker" and Section 96-1.02Q, "Geosynthetic Bond Breaker"
  - Type: nonwoven polypropylene geosynthetic, 14.7 oz./yd^2 (500 g/m^2), that meets AASHTO M288 specifications
- Microsurfacing:
  - Mix design by VSS International
  - Material and construction following Caltrans Std. Specs. Section 37-3, "Slurry Seals and Micro-Surfacings"
  - Type: Type II gradation
  - Asphalt residue: 9% (by weight of aggregate)
  - Cement content: 1% (by weight of aggregate)
  - Aluminum sulfate content: 0% to 2% (by weight of aggregate); the aluminum sulfate controls the breaking time of the asphalt emulsion; the aluminum sulfate content is adjusted in place depending mainly on the paving weather conditions

2.3 Test Track Design

The main goal of the test track is to provide the experimental data required for improving the understanding of JPCP slab-base interaction. Its design focuses on two of the questions that were formulated in this research project:

- Why does JPCP perform considerably worse, in terms of cracking, with LCB than with HMA base?
- Can the performance of JPCP with LCB be improved by using an engineered interlayer? If yes, which interlayer?

Two base materials were used for the test track. The first material is an LCB and the second is an RHMA-G, both described in Section 2.1. Both materials were designed and built according to Caltrans Std. Specs. guidelines. Two of the interlayers used in the test track construction, the curing compound and geotextile, were selected and placed following Caltrans Std. Specs. Section 36-2, "Base Bond Breaker." The third one, the microsurfacing, was designed and placed following Caltrans Std. Specs. Section 37-3, "Slurry Seals and Micro-Surfacings," although it is not one of the bond breaker options allowed by Caltrans.

The concrete pavement was built with portland limestone cement (PLC), as this type of cement is progressively replacing portland cement in California due to its lower embodied carbon. The concrete mixture design is based on an existing design provided by CEMEX, the concrete supplier for the test track construction. The portland limestone cement concrete (PLCC) mixture design, shown in Table 2.1, meets Caltrans Std. Specs. Section 40, "Concrete Pavement" and Section 90, "Concrete."

Table 2.1: Portland Limestone Cement Concrete Mixture Design

Material	Description	Design Quantity (per 1 yd^3)	Design Quantity (per 1 m^3)
Coarse aggregate	Gravel	1,900 lb.	1,127 kg
Fine aggregate	Sand	1,312 lb.	778 kg
Cement	Type IL, ASTM C595	413 lb.	245 kg
Ground granulated blast furnace slag	Slag, Grade 120, ASTM C989	177 lb.	105 kg
Water reducer	Master Glenium 7500	4 oz./cwt	640 mL
Water	—	34.0 gal.	168 L

Only one slab per section was built due to space and budget limitations, which means that the sections were not provided with transverse joints. This choice of design, however, is not regarded as a limitation. The goal of the test track was to evaluate how the type of base and the interlayer impact the capacity of the slab to support loading. For that reason, large curling/warping of the slabs is desired. Curling/warping is expected to be larger for single (isolated) slabs than for jointed slabs with doweled transverse joints, as dowels restrict slab curling/warping. Further, the corner deflections under FWD loading will be larger on a single slab than on jointed slabs, particularly if the transverse joints are provided with dowels. Consequently, the effects of the type of base and interlayer will be better captured on single (isolated) slabs than on jointed slabs.

The thickness of the slab was 7 in. (178 mm), which is relatively thin for JPCP. The reason for the selection of a relatively small thickness was to increase curling/warping of the slabs. According to the Caltrans *HDM*, the thickness of the RHMA-G is 3 in. (76 mm), which is required for the JPCP HMA base, and the thickness of the LCB is 4.2 in. (107 mm), as specified for JPCP LCB *(15)*. The configuration of the test track is shown in Figure 2.1.

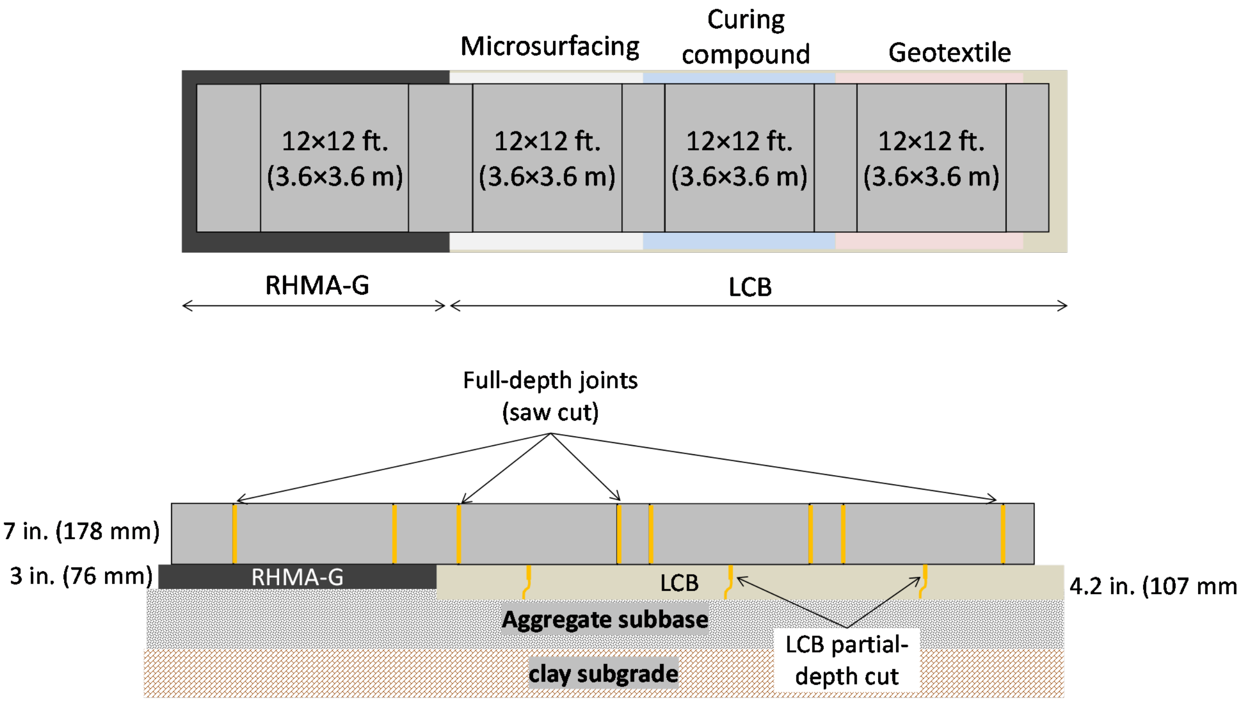

Figure 2.1: Test track layout.

The instrumentation installed in each of the four sections, shown in Figure 2.2, focuses on measuring the response to the ambient environmental loading. The instrumentation of each slab includes the following:

- Two thermocouple rods for measuring the temperature profile in the slab and base
- Three pairs of GeoKon 4200 vibrating wire strain gauges (VWSG) located at the center of the slab and at two corners, with each pair consisting of one VWSG positioned 1.0 in. (25 mm) from the top of the slab and another VWSG positioned 1.0 in. (25 mm) from the bottom

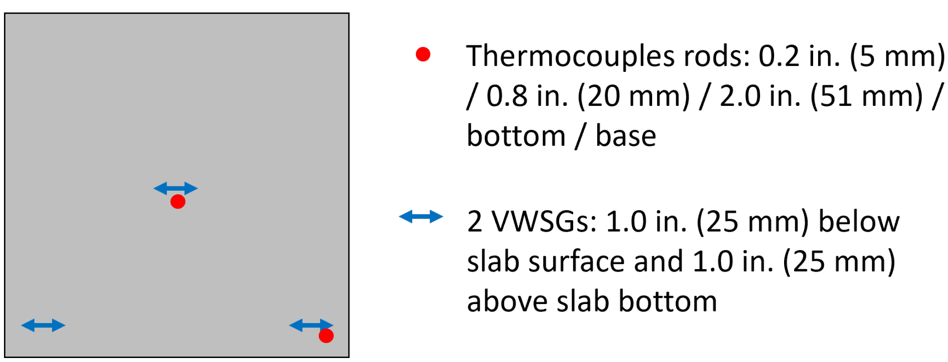

Figure 2.2: Test section instrumentation layout.

Sensor data were collected by a Campbell Scientific data acquisition system located next to the test sections. The data were collected every 10 minutes, starting before the construction of the concrete slabs. The different test track sections are listed in Table 2.2. The short names are used in several figures throughout this report.

Table 2.2: Test Track Section Short Names

Base	Interlayer	Section Short Name
Rubberized hot mix asphalt–gap-graded (RHMA-G)	None	RHMA
Lean concrete base (LCB)	Microsurfacing	MIC
	Curing compound	CC
	Geotextile	GEO

2.4 Methodology for Laboratory Testing of JPCP Asphalt Concrete Bases

A methodology for laboratory testing of JPCP asphalt concrete bases was proposed. To develop the testing methodology, the following three questions are addressed:

(1) What are the goals of the JPCP base?

(2) What are the base material properties required to accomplish the goals?

(3) How do we measure each property in the laboratory, considering the material is asphalt concrete?

Questions 1 and 2 are addressed in Section 2.4.1, while Question 3 is addressed in Section 2.4.2.

2.4.1 The Goals of the JPCP Base and the Required Base Material Properties

The following are goals of the JPCP base and the corresponding required material properties:

- Goal 1: Help JPCP slabs carry traffic loading.

  To achieve Goal 1, the following properties are required for the JPCP base:

  - High stiffness under rapid loading (~10 Hz)
  - Capacity to remain bonded to the concrete slab (relevant to thin slabs)

  While the thickness of the base is important to resist traffic loading, it is not included in the list as it is not a material property.

- Goal 2: Absorb hygrothermal movements of the concrete slabs while imposing minimum slab restraint and preventing slab-base separation, the “cushion effect” (see slab-base separation in Figure 1.2).

  To achieve Goal 2, the following properties are required for the JPCP base:

  - Low stiffness under slow loading (<0.001 Hz)
  - Capacity to deform (without damage and/or cracking) under slow loading (<0.001 Hz)
  - Capacity to remain bonded to the concrete slab

- Goal 3: Help traffic load transfer between slabs (shown in Figure 2.3).

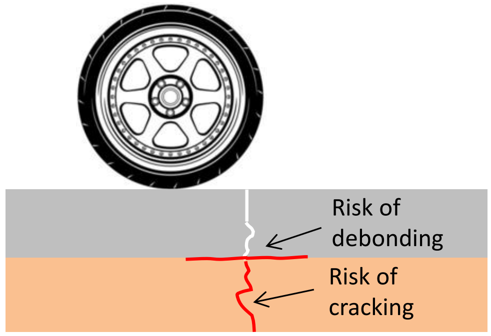

Figure 2.3: Base contributing to transferring traffic load between slabs.

To achieve Goal 3, the following properties are required for the JPCP base:

- ○ High stiffness under rapid loading (~10 Hz)
- ○ Erosion resistance
- ○ Fatigue resistance (relevant to thin slabs with undoweled joints)
- ○ Capacity to remain bonded to the concrete slab (relevant to thin slabs with undoweled joints)

- Goal 4: Resist construction traffic without raveling or rutting.

  To achieve Goal 4, the following properties are required for the JPCP base:

  - ○ Early-age rutting/raveling resistance

- Goal 5: Long-term structural and material integrity of the JPCP base.

  To achieve Goal 5, the following are required properties of the JPCP base where the properties are classified by the main actions that may jeopardize the long-term integrity of the base:

  - ○ Traffic:
    - ▪ Erosion resistance
    - ▪ Fatigue resistance (relevant to thin slabs with undoweled joints; related to load transfer between slabs)
  - ○ Slabs curling/warping:
    - ▪ Capacity to deform without cracking under slow loading (<0.001 Hz)
  - ○ Water:
    - ▪ Erosion resistance
    - ▪ Resistance to water-induced damage
  - ○ Chemical reactions:
    - ▪ Resistance to material-related distresses (e.g., resistance to sulfate attack and alkali-silica reaction for bases treated with portland cement; not relevant to asphalt bases)

The required properties and the corresponding goals, listed above, are noted in the matrix presented in Table 2.3.

Table 2.3: Required Properties of the JPCP Base and Corresponding Goals

Property	Goals[a]				
	1	2	3	4	5
High stiffness under rapid loading (~10 Hz)	Required		Required		
Capacity to remain bonded to the concrete slab	Required	Required	Required		
Low stiffness under slow loading (<0.001 Hz)		Required			
Capacity to deform under slow loading (<0.001 Hz)		Required			Required
Erosion resistance			Required		Required
Fatigue resistance (relevant to thin slabs with undoweled joints)			Required		Required
Early-age rutting/raveling resistance				Required	
Resistance to water-induced damage					Required
Resistance to material-related distresses					Required

[a] The following are the details of each JPCP base goal: (1) Goal 1: Help JPCP slabs to resist traffic loading, (2) Goal 2: Absorb hygrothermal movements of the concrete slabs while imposing minimum slab restraint and preventing slab-base separation, the "cushion effect," (3) Goal 3: Help traffic load transfer between slabs, (4) Goal 4: Resist construction traffic without raveling or rutting, and (5) Goal 5: Long-term structural and material integrity.

2.4.2 Selected Laboratory Testing Procedures for JPCP Asphalt Concrete Bases

In the list of required material properties for a JPCP base shown in Table 2.3, one of the properties, fatigue resistance, is only applicable to thin slabs, which are not part of the scope of this study and therefore not specifically addressed in this study. In addition, while early-age rutting/raveling resistance is critical for constructability, asphalt concrete is known to be able to resist construction traffic as soon as it cools down to ambient temperatures. Consequently, no specific test for the evaluation of early-age rutting/raveling resistance was performed in this study.

The following required properties are relevant to JPCP asphalt concrete bases:

- High stiffness under rapid loading (~10 Hz)
- Low stiffness under slow loading (<0.001 Hz)
- Capacity to deform without cracking under slow loading (<0.001 Hz)
- Capacity to remain bonded to the concrete slab
- Erosion resistance
- Resistance to water-induced damage

Each of these properties and the selected testing procedures are discussed in the following sections.

2.4.2.1 High Stiffness Under Rapid Loading

A standardized test, AASHTO T 378-22, for measuring the stiffness of asphalt concrete under rapid (traffic) loading already exists. This test was selected for this study. The dynamic modulus testing includes a frequency sweep conducted at different temperatures.

For this study, the following test conditions were applied:

- Frequency range: 0.1 to 25 Hz

- Temperatures: 40°F, 70°F, 100°F, and 130°F (4°C, 21°C, 38°C, and 54°C)

The test specimens were cylinders, 4 in. (100 mm) in diameter and 6 in. (150 mm) in height, cored and trimmed from larger cylinders prepared with the gyratory compactor at the UCPRC laboratory.

2.4.2.2 Low Stiffness Under Slow Loading

A standardized test for measuring the stiffness of asphalt concrete under tensile slow loading, below 0.001 Hz, does not exist. The mechanism that puts the asphalt base in tension is explained in Section 1.1 and shown in Figure 1.2 (right). The loading must be tensile to represent the slabs pulling up the base that is bonded to them as they curl/warp due to the hygrothermal actions, shown in the figure. The laboratory loading must be slow to represent the diurnal (within a day), seasonal, and long-term changes in the curvature of the JPCP slabs. The diurnal changes in the slab curvature, mainly associated with thermal changes, have a loading frequency in the order of 10^{-5} Hz (one day has 86,400 seconds; frequency is the inverse, which is 1.16×10^{-5}). The changes in slab curvature from the seasonal variation in drying shrinkage occur at an even slower frequency.

A test was developed for this study to evaluate the tensile stiffness of asphalt concrete subjected to slow tensile loading. The test is referred to as the "hanging test" as the specimen is hung from a loading frame and the loading is applied by a dead weight hanging from the specimen (Figure 2.4 and Figure 2.5). The asphalt concrete strain is measured by three linear variable differential transformer (LVDT) sensors, 120 degrees apart, fixed to the specimen. The test is conducted in a temperature-controlled room.

Figure 2.4: Hanging test.

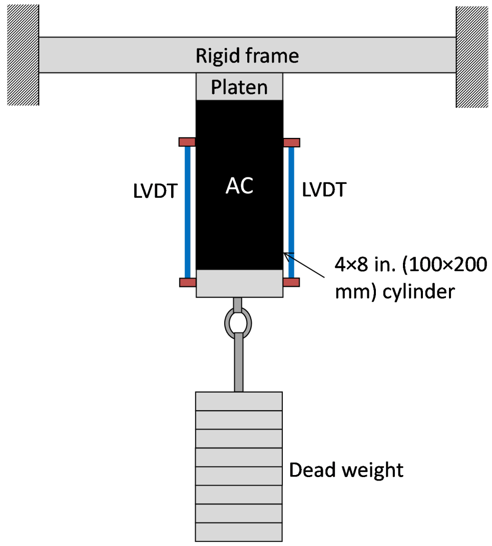

Figure 2.5: Hanging test layout.

The load applied to the specimen, the weight of the steel plates plus the weight of the specimen, is constant. Consequently, the measured strain normalized by the applied stress is the creep compliance of the material.[2]

An example of the LVDT readings and the corresponding asphalt strain in the hanging test is shown in Figure 2.6. The asphalt strain was calculated as the average of the three LVDT readings divided by the LVDT span. The asphalt strain divided by the applied stress (1 psi [7 kPa] in the example) is the creep compliance of the material (Equation 2.1). Finally, a power function ($D_1 \times t^n$, where D_1 and n are the fitting parameters and t is time in seconds) was fitted to the creep compliance data (Figure 2.7).

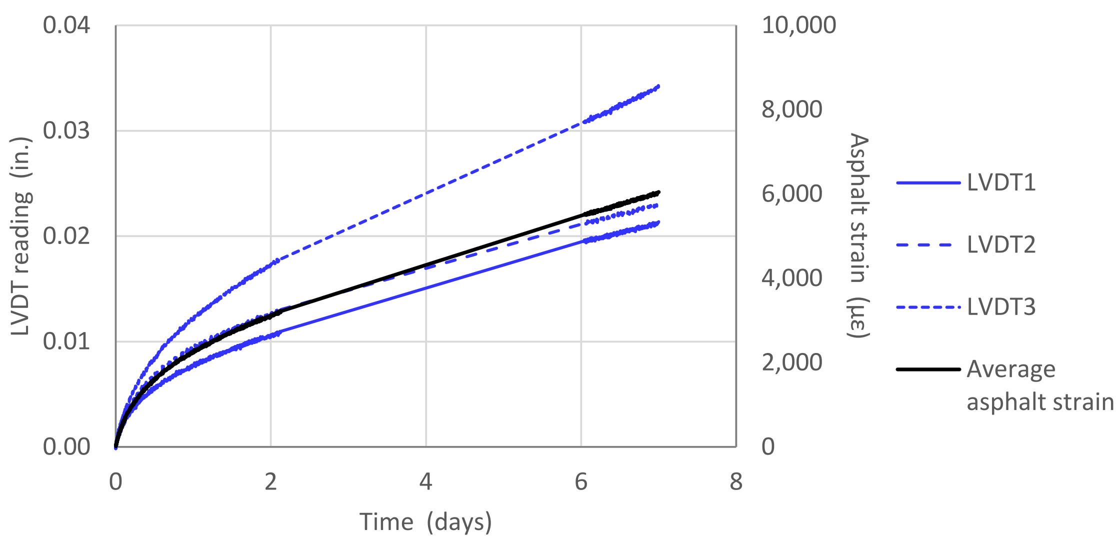

Note: Test tensile stress: 1 psi (7 kPa).

Figure 2.6: Hanging test measurements example (HMA).

[2] In viscoelasticity, the creep compliance is defined as the strain variation under constant unit stress; its units are stress^{-1}.

$$Creep\ compliance(t)\ = \frac{Asphalt\ strain(t)}{Stress} \tag{2.1}$$

Where:

Stress = constant tensile stress applied in the test

t = time

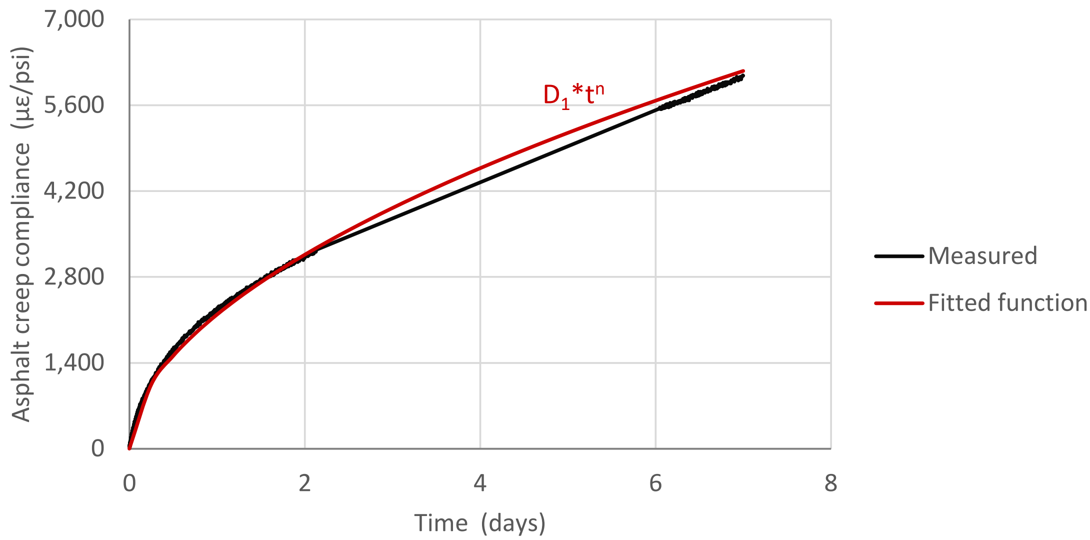

Note: Raw data are shown in Figure 2.6.

Figure 2.7: Fitting power creep function to the measured creep compliance.

The weight of the steel plates was determined through a trial-and-error process with the goal of obtaining around 10,000 με (in the asphalt concrete specimen) within 7 days. The 10,000 με (1%) limit was selected to prevent cracking of the asphalt concrete specimen. These criteria for selecting the weight, along with the test temperature, were chosen to provide results in a practical timeframe while capturing the stiffness with the slowest possible loading rate.

In this study, the following test conditions were applied:

- Test duration: 7 days
- Target strain: 10,000 με in 7 days (steel plates' weight chosen accordingly to achieve around 10,000 με in 7 days)
- Temperature: 77°F (25°C)

The test specimens are similar to those used in the dynamic modulus test with the Asphalt Mixture Performance Tester (AMPT) device: cylinders with a 4 in. (100 mm) diameter and 6 in. (150 mm) height, cored and trimmed from larger cylinders prepared with a gyratory compactor.

2.4.2.3 Capacity to Deform Without Cracking Under Slow Loading

The capacity of the asphalt concrete to deform in tension without presenting damage and/or cracking was evaluated using a universal testing machine (UTM). This test consists of deforming the asphalt mix at a constant rate, whereas the hanging test previously described measures deformation under a constant stress. Specifically designed for this research study, this test is referred to as the "UTM-ramp test" in this report. The UTM-ramp test involves applying a constant displacement rate on an asphalt concrete cylindrical specimen until failure (Figure 2.8 and Figure 2.9). The displacement rate causes the specimen to reach around 4% average strain (top versus bottom) within three hours. This 4% strain target is such that the cracking of the specimen is almost certain to occur, while the three-hour duration is practical enough to allow testing two specimens per day. The goal is to test the specimen as slowly as possible to mimic the deformation imposed by the hygrothermal actions, while keeping the test practical in terms of time. The asphalt concrete strain is measured using three LVDT sensors positioned 120 degrees apart and fixed to the specimen. The fixtures used are the same as those used in the AMPT testing.

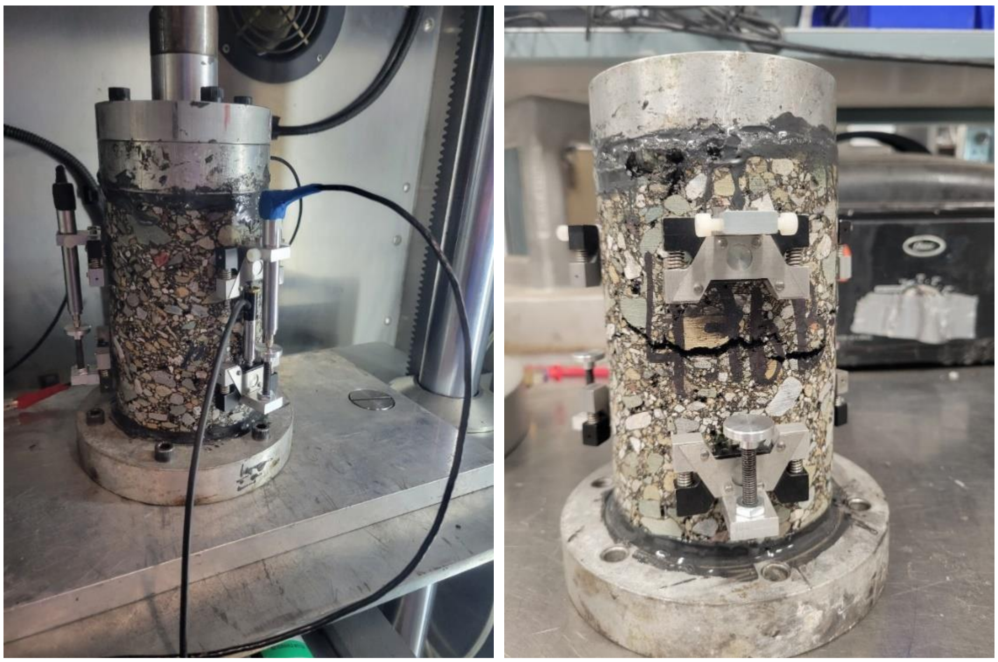

Figure 2.8: UTM-ramp test specimen before testing (left) and specimen cracked after testing (right).

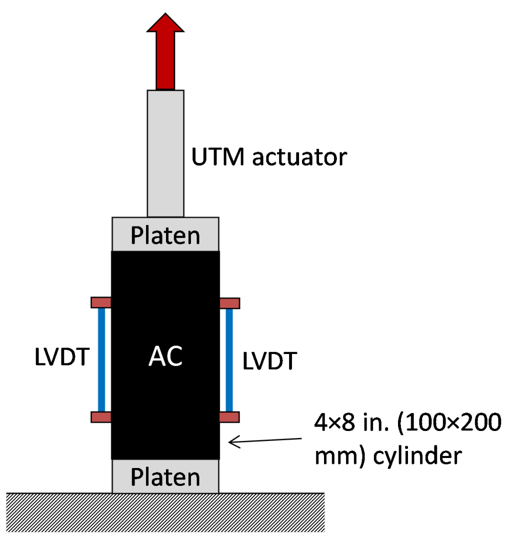

Figure 2.9: UTM-ramp test layout.

In this study, the following test conditions were applied:

- Test duration: three hours
- Target displacement rate: 2×10^{-5} in./sec (5×10^{-4} mm/sec) (for a specimen 6 in. (150 mm) in height, this displacement rate produces a 3.6% average strain in three hours)
- Temperature: 77°F (25°C)

The test specimens are AMPT type: cylinders, 4 in. (100 mm) in diameter and 6 in. (150 mm) in height, cored and trimmed from bigger cylinders prepared with the gyratory compactor.

An example of the applied force and LVDT readings in the UTM-ramp test is shown in Figure 2.10. The force increases at the beginning of the test as the displacement increases. Then, due to the damage produced in the asphalt concrete, the force rate decreases and eventually zeroes out and becomes negative (at around 2,000 seconds in the example).

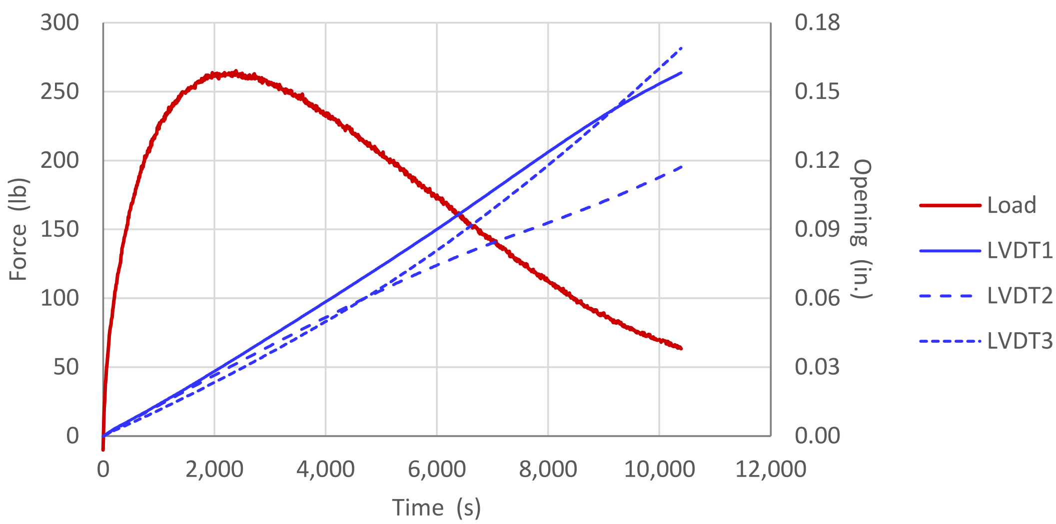

Figure 2.10: UTM-ramp test measurements example (HMA).

The analysis of the collected data was conducted as follows (Figure 2.11 and Figure 2.12):

- The imposed strain (ε) is calculated from the three LVDT readings (average of the three LVDT readings divided by the LVDT span).
- The predicted viscoelastic stress (σ_{ve}) is calculated under the assumption that the asphalt concrete specimen does not suffer any damage during the test. The σ_{ve} is defined by the convolution integral, shown in Equation 2.2. A numerical version of the equation was programmed in Excel.

$$\sigma_{ve}(t) = \int_0^t D(t-\tau) \cdot d\varepsilon(\tau) \quad \textbf{(2.2)}$$

Where:

ε = the imposed strain

D = creep compliance of the asphalt concrete determined from the hanging test ($D_1 \times t^n$)

t = time

- The σ_{ve} is scaled to match the measured stress at the beginning of the test when the asphalt damage is negligible. The scaling is required for two main reasons. The first reason is to account for specimen-to-specimen variability. The creep compliance function is obtained as the average of several specimens tested in the hanging test, and it is not determined on the very same specimen tested in the UTM-ramp test. The second reason is to account for non-linearities in the material, as the stress levels in the two tests (hanging and UTM-ramp) differ from each other. The resulting stress is referred to as scaled viscoelastic stress ($S\sigma_{ve}$), calculated using Equation 2.3.

$$S\sigma_{ve}(t) = k \cdot \sigma_{ve}(t) \quad \textbf{(2.3)}$$

Where:

k = constant

σ_{ve} = predicted viscoelastic stress

t = time

- The separation between $S\sigma_{ve}$ and the applied stress (σ_{UTM}) as the test progresses indicates damage in the asphalt concrete. The applied stress (σ_{UTM}) is the force applied by the UTM divided by the specimen cross-sectional area. Figure 2.11 shows a comparison of the applied stress series versus the scaled viscoelastic stress series. In this study, the damage is characterized as the specimen integrity (I), calculated using Equation 2.4.

$$I(t) = \frac{\sigma_{UTM}(t)}{S\sigma_{ve}(t)} \quad \textbf{(2.4)}$$

Where:

σ_{UTM} = applied stress

$S\sigma_{ve}$ = scaled viscoelastic stress

t = time

- The final step is plotting the specimen integrity (I) versus the imposed strain (ε), shown in Figure 2.12. The relationship between I and ε can be used to evaluate the asphalt concrete's capacity to resist slow tensile deformations without cracking (the higher the specimen integrity, the higher the capacity). The relationship between I and ε can also be used to rank mixes and calibrate damage models for FEM analysis.

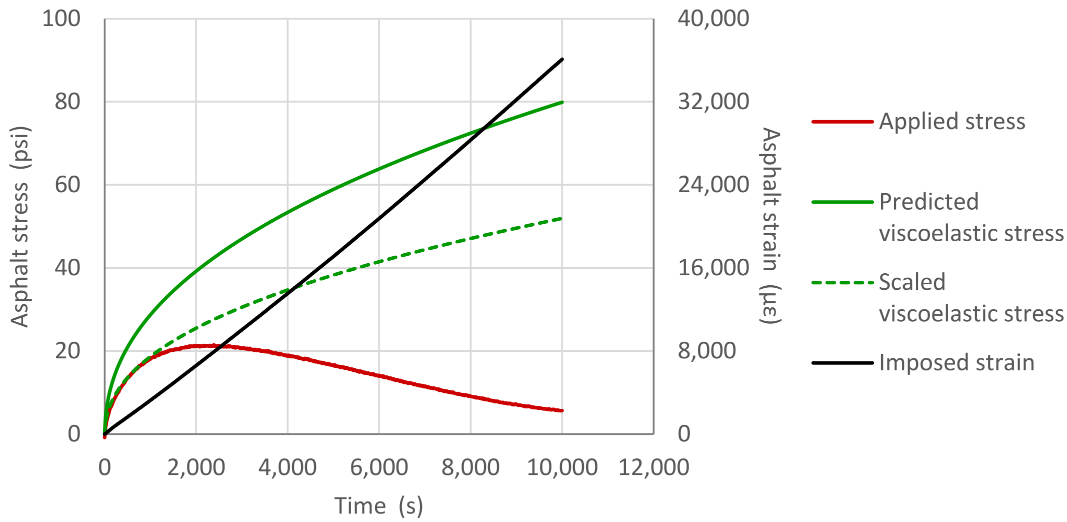

Note: Raw data are shown in Figure 2.10.

Figure 2.11: Example of analysis of UTM-ramp test results (part 1).

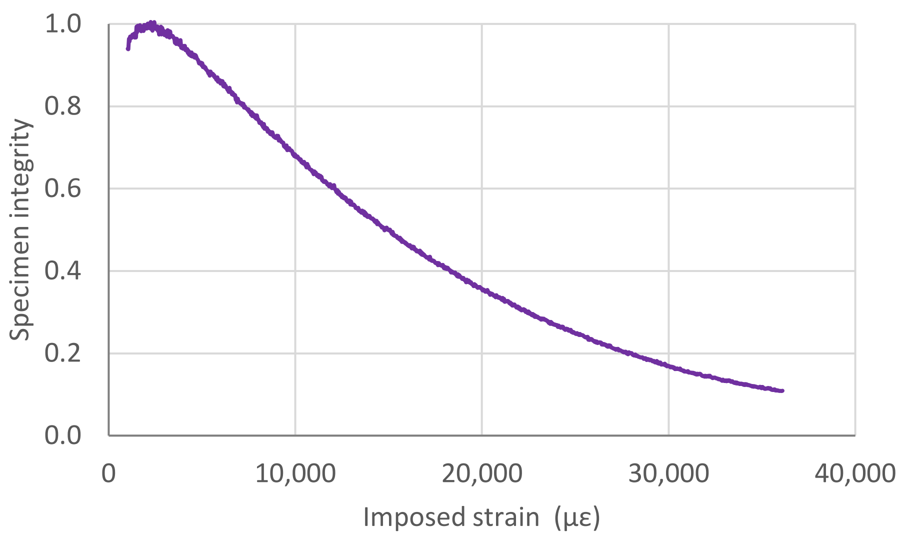

Note: Raw data are shown in Figure 2.10.

Figure 2.12: Example of analysis of UTM-ramp test results (part 2).

2.4.2.4 Capacity to Remain Bonded to the Concrete Slab

The capacity of the asphalt base to remain bonded to the concrete slab is relevant for different reasons. For short-jointed plain concrete pavements (thin slabs), which are not the focus of this study, the bonding helps slabs resist traffic loading (Section 2.4.1, Goal 1) and transfer traffic loads across transverse joints (Section 2.4.1, Goal 3). For JPCP, the bonding helps to absorb hygrothermal movements of the concrete slabs (Section 2.4.1, Goal 2). If the slabs separate from the base as they curl/warp, they function as cantilever slabs rather than as slabs supported by a multilayer structure. Consequently, traffic loading applied close to or at the joints would produce considerable tensile stresses at the top of the slabs, potentially leading to top-down cracking (Figure 1.2, left).

Currently, there is no established test or methodology to evaluate the capacity of the asphalt base to remain bonded to the concrete slab and very little is known about the slab-base bonding performance. Based on Caltrans PPRC Project 4.58B*,* the curling/warping of the slabs plays a main role in the bonding performance, most likely more important than traffic loading *(3)*. Therefore, this research study evaluates only the capacity of the asphalt concrete to remain bonded to the concrete slabs as they curl/warp (slow loading). Traffic-related stresses and moisture damage were not considered. While this approach entails a considerable simplification of the real phenomenon, it is regarded as valid for the goals pursued in this research.

The capacity of the asphalt concrete to remain bonded to the concrete slab under slow loading was evaluated by conducting the UTM-ramp test on composite specimens (concrete cast on top of asphalt). The only differences between testing the material and testing the bonding are the type of specimen and the LVDT arrangement. The three LVDTs are placed so that they bridge the concrete-asphalt base interphase as shown in Figure 2.13. The main outcome from this test is the location of the failure and whether it occurs at the interphase (bond failure) or in the asphalt concrete base. The findings reported later in Section 5.1 note that the failure occurred in the asphalt concrete base for all composite specimens tested in this study (concrete on HMA and concrete on RHMA-G).

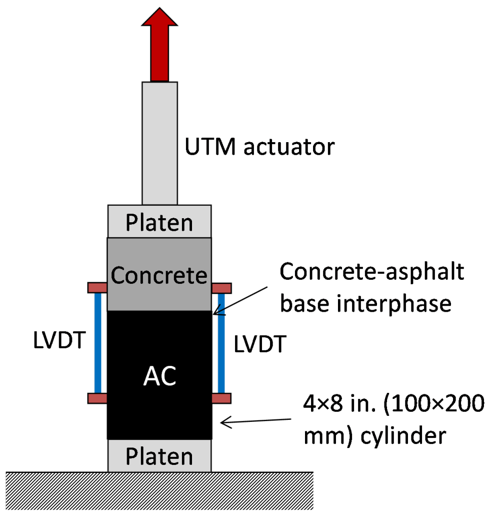

Figure 2.13: Composite specimen UTM-ramp test layout.

The analysis of the test data was conducted in the same manner as the UTM-ramp test on homogeneous asphalt concrete specimens (previously explained). The only difference is that the LVDT span used to calculate the imposed strain (ε) is just the asphalt portion of the LVDT span. For composite specimens, the strain ε represents the average strain of the asphalt concrete base and the concrete-asphalt base interphase. Other than this factor, the data analysis is identical to that of the homogeneous asphalt concrete specimens. Each test is summarized as a curve of specimen integrity (I) versus imposed strain (ε).

The I-ε curves obtained for the composite specimens can be compared with the curves obtained for the homogeneous asphalt concrete specimens. The similarity between both sets of curves would be an indication of good bonding between the concrete and the asphalt concrete base. The opposite conclusion would be reached if the set of I-ε curves of the composite specimens lies below (lower I for the same ε) the set of curves of the homogeneous asphalt concrete specimens.

The composite specimens can be prepared by casting the concrete on asphalt gyratory cylinders. The top surface of the gyratory cylinder must be uncut to mimic the concrete-asphalt interphase in JPCP construction. The composite specimens can also be prepared by casting the concrete on an asphalt slab, prepared with a rolling wheel compactor, segmented compactor, or other similar compactor, and then coring the cylindrical specimens afterward. The preferred method, and the one used in this study, is casting the concrete on asphalt slabs prepared with the rolling wheel compactor. The reason why this is the preferred method is that the rolling wheel compactor is also the compaction method used in the field, and, consequently, it should produce a realistic asphalt surface. It is recommended that at least 28 days pass between casting the concrete and testing the composite specimen.

2.4.2.5 Erosion Resistance

A widely accepted test for measuring the erosion resistance (or erodibility) of a JPCP base material does not exist. For example, *AASHTOWare Pavement ME Design* defines the erosion resistance of the base by the "erodibility class," ranging from 1 to 5, which is selected as a function of the material type (1 for very erodible materials like untreated subgrade soils; 5 for highly erosion-resistant materials like lean concrete or HMA), but no test is recommended. The erodibility class is used for faulting calculations in *AASHTOWare Pavement ME Design*.

In this research study, the erosion resistance of the base was tested with a Hobart mixer following the approach in ASTM D7196-18. In this test, a cylindrical specimen is subjected to a rotating rubber hose that exerts an abrasion force on the specimen for a preset period (Figure 2.14). The loss of material is calculated by comparing the pre- and post-test dry weights of the specimen. While this test was conceived for measuring the early-age traffic raveling resistance of emulsified asphalt, it is considered applicable to asphalt concrete materials.

Figure 2.14: Erosion test on HMA.

The conditioning of the asphalt concrete specimens differed from ASTM D7196-18. Since the erosion of the base is expected to occur mainly in the presence of water, the specimens must be wet-conditioned for the erosion test. The wet conditioning was conducted in this study with the Moisture-Induced Stress Tester (MiST) device (Figure 2.15), following ASTM D7870-20.

Figure 2.15: MiST device: specimens added to the chamber (left), chamber filled with water (center), and ongoing test (right).

In the MiST conditioning, the asphalt specimen is submerged in water inside a pressure chamber, which is immediately set to high temperature, 122°F to 140°F (50°C to 60°C); then the specimen inside the chamber is subjected to 3,500 water pressure cycles. Each cycle consists of a one-second-long pressure pulse of 40 psi (280 kPa). The MiST is intended to simulate the pore pressure induced in a wet pavement by the passing/moving traffic loading.

In this study, the following test conditions were applied:

- MiST conditioning temperature: 140°F (60°C) (this is the temperature prescribed in ASTM D7870-20 for mixes with asphalt binder high PG above 60°C) and is intended to accelerate moisture damage
- Specimen conditioning before the erosion test (right after MiST): two hours in water at 77°F (25°C)
- Erosion test time: 15 minutes

The test specimens were 6 in. (150 mm) diameter cylinders prepared with the gyratory compactor. The specimen height was 1.8 in. (70 mm).

2.4.2.6 Resistance to Water-Induced Damage

The resistance to water-induced damage of asphalt concrete has been traditionally evaluated by the AASHTO T283 test. In this test, two sets of asphalt specimens are tested for indirect tensile strength. The first set is dry, while the second set is water-saturated (70% to 80% saturation) and subjected to a freeze cycle followed by a warm bath at 140°F (60°C) for 24 hours before the strength testing. The strength of the second set (wet) and the comparison versus the strength of the first set (dry) provide an indication of the resistance of the asphalt concrete to water-induced damage, focusing on damage to the chemical bonding between the asphalt and aggregate, which is called “adhesive” damage.

Some concerns have been raised about the AASHTO T283 test, in particular its ability to simulate the asphalt "cohesive" damage induced by water pressure pulses developed under traffic loading *(16)*. The water pressure pulses may result in an emulsification process that weakens the bond between asphalt binder molecules; this process cannot be reproduced by the static nature of AASHTO T283 wet conditioning. The MiST conditioning was developed to overcome this limitation, which is why the MiST includes water pressure pulses rather than a simple water bath.

The MiST conditioning was selected for this study (instead of the AASHTO T283 test) since the long-term moisture resistance of the asphalt concrete base is critical to JPCP performance. Further, instead of determining only the indirect tensile strength of the two sets of specimens (dry and wet), the IDEAL cracking tolerance (IDEAL-CT) test was conducted, following ASTM D8225-19. The IDEAL-CT test provides not only the indirect tensile strength but also the failure energy and other parameters, including the cracking tolerance index (CT_{Index}), that can be used to evaluate the mechanical properties of the asphalt concrete.

In this study, the following test conditions were applied:

- MiST conditioning temperature: 140°F (60°C)
- Specimen conditioning before the IDEAL-CT test (right after MiST): two hours in water at 77°F (25°C)
- IDEAL-CT test conducted according to ASTM D8225-19

The test specimens were cylinders 6 in. (150 mm) in diameter and 2.5 in. (62 mm) in height, prepared with the gyratory compactor.

2.5 Preliminary Considerations for Developing a Methodology for Testing Interlayers

The methodology presented in Section 2.4 is applicable to asphalt concrete to be used as the base of a JPCP pavement. It is not directly applicable to interlayers to be used between the JPCP slab and a rigid base like lean concrete. While a methodology for laboratory testing of such interlayers is not available yet, some considerations regarding the role of the slab-rigid base interlayer and the testing requirements include the following:

- From the structural point of view, the goal of the interlayer is not to resist traffic loading but to provide the bond between the slab and the rigid base so that the two work together to resist bending under traffic loading. The structural capacity of two bonded layers is higher than the sum of the structural capacity of the two independent layers. The bonding is particularly relevant to thin slabs.
- The "cushion" to absorb hygrothermal movements of the concrete slabs while imposing minimum slab restraint and preventing slab-base separation must be provided by the interlayer rather than the rigid base. In other words, the deformation capacity of the interlayer-rigid base system relies almost exclusively on the interlayer. As the interlayer is much thinner than the typical asphalt base, the deformation requirements (capacity to deform without cracking) are much more demanding for the interlayer than for the asphalt base.
- The requirements for erosion resistance are the same for the interlayer as for the asphalt base.
- The requirements for resisting construction traffic without raveling are the same for the interlayer as for the asphalt base.

- The requirements for long-term structural and material integrity are the same for the interlayer as for the asphalt base, with the added challenge of the higher deformations induced by the hygrothermal movements of the slabs. The resistance to moisture-induced damage is as critical for the interlayer as it is for the asphalt base or even more critical because water will come through concrete joints and get trapped at the interphase.

2.6 Asphalt Concrete Specimen Preparation in the Laboratory

All asphalt concrete specimens evaluated in this research study were prepared from mixes fabricated in a plant. The plant-produced (field) mix was sampled in metal buckets and stored at room temperature until it was reheated for preparing the specimens in the laboratory. No short-term oven aging conditioning was applied to the mix as the plant mix is already short-term aged. The plant mix reheating (to fabricate test specimens) was conducted as follows:

(1) The metal buckets were heated with the lid on for four hours at either 275°F (135°C) for HMA or 302°F (150°C) for RHMA-G.

(2) The heated mix was split from the buckets into pans and immediately moved to an oven set to the compaction temperature. The compaction temperature was 286°F (141°C) for HMA and 320°F (160°C) for RHMA-G.

(3) The mix in the pans was kept in the oven at the compaction temperature for one to two hours before being used for specimen preparation.

No mid-term or long-term oven aging was applied to the loose mix or to the asphalt concrete specimens. This is not regarded as a limitation as the aging expected under the concrete pavement in the field is negligible, mainly because of the absence of high temperatures due to the thermal insulation produced by the concrete layer. The lab testing was conducted between a minimum of two weeks and a maximum of two months, with the period counted from specimen preparation.

3 TEST TRACK CONSTRUCTION

The test track is located at the Davis, California, site of the UCPRC. The aggregate subbase, prepared using material purchased to meet Caltrans C2 aggregate base specifications, was constructed by the UCPRC team in April 2022. The construction of the remaining layers is presented in chronological order in the following discussion.

3.1 Construction of the Lean Concrete Base

The lean concrete was supplied by an Elite Ready Mix plant located 45 miles (72 km) from the test track site, and it was placed and consolidated by the paving contractor (Vanguard) on May 6, 2022 (Figure 3.1). The lean concrete used for the test track construction is a material commonly used in Caltrans JPCP bases. Its design and construction followed Caltrans Std. Specs. Section 28. Some details of the LCB material design are described in Section 2.1. Lean concrete specimens were prepared from a fresh mixture sampled during the construction and tested in the laboratory (results presented in Section 5.2).

The LCB on the test section was cured following Caltrans specifications, which prescribe two applications for curing compound spray, beginning immediately after the construction of the LCB:

- First spray: 1 gal./150 ft^2 (0.27 L/m^2) (Figure 3.2)
- Second spray (within 4 days after construction): 1 gal./200 ft^2 (0.20 L/m^2)

The curing compound was ASTM C309 Type 2B (white pigmented, resin-based). The curing compound used for LCB curing was the same as the bond breaker in the curing compound part of the test sections (see Figure 2.1) and also the curing compound used for curing the PLCC. The LCB was saw-cut approximately every 20 ft (6.1 m), matching the mid-slab locations shown in Figure 2.1. The saw-cut depth was 1.4 in. (36 mm), one-third of the LCB thickness (Figure 3.3).

Figure 3.1: Lean concrete base (LCB) construction.

Figure 3.2: Curing compound application on lean concrete base (LCB).

Figure 3.3: Lean concrete base (LCB) partial depth saw-cut.

3.2 Construction of the RHMA-G Base

The RHMA-G was supplied by a local plant (Teichert), located 25 miles (40 km) from the test track site, and placed and compacted by a local contractor (Helmers and Sons) on May 6, 2022 (Figure 3.4). The 1/2 in. nominal maximum aggregate size of the RHMA-G used for the test track construction is the material commonly used as a 1.5 to 2.4 in. (45 to 60 mm) thick surface overlay in Caltrans asphalt pavements. Its design and construction followed Caltrans Std. Specs. Section 39. Some details of the RHMA-G material design are described in Section 2.1.

Loose mix was sampled in buckets during the construction and stored indoors at room temperature. The sampled mix was used for the fabrication of specimens for laboratory testing (test results shown in Section 5.1).

Figure 3.4: RHMA-G paving.

3.3 Construction of the Interlayers

3.3.1 Curing Compound Interlayer

The curing compound interlayer was applied to the LCB the day before the concrete paving. Following Caltrans Std. Specs. Section 36-2, “Base Bond Breaker,” it consisted of a spray of 0.12 gal./yd^2 (0.54 L/m^2) of ASTM C309 curing compound. The compound was ASTM C309 Type 2B (white pigmented, resin-based). The section with the curing compound bond breaker before PLCC paving is shown in Figure 3.5.

Figure 3.5: Section with curing compound bond breaker before portland limestone cement concrete (PLCC) paving.

3.3.2 Geotextile Interlayer

The geotextile was selected and placed following Caltrans Std. Specs. Section 36-2, “Base Bond Breaker” and Section 96-1.02Q, “Geosynthetic Bond Breaker.” It consisted of a nonwoven polypropylene geosynthetic, 14.7 oz./yd^2 (500 g/m^2). The section with the geotextile bond breaker before PLCC paving is shown in Figure 3.6.

Figure 3.6: Section with geotextile bond breaker before portland limestone cement concrete (PLCC) paving.

3.3.3 Microsurfacing Interlayer

The microsurfacing was produced and placed by VSS International on May 20, 2022. The paving operation is shown in Figure 3.7, and the finalized interlayer (microsurfacing on top of the LCB) is shown in Figure 3.8. The material used for the test track construction is a microsurfacing commonly used for street paving applications in central California. Its design and construction followed the Caltrans Std. Specs. Section 37-3, “Slurry Seals and Micro-Surfacings,” Type II gradation. Some details of the microsurfacing material design are shown in Section 2.2. The amount of microsurfacing applied to the section, based on the paver metering system, divided by the actual surface of the paved area resulted in a dose of 15.7 lb./yd^2 (8.5 kg/m^2). For a density of 100 lb./ft^3 (1600 kg/m^3), the average microsurfacing thickness is 0.2 in. (5 mm).

Figure 3.7: Microsurfacing paving.

Figure 3.8: Lean concrete base (LCB) with microsurfacing on top.

3.4 Construction of the Concrete Slabs

PLCC was used for building the slabs. The PLCC was supplied by a local plant, CEMEX, located 25 miles (40 km) from the test track site, and placed and consolidated by the UC Davis Transportation and Parking Services concrete masonry construction crew on June 6, 2022 (Figure 3.9). The PLCC used for the test track construction was based on an existing design with Type II cement, developed by CEMEX, that is frequently used for JPCP paving in California. The Type II cement was replaced by Type IL (portland limestone cement) in the mix design. The PLCC design and construction followed Caltrans Std. Specs. Section 40, "Concrete Pavement," and Section 90, "Concrete." Some details of the PLCC material design are described in Section 2.3.

Figure 3.9: Portland limestone cement concrete (PLCC) construction.

The PLCC was consolidated using a vibrating roller screed and finished with a trowel. No surface texturing was applied. The curing was conducted with a white pigmented, resin-based curing compound that meets ASTM C309 Type 2B specifications and was applied at a nominal rate of 1 gal./150 ft^2 (0.27 L/m^2) (Figure 3.10). Three ready-mix truckloads were used in the construction of the slabs. The slump and the air content of the fresh concrete, measured in each of the three trucks, varied from 5.5 to 6.0 in. and from 2.3% to 3.6%, respectively. The concrete was not air-entrained. PLCC cylindrical specimens and beams were prepared during construction, cured, and tested in the laboratory (results are shown in Section 5.3). The transverse joints (see the location of transverse joints in Figure 2.1) were sawed full depth once the PLCC had hardened enough to resist cutting without spalling (Figure 3.11).

Figure 3.10: Curing compound application on portland limestone cement concrete (PLCC).

Figure 3.11: Full-depth cutting of transverse joints on portland limestone cement concrete (PLCC).

4 TEST TRACK MONITORING

This chapter reviews the test track monitoring results, including the curling and warping of the slabs and FWD evaluations.

4.1 Slabs Curling/Warping

The slabs were instrumented with VWSGs to measure strain due to hygrothermal actions, including drying shrinkage and thermal effects. The instrumentation layout is shown in Figure 2.2. The strain sign criterion adopted in this study indicates that positive values signify expansion and negative values signify contraction.

A “field setting time” of four hours, measured from the ready-mix truck batching, has been adopted as a reference for strain calculation (with strain set to zero at the field setting time). This four-hour timeframe is based on the set time testing according to ASTM C403. The fresh mixture was sampled during the construction and tested following ASTM C403. The initial set time, corresponding to a penetration resistance of 500 psi (2.45 MPa), was three hours and 25 minutes, while the final set time, corresponding to a penetration resistance of 4,000 psi (27.6 MPa), was four hours and 30 minutes from the ready-mix truck batching. The field setting time of four hours is halfway between the initial (start) and final (end) set times.

The strain data collected by the VWSG sensors in the slabs were used to calculate the mean and differential strains, ε_{mean} and ε_{diff}, respectively. The strain ε_{mean} is the average of the strain measured at the top and bottom of the slab, quantifying overall slab expansion/contraction. The strain ε_{diff} is the difference between the strain measured at the top and bottom of the slab, quantifying slab curling/warping. The ε_{mean} and ε_{diff} calculation formulas are shown in Figure 4.1.

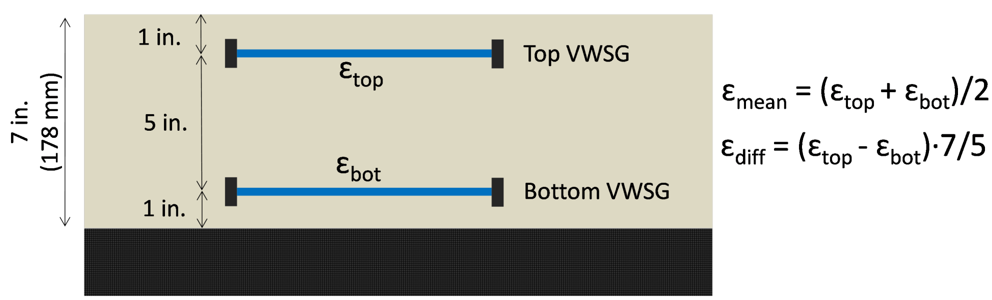

Figure 4.1: Calculation of ε_{mean} and ε_{diff}.

The strains measured at the corners were analyzed in this report. At the corners, little restriction to slab expansion/contraction and curling/warping was present, regardless of the base and interlayer type; consequently, no section-to-section differences are expected. The average of all VWSG (two instrumented corners per section, four sections) at the top and bottom of the slabs was used to calculate ε_{mean} and ε_{diff}.

The strains ε_{mean} and ε_{diff} throughout the evaluation period presented in this report (June 2022 to September 2023) are shown in Figure 4.2. The negative sign of ε_{mean} indicates slab contraction, while the negative sign of ε_{diff} indicates that the curvature of the slabs is concave upward. The mean strain reached values as low as -700 με (contraction), while the differential strain reached values as low as 600 με. Both ε_{mean} and ε_{diff} presented strong seasonal variation: ε_{mean} reached the minimum values (maximum contraction) during the winter due to low temperatures, while ε_{diff} reached the minimum values (maximum concave upward curvature) during the summer due to high differential drying shrinkage (the top of the slab dries more than the bottom).

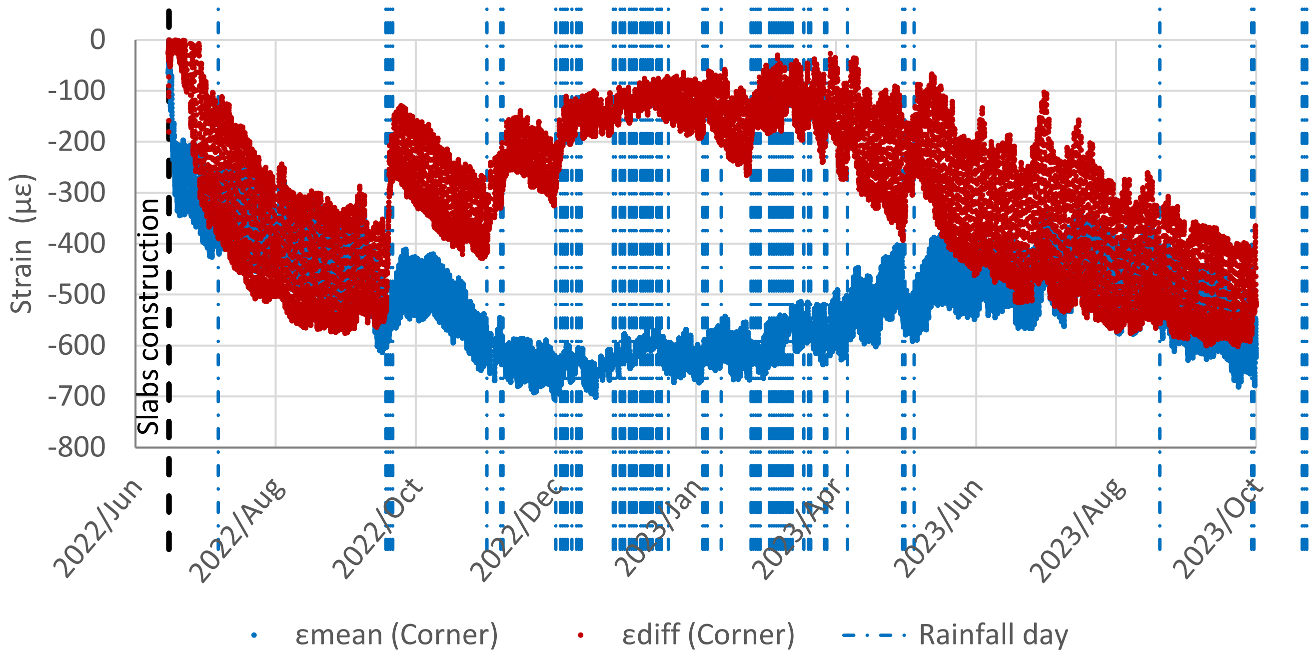

Figure 4.2: Strains ε_{mean} and ε_{diff} at the corner of the slabs.

Figure 4.3 shows an example of the diurnal variations of the strain and temperature. In this figure, the parallel between the variation of ε_{mean} and the variation of T_{mean} (average of slab top and bottom temperatures) can be seen. The same applies to variations of ε_{diff} and T_{diff} (difference between the slab top and bottom temperatures).

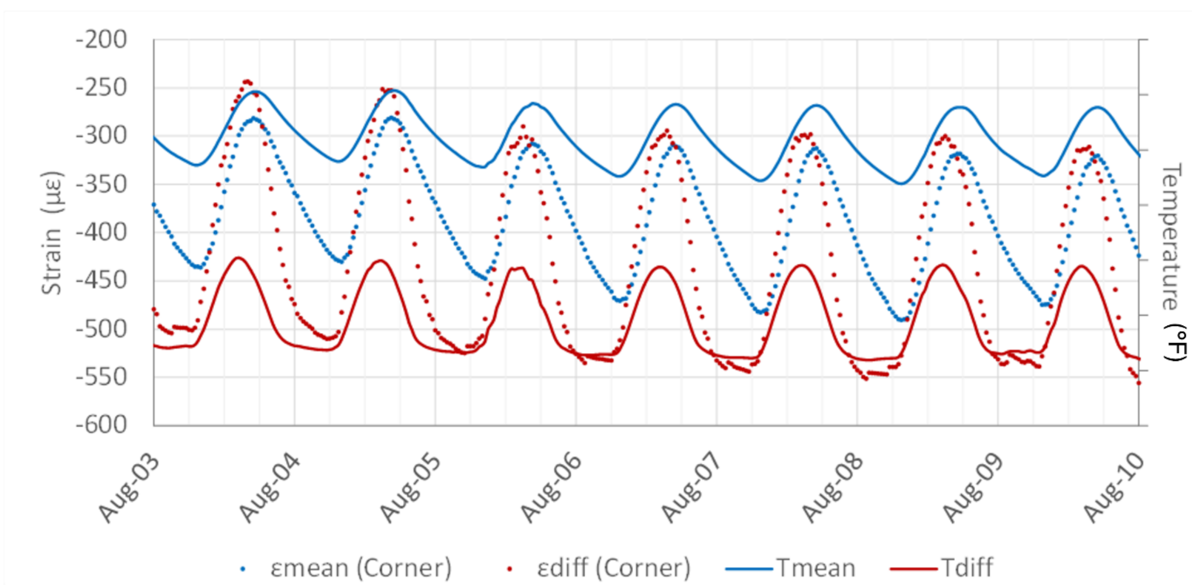

Notes: T_{mean} is the average of the top and bottom of the slab temperatures; T_{diff} is the top minus bottom of the slab temperatures.

Figure 4.3: Example of diurnal variation of strain and temperature at the corners of the slabs.

The curvature of the slabs is expected to impact the deflections measured at the corner under the FWD loading. As a corner lifts up due to the curvature (curling and warping), the slab loses support below the corner and, consequently, the deflection produced by the FWD loading increases. While this is expected to impact all sections regardless of the base type and interlayer, the magnitude of the impact is expected to be different from one section to another. The impact is presented in Section 4.2.

4.2 Falling Weight Deflectometer Deflections

The sections were periodically evaluated with the FWD. The goal of the FWD evaluations was to determine how the corner deflection changes versus the curvature of the slab and how the change varies from section to section. The type of base and interlayer is expected to play a main role in the relationship between slab curvature and corner deflection. In this study, the curvature of the slabs is quantified as ε_{diff}.

Six FWD evaluations were conducted (Table 4.1). In each of the six FWD evaluations, each slab was tested at the center and corners (Figure 4.4) twice a day (morning and afternoon). The curvature of the slabs varied considerably from one evaluation to another and also from morning to afternoon (see ε_{diff} seasonal and diurnal variation in Figure 4.2 and Figure 4.3, respectively). Three load levels were applied: 6.7 kips, 11.2 kips, and 15.7 kips (30 kN, 50 kN, and 70 kN).

Table 4.1: Falling Weight Deflectometer Evaluations

FWD Evaluation	Date
1	June 28, 2022
2	August 19, 2022
3	November 10, 2022
4	February 2, 2023
5	June 28, 2023
6	September 20, 2023

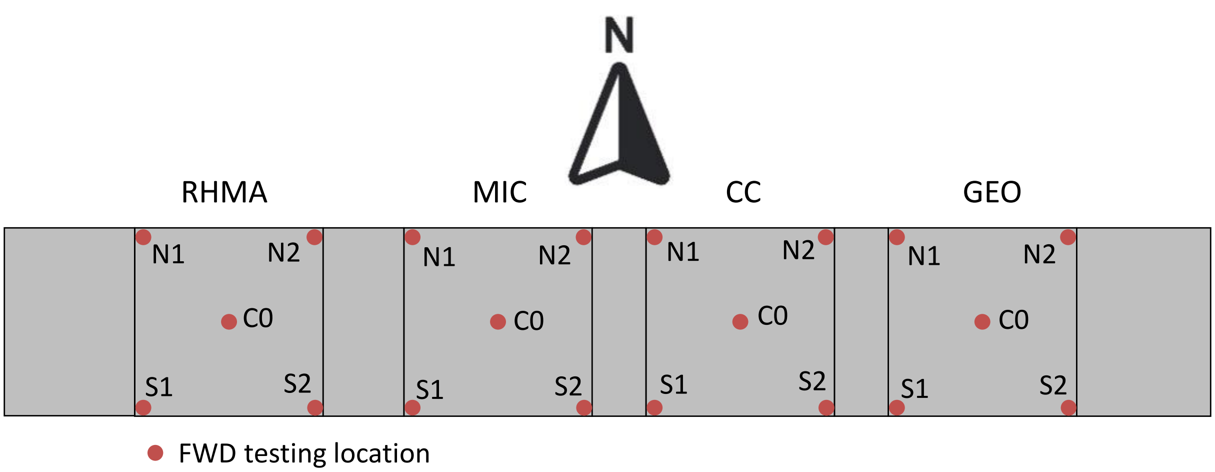

Figure 4.4: FWD evaluation locations.

For example, the deflections measured in the section with curing compound during Evaluation 2, conducted on August 19, 2022, are shown in Figure 4.5. The lower deflection at the center (C0) of the slab, compared with the deflections at the corners (S1, S2, N1, and N2), is evident in the figure. Additionally, the higher corner deflection in the morning (Replicate 1), when the temperature difference causes the most concave curling, is contrasted with the afternoon (Replicate 2), when the concave curling is least pronounced. The greater curling occurs in the morning because the top of the slab is cooler and more contracted than the bottom of the slab; conversely, the opposite is true in the afternoon. The fact that there is still a concave shape in the afternoon is due to the warping caused by lower humidity and the corresponding greater drying shrinkage at the surface of the concrete compared with its bottom. The approximately linear increase in corner deflections up to the highest load indicates that the corners do not deflect downward enough to make full contact with the LCB. If the FWD load was sufficient to cause the corner of the slab to come into full contact with the LCB, it would be expected that the deflection would increase at a lower rate with increasing load for that and all greater loads *(13)*. Considerable corner-to-corner variability is also evident in Figure 4.5.

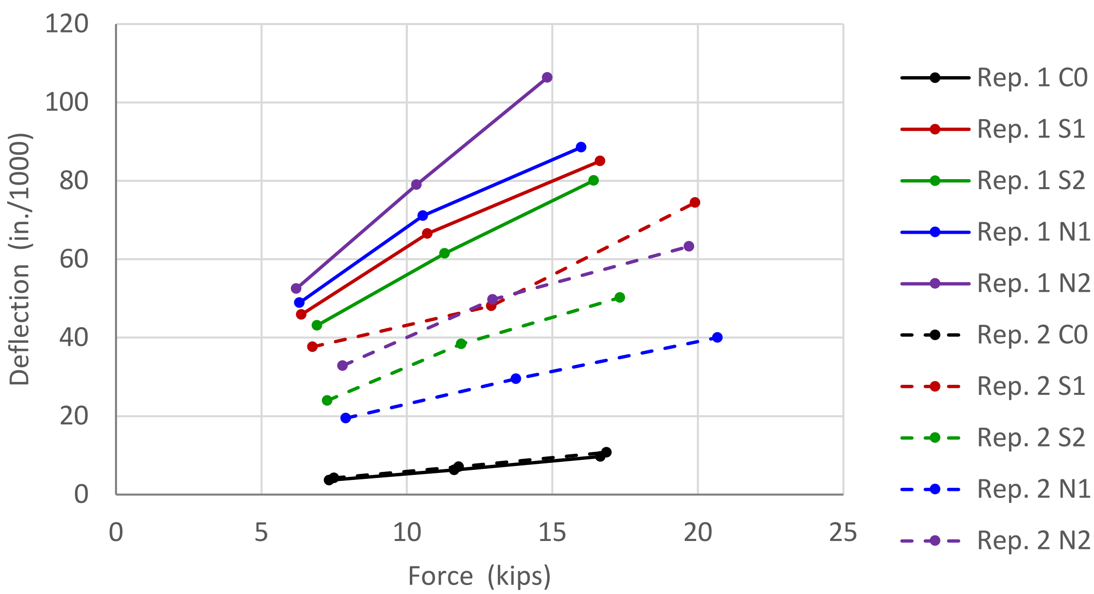

Notes: Replicate 1 (Rep. 1) is conducted in the morning; Rep. 2 in the afternoon. C0 location is slab center; N1 (north 1), N2 (north 2), S1 (south 1), and S2 (south 2) locations are slab corners; see locations in Figure 4.4.

Figure 4.5: Example of FWD evaluation at the section with curing compound; FWD Evaluation 2 (August 19, 2022).

The corner deflection varied considerably between the four sections, the six evaluations, and the replicates (Replicate 1 in the morning and Replicate 2 in the afternoon). This outcome can be inferred from Figure 4.6 and Figure 4.7. Figure 4.6 shows the deflections for the FWD Evaluation 1, conducted on June 28, 2022, Replicate 2 (afternoon), where relatively low corner deflections were measured. In contrast, Figure 4.7 shows the deflections for the FWD Evaluation 2, conducted on August 19, 2022, Replicate 1 (morning), where relatively high corner deflections were measured.

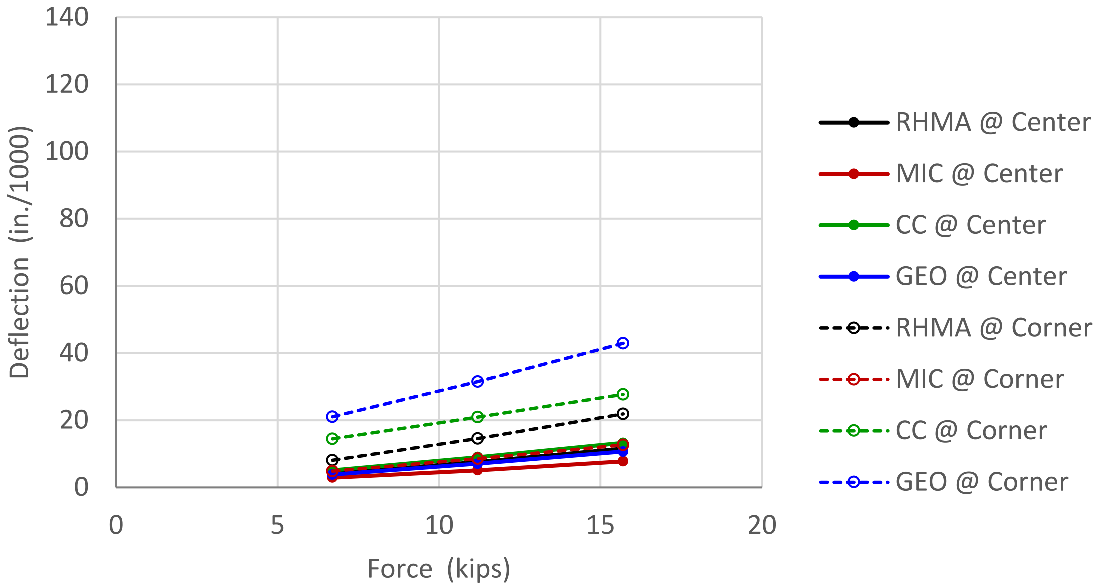

Note: The sections with LCB and interlayers are referred to as MIC (microsurfacing), CC (curing compound), and GEO (geotextile).

Figure 4.6: Center and corner deflections in different sections; FWD Evaluation 1 (June 28, 2022), Replicate 2 (afternoon).

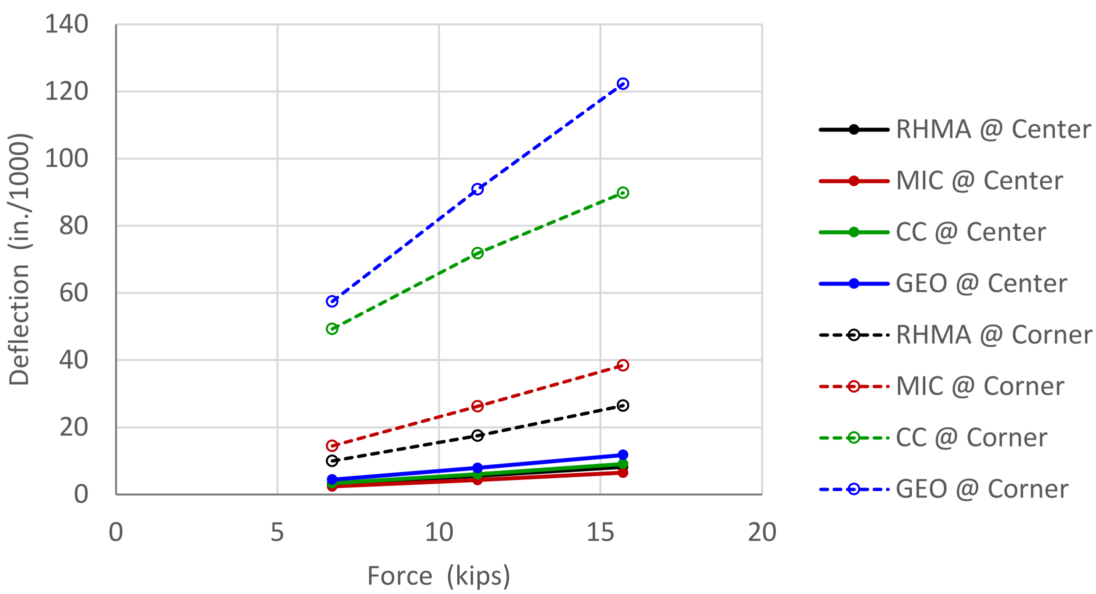

Note: The sections with LCB and interlayers are referred to as MIC (microsurfacing), CC (curing compound), and GEO (geotextile).

Figure 4.7: Center and corner deflections in different sections; FWD Evaluation 2 (August 19, 2022), Replicate 1 (morning).

According to the hypothesis formulated in the introduction and depicted in Figure 1.2, the large variations in corner deflection between evaluations and between replicates (morning versus afternoon) within the same section are due to differences in the curvature of the slabs. In order to test this hypothesis, a single load level was selected (15.7 kips [70 kN]), and the corner deflections (average of four corners per section) were plotted versus ε_{diff} (slab curvature measured with VWSG), shown in Figure 4.8. The negative sign of ε_{diff} indicates that the slabs are curled concave upward (nighttime-type curvature). As the figure shows, the corner deflections for each section condense into a single line when plotted versus ε_{diff}. This outcome supports the aforementioned hypothesis. Several conclusions can be extracted from Figure 4.8:

- While the deflection at the center of the slab remains stable versus ε_{diff} and varies little from section to section, the deflection at the corner changes considerably versus ε_{diff} and from one section to another.
- As expected, the corner deflection increases as the magnitude of ε_{diff} increases.
- The relationship between corner deflection and ε_{diff} strongly depends on the type of base and interlayer.
- The corner deflection in the section with LCB and curing compound interlayer increases versus ε_{DIFF} much more than in the section with RHMA-G base. In the summer evaluations, the corner deflection in the section with LCB and curing compound is up to three times larger than the corner deflection in the section with RHMA-G base. This outcome corresponds with the poorer cracking performance of JPCP with LCB compared with JPCP with asphalt concrete base.
- The geotextile did not improve, but rather diminished, the performance of the section with curing compound interlayer in terms of the reduction of corner deflections.
- The section with microsurfacing interlayer considerably improved the deflection performance of the section with curing compound interlayer. In fact, the corner deflection in the section with LCB and the microsurfacing interlayer changed little versus $\varepsilon_{diff,}$ and it was similar to the corner deflection in the section with RHMA-G base.

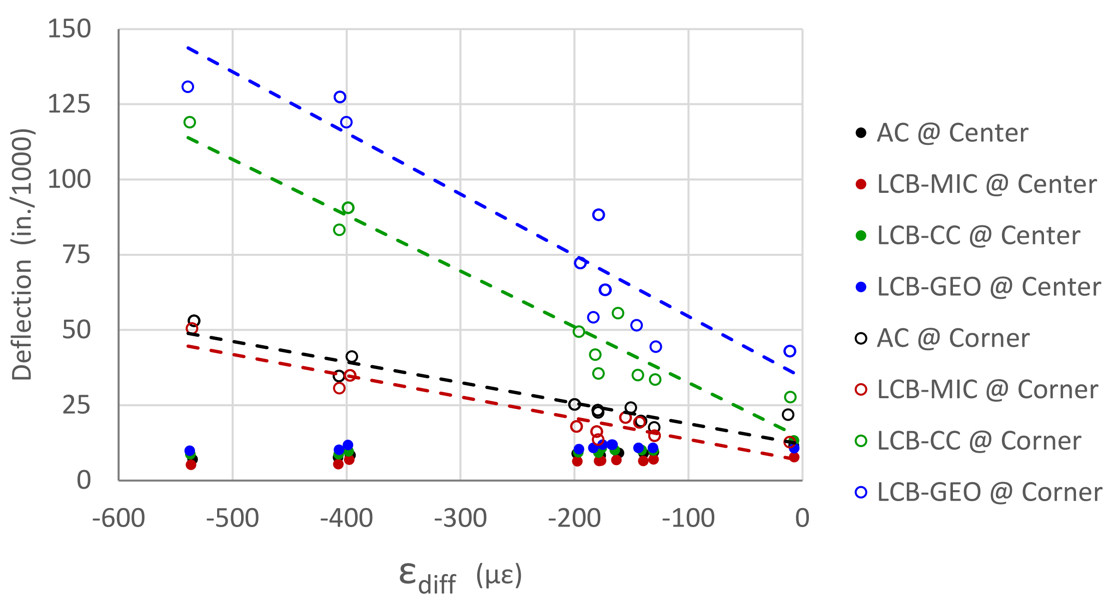

Note: The sections with LCB and interlayers are referred to as MIC (microsurfacing), CC (curing compound), and GEO (geotextile).

Figure 4.8: Summary of FWD evaluations at 15.7 kips (70 kN) loading.

5 LABORATORY TESTING OF BASE MATERIALS AND CONCRETE

This chapter reviews the laboratory testing results for the HMA, RHMA-G, LCB and PLCC specimens.

5.1 Testing of Hot Mix Asphalt and Rubberized Hot Mix Asphalt–Gap-Graded

Loose mix was sampled in metal buckets during the construction of the test track, and the buckets were stored at room temperature. Then, the specimens were produced and tested in the laboratory, as described in the following discussion. No oven aging was applied to the loose mix or the prepared specimens. All specimens were compacted at 7% air-void content with a tolerance of ±0.5%.

5.1.1 Stiffness Under Rapid Loading

The stiffness of the asphalt concrete mixes was measured by conducting the axial dynamic modulus testing following AASHTO T 378-22. The testing was conducted at four temperatures: 40°F, 70°F, 100°F, and 130°F (4°C, 21°C, 38°C, and 54°C), applying sinusoidal loading with a frequency of 0.1 to 25 Hz. Testing details are included in Section 2.4.2.1.

The results of the axial dynamic modulus testing were fitted with a sigmoidal master curve, considering the time-temperature superposition principle, shown in Equation 5.1 and Equation 5.2.

$$log(E) = \delta + \frac{\alpha}{1+e^{\beta+\gamma \cdot log(f_{red})}} \quad \textbf{(5.1)}$$

Where:

E = axial dynamic modulus

δ, α, β, and γ = fitting parameters

f_{red} = reduced frequency

$$f_{red} = f \cdot a_T \quad \textbf{(5.2)}$$

Where:

f = frequency

a_T = time-temperature shift factor; a_T is assumed to depend on temperature as follows:

$$log\,(a_T) = \beta_T \cdot (T - T_{Ref})$$

Where:

T = test temperature

T_{Ref} = master curve reference temperature, 68°F (20°C)

β_T = fitting parameter

The master curves of the two asphalt concrete mixes are shown in Figure 5.1. As expected, the stiffness of the HMA is higher than the stiffness of RHMA-G for intermediate and high reduced frequencies. The opposite occurs at low reduced frequencies.

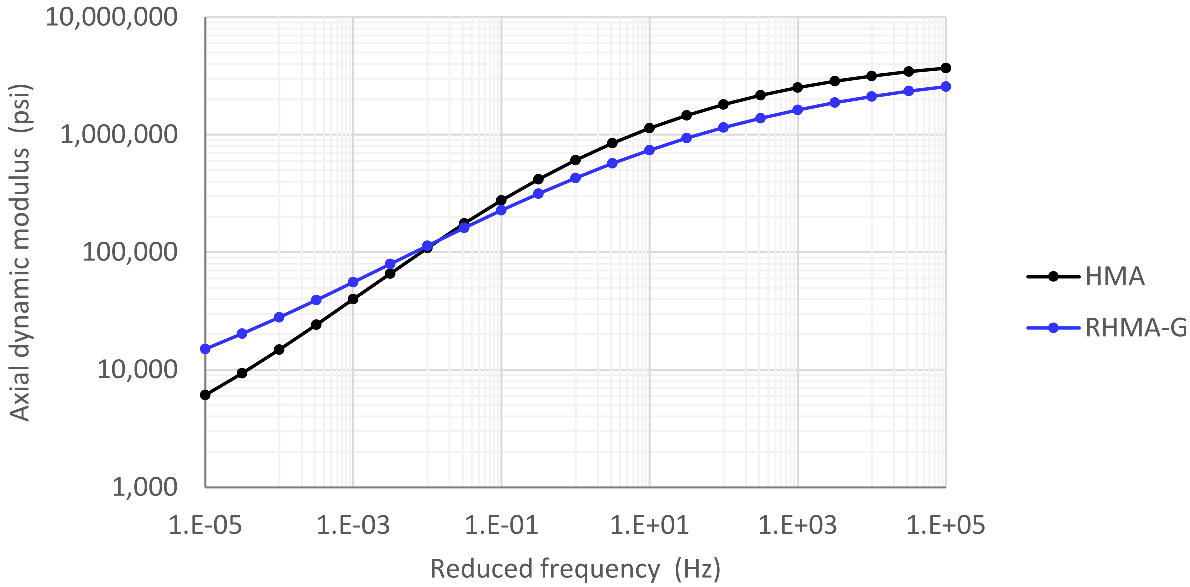

Figure 5.1: Dynamic modulus of the asphalt concrete mixes at 68°F (20°C).

5.1.2 Stiffness Under Slow Loading

The stiffness of the asphalt concrete mixes under slow loading was measured by conducting the hanging test at a temperature of 77°F (25°C). The hanging test was developed for this study, and it is not included in any ASTM or AASHTO standard. Testing details and data analysis procedures are shown in Section 2.4.2.2. The outcome of the hanging test is the tensile creep compliance (strain under constant stress) of the asphalt concrete. The creep compliance data were fitted with a power function, shown in Equation 5.3, and were demonstrated in Figure 2.7.

$$Creep\ compliance(t) \ = D_1 \cdot t^n \tag{5.3}$$

Where:

D_1 and n = fitting parameters

t = time

The creep compliance of the two asphalt concrete mixes is shown in Figure 5.2. As shown in this figure, the creep compliance of the RHMA-G is lower than the creep compliance of the HMA (for the time range captured in the hanging test), indicating that the RHMA-G is stiffer than the HMA for slow loading. This outcome agrees with the dynamic modulus master curve data shown in Figure 5.1, which shows that for low reduced frequency, the RHMA-G has a higher dynamic modulus than the HMA.

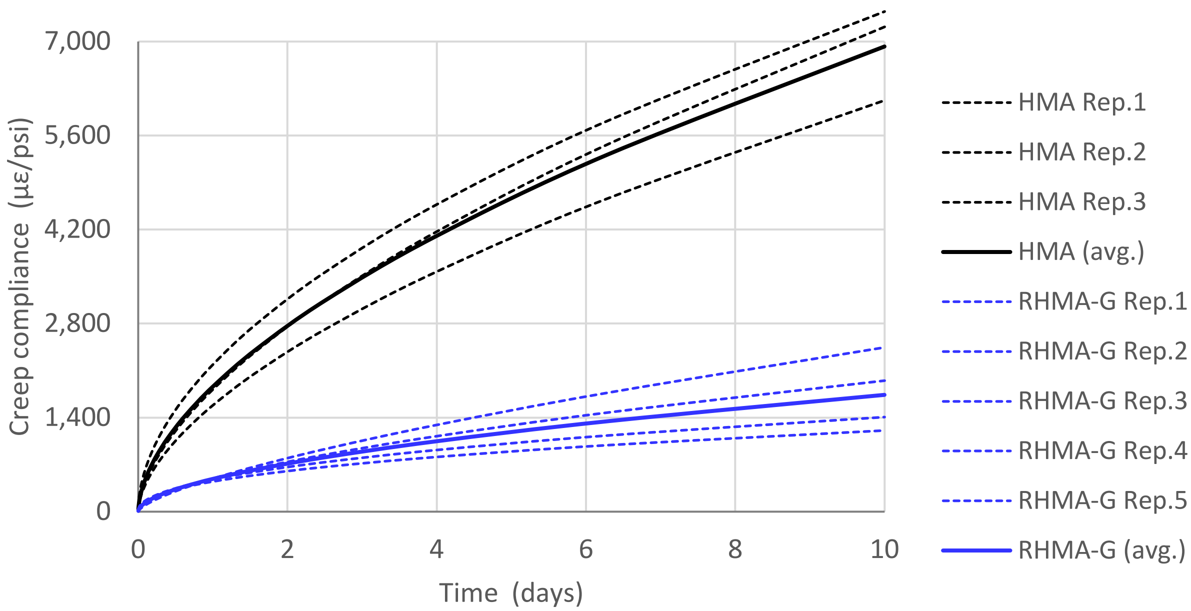

Figure 5.2: Creep compliance of the asphalt concrete mixes at 77°F (25°C) from the hanging test.

5.1.3 Capacity to Deform Under Slow Loading

The capacity of the asphalt concrete mixes to deform in tension without presenting damage and/or cracking was measured by conducting the UTM-ramp test at a temperature of 77°F (25°C). The UTM-ramp test consists of applying a constant displacement rate on an asphalt concrete cylindrical specimen until failure. The test was developed for this study, and it is not standardized in any ASTM or AASHTO specifications. Testing details and the data analysis procedure are shown in Section 2.4.2.3.

The outcome of the UTM-ramp test is the curve specimen integrity (I), defined in Equation 2.4, versus imposed strain (ε). The I-ε curves can be used to evaluate the asphalt concrete capacity to resist slow tensile deformations without cracking, with a larger difference between the curves indicating greater damage and a higher likelihood of cracking. The I-ε curves of the two asphalt concrete mixes are shown in Figure 5.3. As discussed in Section 2.4.2.3, a higher integrity indicates that the stress needed to deform the specimen in the UTM-ramp test is closer to what it would be for an undamaged specimen (an undamaged specimen has an integrity value of 1.0). As shown in the figure, the HMA specimens have higher integrity than the RHMA-G specimens for the same imposed strain, which means that the capacity to deform under slow loading with less damage and a lower likelihood of cracking is slightly better for the HMA than for the RHMA-G (i.e., better cushion effect).

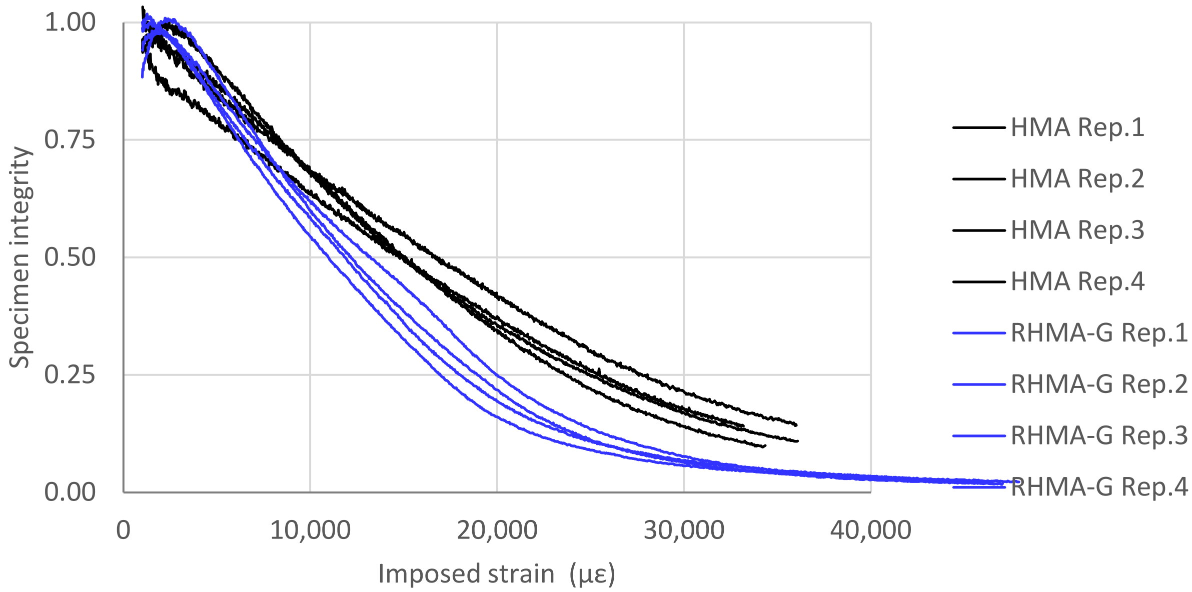

Figure 5.3: Strain capacity of the asphalt concrete mixes at 77°F (25°C).

5.1.4 Capacity to Remain Bonded to the Concrete Slab Under Slow Loading

The capacity of the asphalt concrete to remain bonded to the concrete slab under slow loading is evaluated by conducting the UTM-ramp test on composite specimens (concrete cast on top of asphalt). Testing details and data analysis procedures are shown in Section 2.4.2.4. The UTM-ramp test on composite specimens is conducted and analyzed in the same way as the UTM-ramp test on homogeneous asphalt concrete specimens. The outcome of the test is also the curve of specimen integrity (I) versus imposed strain (ε).

The comparison of the I-ε curves obtained for the composite specimens versus the curves obtained for the homogeneous asphalt concrete specimens indicates the bonding between the concrete and the asphalt concrete base. The comparison is shown in Figure 5.4 (HMA) and Figure 5.5 (RHMA-G). In both cases, the curves obtained for the composite specimens are close to the curves obtained for the homogeneous asphalt concrete specimens. This outcome indicates that the concrete-asphalt interphase is not contributing to the deformation of the composite specimen, which is an indication of good bonding between the concrete and the asphalt concrete base.

All composite specimens tested in the UTM-ramp failed in the asphalt base rather than at the concrete-asphalt interphase, shown in Figure 5.6 (HMA) and Figure 5.7 (RHMA-G). This is another outcome that indicates good bonding between the concrete and the asphalt concrete base.

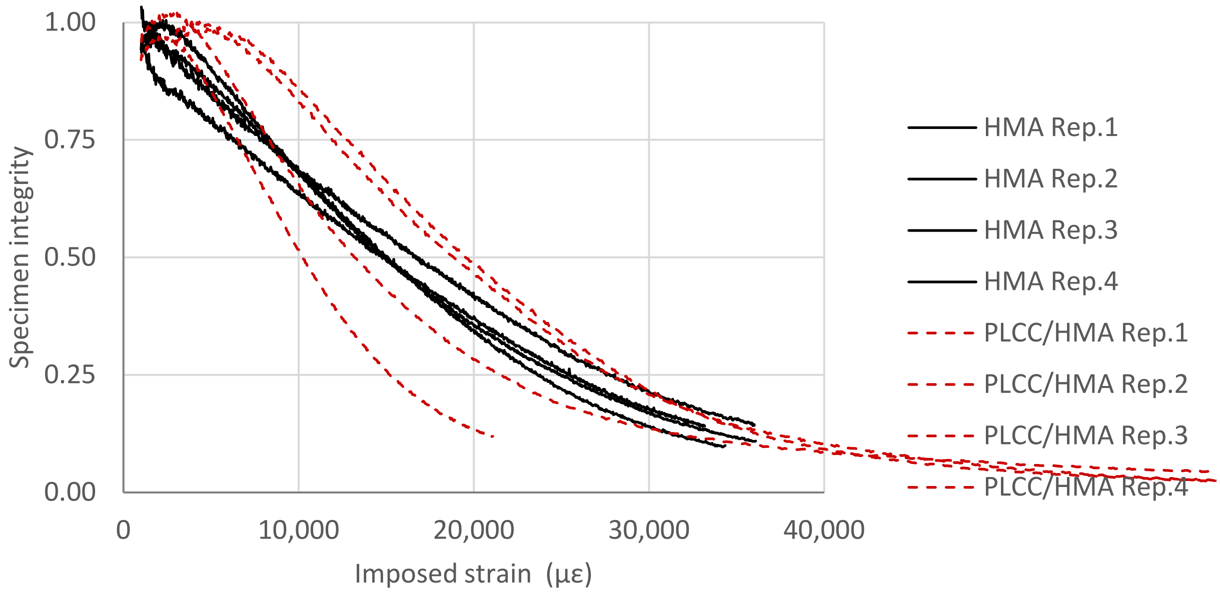

Figure 5.4: Strain capacity of the asphalt concrete mixes at 77°F (25°C): Comparison of homogeneous versus composite specimens (HMA).

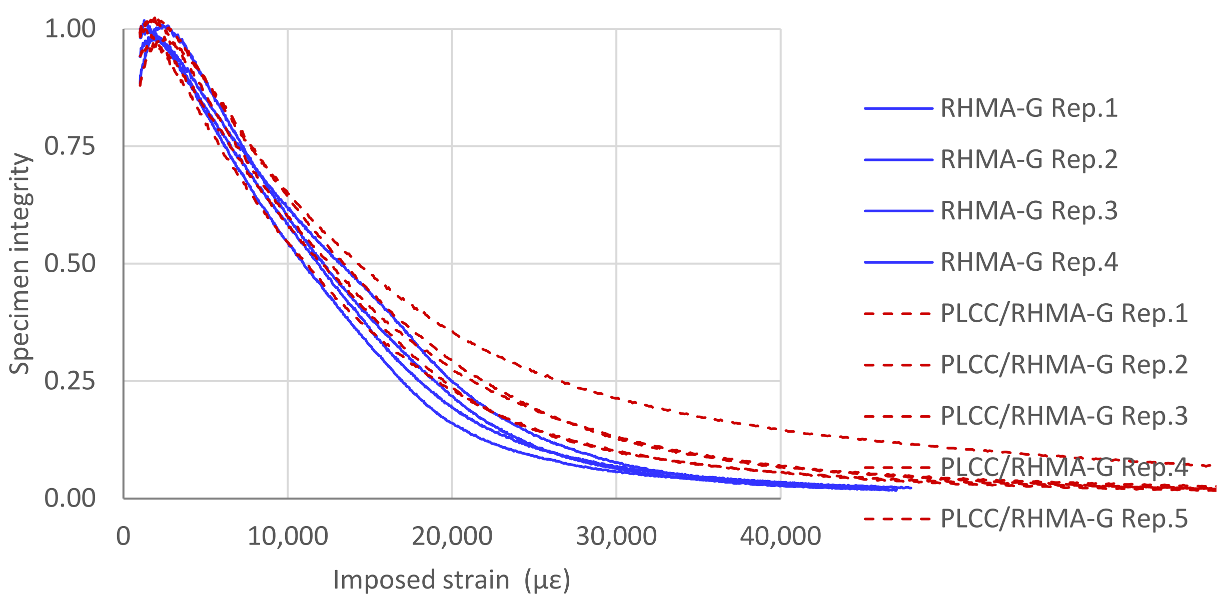

Figure 5.5: Strain capacity of the asphalt concrete mixes at 77°F (25°C): Comparison of homogeneous versus composite specimens (RHMA-G).

Figure 5.6: Composite specimens after UTM-ramp testing (PLCC on HMA).

Figure 5.7: Composite specimens after UTM-ramp testing (PLCC on RHMA-G).

5.1.5 Erosion Resistance

The erosion resistance of the asphalt concrete mixes was measured by conducting the ASTM D7196-18 erosion test on asphalt concrete specimens that had been previously subjected to MiST conditioning. In the ASTM D7196-18 erosion test, a cylindrical specimen is subjected to a rotating rubber hose that exerts an abrasion force on the specimen for a preset period of 15 minutes in this study. The MiST conditioning in this study followed ASTM D7196-18 and includes 3,500 water pressure cycles at 40 psi (280 kPa) and a high temperature of 140°F (60°C). Testing details and data analysis procedures are shown in Section 2.4.2.5.

The outcome of the erosion test is the specimen mass loss, which is determined by comparing the weight of the dry specimen before and after the test. In this study, two sets of specimens were prepared for each asphalt concrete mix. The first set was subjected to MiST conditioning exclusively, while the second set was subjected to MiST conditioning followed by the erosion test. The mass losses of the two sets for the two asphalt concrete mixes are shown in Table 5.1.

Table 5.1: Erosion Test Results

Material	Weight Loss Due to MiST (%)	Weight Loss Due to MiST + Erosion (%)
HMA	0.0	0.0
RHMA-G	0.3	0.4

As shown in Table 5.1, the mass loss is negligible for both HMA and RHMA-G mixes. These results agree with *AASHTOWare Pavement ME Design* default classification of HMA as a "highly erosion-resistant material" (class 5) (RHMA-G is not considered in *AASHTOWare Pavement ME Design*) *(10)*.

5.1.6 Resistance to Water-Induced Damage

The resistance to water-induced damage of the asphalt concrete mixes was evaluated by comparing the indirect tensile strength of asphalt concrete specimens before and after the MiST conditioning. The MiST conditioning followed ASTM D7196-18 and includes 3,500 water pressure cycles at 40 psi (280 kPa) at a high temperature of 140°F (60°C). The indirect tensile strength was measured following ASTM D8225-19, "Determination of Cracking Tolerance Index of Asphalt Mixture Using the Indirect Tensile Cracking Test at Intermediate Temperature," also known as the IDEAL-CT test. Testing details and data analysis procedures are shown in Section 2.4.2.6.

The load-displacement curves measured in the IDEAL-CT test are shown in Figure 5.8. Each of the curves in this figure is the average of three to five specimens. The IDEAL-CT test temperature is 77°F (25°C). For the two asphalt concrete mixes, the MiST conditioning resulted in a reduction of the peak strength, as expected. The retained strength ("MiSTed" versus dry), also known as the indirect tensile strength (ITS) ratio, is very high for the two mixes, 88% for the HMA and 84% for the RHMA-G (Figure 5.9). This outcome is an indication of the good long-term resistance to water-induced damage of both the tested HMA and RHMA-G.

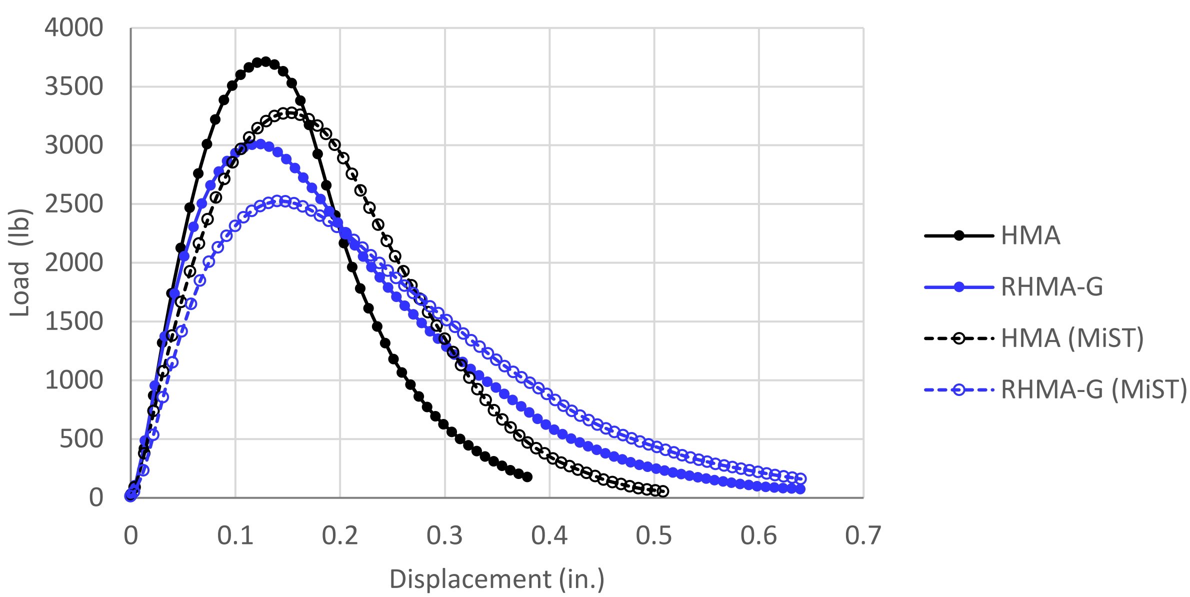

Figure 5.8: IDEAL-CT test results: Load versus displacement.

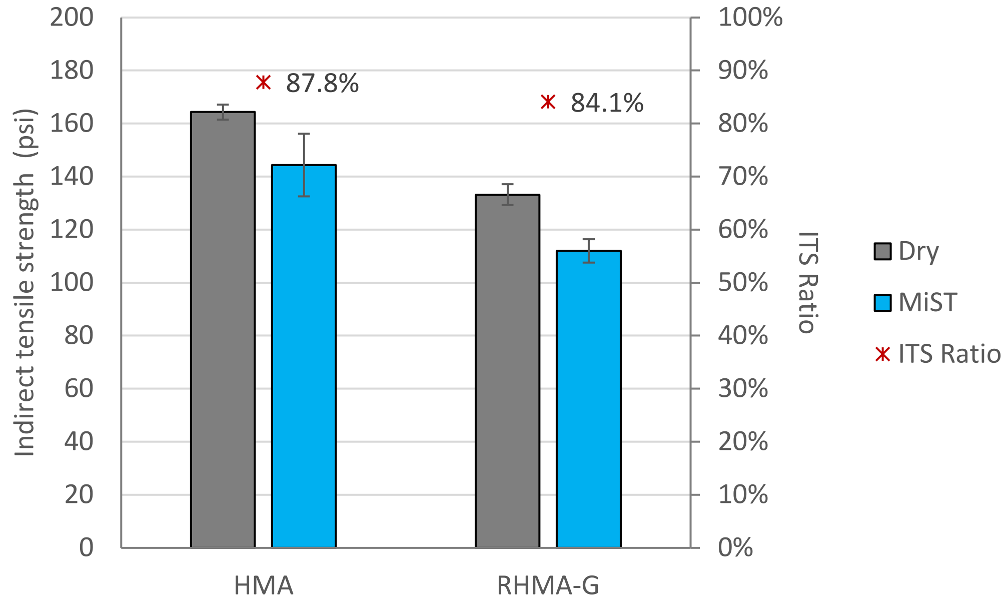

Figure 5.9: Indirect tensile strength ratio (MiST effect).

5.2 Testing of Lean Concrete Base

LCB specimens were prepared from the fresh mixture sampled during the construction of the test track. The specimens were prepared following ASTM C31-21, “Making and Curing Concrete Test Specimens in the Field,” and stored in a curing box. Then, some specimens were demolded after three days for testing. The rest were demolded after seven days for either seven-day testing or storing in lime water until testing. Two sets of specimens were prepared as follows:

- Set of 4 × 8 in. (100 × 200 mm) cylinders for compressive strength testing following ASTM C39-21, “Compressive Strength of Cylindrical Concrete Specimens.” Three specimens were tested at each age (3 days, 7 days, 28 days, and one year).
- Set of 6 × 12 in. (150 × 300 mm) cylinders for modulus of elasticity testing following ASTM C469-02, “Static Modulus of Elasticity and Poisson's Ratio of Concrete in Compression.” Three specimens were tested at 3 days, and another three specimens were tested at 7 days, 28 days, and one year, though the one-year testing results were discarded as they did not look consistent with previous results.

The results are shown in Figure 5.10 (compressive strength) and Figure 5.11 (modulus of elasticity). The lean concrete fulfills the Caltrans minimum compressive strength requirement of 530 psi (3.7 MPa) at seven days of age (Caltrans Std. Specs. Section 28).

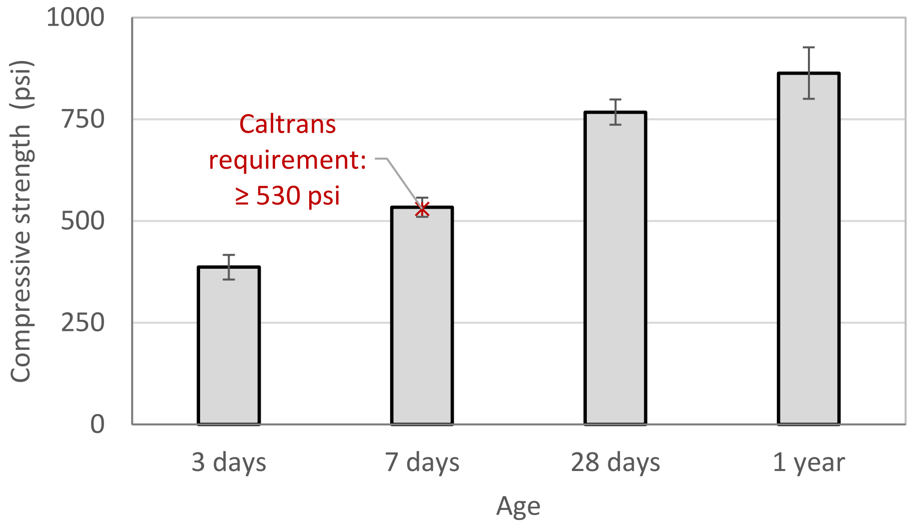

Note: The error bars correspond to ±1 std. deviation.

Figure 5.10: Compressive strength (lean concrete).

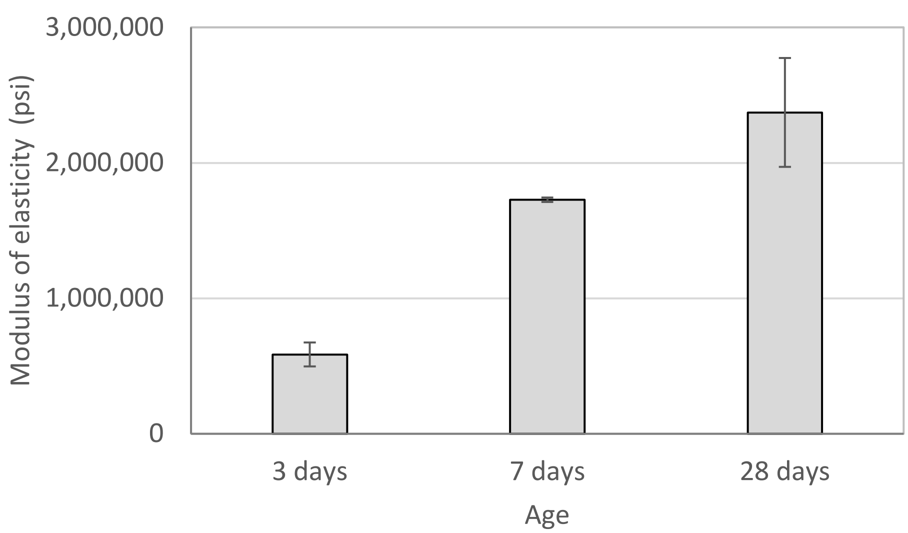

Note: The error bars correspond to ±1 std. deviation.

Figure 5.11: Modulus of elasticity (lean concrete).

5.3 Testing of Portland Limestone Cement Concrete

PLCC specimens were prepared from the fresh mixture sampled during the construction of the test track. The specimens were prepared following ASTM C31-21, "Making and Curing Concrete Test Specimens in the Field," and were stored in a curing box, demolded in 24 hours, and stored in lime water until testing. Five sets of specimens were prepared as follows:

- Set of 6 × 6 × 12 in. (150 × 150 × 450 mm) beams for flexural strength testing following ASTM C78-22, "Flexural Strength of Concrete (Using Simple Beam with Third-Point Loading)." Three specimens were tested at each age (10 days, 28 days, and one year).

- Set of 4 × 8 in. (100 × 200 mm) cylinders for compressive strength testing following ASTM C39-21, "Compressive Strength of Cylindrical Concrete Specimens." Three specimens were tested at each age (10 days, 28 days, and one year).
- Set of 6 × 12 in. (150 × 300 mm) cylinders for modulus of elasticity testing following ASTM C469-02, "Static Modulus of Elasticity and Poisson's Ratio of Concrete in Compression." Three specimens were tested at 10 days, and another three specimens were tested at 28 days and one year.
- Set of 4 × 8 in. (100 × 200 mm) cylinders for coefficient of thermal expansion (CTE) testing following AASHTO T 336-15, "Coefficient of Thermal Expansion of Hydraulic Cement Concrete." Three specimens were tested at 42 days of age.
- Set of 4 × 4 × 10 in. (100 × 100 × 250 mm) prisms for drying shrinkage testing following ASTM C157-17, "Length Change of Hardened Hydraulic Cement Mortar and Concrete," except for the age when drying begins (8 days was adopted rather than the 28 days specified in the ASTM standard). Four prisms were evaluated.

The results are shown in Figure 5.12 (flexural strength), Figure 5.13 (compressive strength), Figure 5.14 (modulus of elasticity), Figure 5.15 (CTE), and Figure 5.16 (drying shrinkage). Overall, all test results fall within the expected range for this concrete.

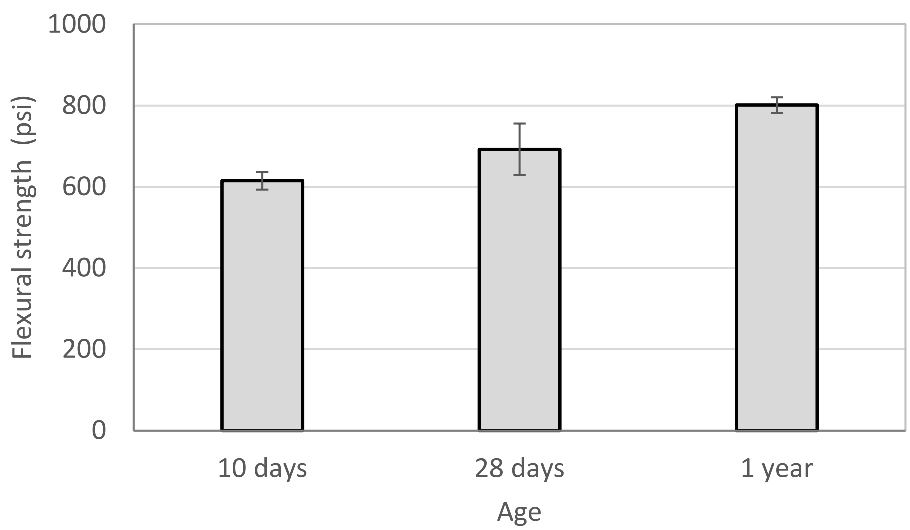

Note: The error bars correspond to ±1 std. deviation.

Figure 5.12: Flexural strength (PLCC).

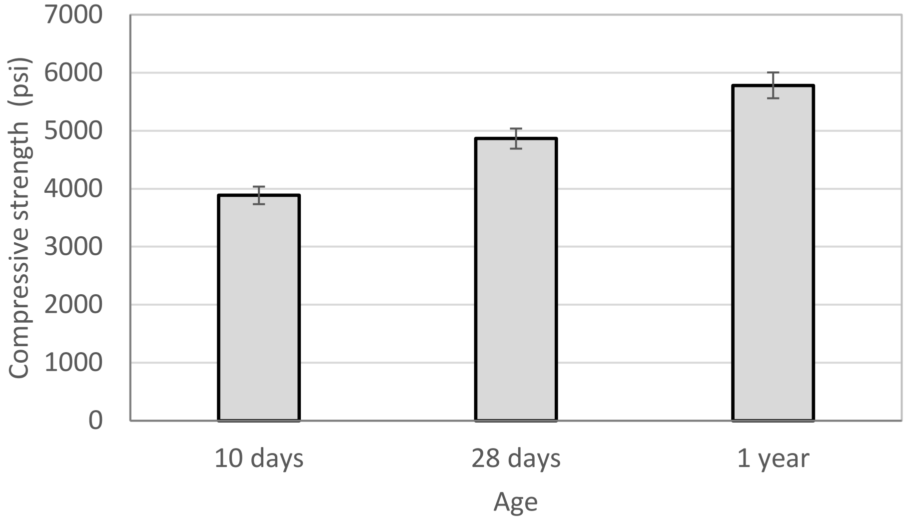

Note: The error bars correspond to ±1 std. deviation.

Figure 5.13: Compressive strength (PLCC).

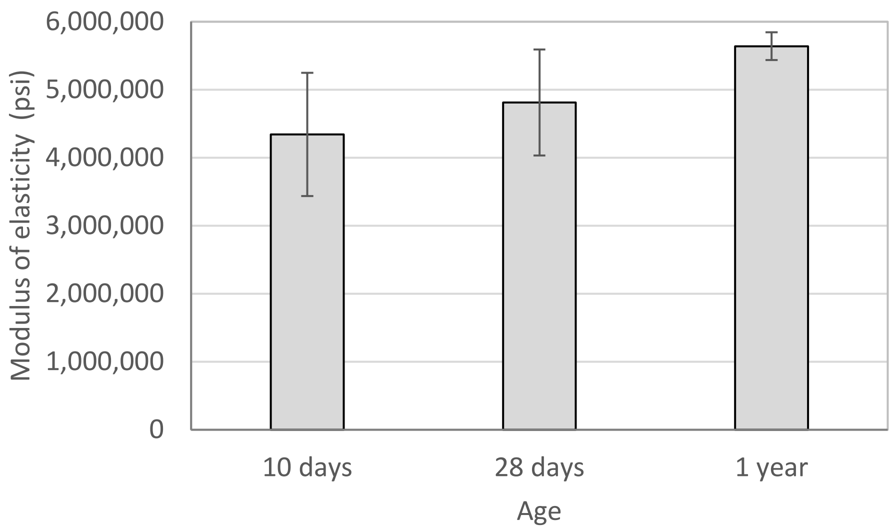

Note: The error bars correspond to ±1 std. deviation.

Figure 5.14: Modulus of elasticity (PLCC).

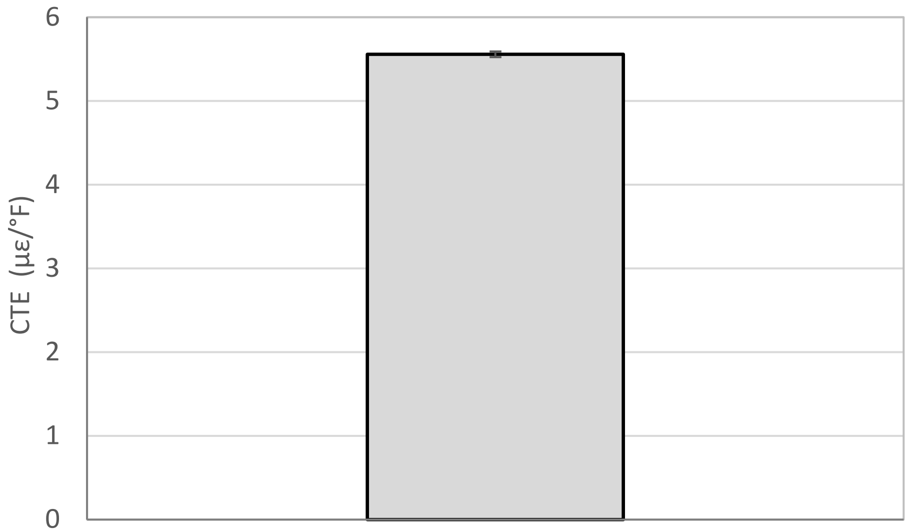

Note: The error bars correspond to ±1 std. deviation.

Figure 5.15: Coefficient of thermal expansion (PLCC).

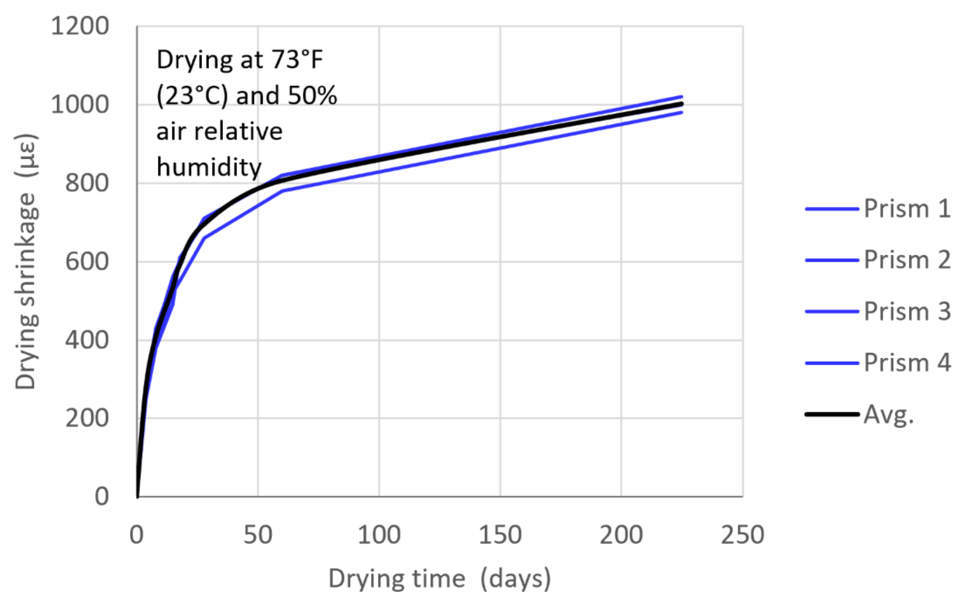

Figure 5.16: Drying shrinkage (PLCC).

6 FINITE ELEMENT METHOD MODELING OF TEST TRACK SECTIONS

Two FEM models have been developed and were used in this research using *Abaqus* software:

1. Structural response model. Its goal is to model the structural response (mainly stress, strain, and deflection) of curled/warped slabs under traffic and FWD loading for different scenarios of slab-base bonding. In this chapter, this model is used to predict the deflections that take place under the FWD loading (Section 6.1).
2. Slab-base debonding model. Its goal is to model the debonding that takes place between the concrete slabs and the base due to the slab curling/warping created by the hygrothermal actions (Section 6.2).

The structural response model was applied to two sections of the test track:

- Section with RHMA-G base (referred to as the RHMA section)
- Section with LCB and curing compound interlayer (referred to as the CC section)

The slab-base debonding model was only applied to the RHMA section. The model was not applied to the CC section because the slabs and the LCB had been debonded since the construction due to the curing compound interlayer.

The other two sections were not modeled for different reasons. The section with LCB and the microsurfacing interlayer was not modeled because the microsurfacing could not be tested in the laboratory, and so the material model parameters were not available. The section with LCB and geotextile interlayer was not modeled since the geotextile is not expected to result in any considerable structural change versus the curing compound interlayer. Both the geotextile and curing compound are expected to break the bond between the slabs and the LCB while providing a negligible cushion effect.

6.1 Modeling the Structural Response Under FWD Loading

6.1.1 Model Definition

The goal of the modeling is to predict the structural response of the slabs under the FWD loading. Except for the slab-base interaction, the modeling was conducted following current standard practice for the mechanistic-empirical design of concrete pavements. Following such practice, the structural problem is assumed to be static and concrete and asphalt are regarded as linear elastic materials. Asphalt stiffness is determined for a frequency that is representative of the FWD loading. The following are details of the modeling:

- Analysis type: Static
- Slab and base finite element type: 8-node linear brick element with incompatible modes and second-order accuracy (this element is referred to as C3D8I in Abaqus)
- Geometry (Figure 6.1):
    - Number of slabs: 1
    - Slab thickness: 7.0 in. (178 mm)

- Base thickness: RHMA-G is 3.0 in. (76 mm); LCB is 4.2 in. (107 mm)

- Subgrade: Tensionless Winkler foundation; k = 368 psi/in. (0.10 MPa/mm), based on FWD backcalculation following the AREA method *(14)*. The finite element is a four-node doubly curved shell with negligible thickness and reduced integration (this element is referred to as S4R in Abaqus).
- PLCC stiffness (linear elastic material): The PLCC elastic modulus was assumed to be the laboratory modulus of elasticity (ASTM C469) of the PLCC sampled during construction (Section 5.3). The laboratory modulus of elasticity increased with time as cement hydration progressed. The PLCC elastic modulus, based on laboratory testing, estimated for each FWD evaluation time is shown in Table 6.1.
- LCB stiffness (linear elastic material): The LCB elastic modulus was assumed to be the laboratory-measured modulus of elasticity (ASTM C469) of the LCB sampled during construction (Section 5.2). The laboratory elastic modulus increased with time as cement hydration progressed. The LCB elastic modulus estimated for each FWD evaluation is shown in Table 6.1.
- RHMA-G (linear elastic material): The elastic modulus was assumed to be the laboratory dynamic modulus (AASHTO T 378) of the RHMA-G sampled during construction (Section 5.1). The laboratory dynamic modulus varied depending on temperature and frequency (see the dynamic modulus master curve in Figure 5.1). The RHMA-G temperature during the FWD evaluations was measured with thermocouples embedded in the RHMA-G. The pulse of the FWD device used in this research has an average frequency of 30Hz. The RHMA-G elastic modulus estimated for each FWD evaluation is shown in Table 6.1.

Table 6.1: Elastic Modulus Estimated for Each FWD Evaluation

FWD Evaluation	Date	PLCC		LCB		RHMA-G	
		Age (days)	E (psi) [MPa]	Age (days)	E (psi) [MPa]	Temp (°F) [°C]	E (psi) [MPa]
1	June 28, 2022	13	4,500,000 [31,000]	53	2,470,000 [17,000]	88°F [31°C]	580,000 [4,000]
2	August 19, 2022	65	5,080,000 [35,000]	105	2,540,000 [17,500]	88°F [31°C]	550,000 [3,800]
3	November 10, 2022	148	5,370,000 [37,000]	188	2,610,000 [18,000]	54°F [12°C]	1,350,000 [9,300]
4	February 2, 2023	232	5,580,000 [38,500]	272	2,610,000 [18,000]	45°F [7°C]	1,610,000 [11,100]
5	June 28, 2023	378	5,730,000 [39,500]	418	2,680,000 [18,500]	83°F [28°C]	670,000 [4,600]
6	September 20, 2023	462	5,800,000 [40,000]	502	2,680,000 [18,500]	80°F [27°C]	700,000 [4,800]

- Slab curvature:
  - Different levels of slab curvature (ε_{DIFF}) were modeled, from 0 με (flat slabs) to -500 με. The definition of the curvature is the same as used with the VWSG, shown in Figure 4.1. ε_{DIFF} is the difference between the strain at the top and at the bottom of the slabs. The negative sign indicates that the slabs are curled concave upward (nighttime-type curvature).
  - The curvature was modeled by introducing a temperature difference (ΔT_{EQ}) between the top and bottom of the slabs: $\Delta T_{EQ} = \varepsilon_{diff}/CTE$. A negative ε_{diff} indicates that the slab top is cooler than the bottom.
- FWD loading:
  - Two different locations: the center and corner of the slab.
  - The FWD loading was applied on a circular surface, 12 in. (300 mm) in diameter.
  - The FWD loading was assumed to be static.
- Loading steps:
  - The problem was modeled in three steps:
    - Step 1: Self weight of the slabs and base.
    - Step 2: Slab curling/warping; see the images on the left in Figure 6.2 and Figure 6.3.
    - Step 3: FWD loading; see the images on the right in Figure 6.2 and Figure 6.3.
    - As previously explained, the three steps were modeled as static.
- Bonding conditions:
  - Section with LCB and curing compound interlayer (CC section):
    - Slabs and LCB were assumed to be debonded.
    - The slab-LCB interaction is modeled as a rigid contact with no bonding. Consequently, the two materials separate from each other when the slabs curl/warp (Figure 6.2, left).
    - Depending on the slab curvature and the FWD loading level, the slab corner may come in contact with the base when the FWD loading is applied (Figure 6.2, right).
  - Section with RHMA-G base (RHMA section):
    - Slabs and RHMA-G were assumed to be bonded except at a delamination band along the slab perimeter (Figure 6.4). Three bonding scenarios were modeled: 0 in., 12 in., and 24 in. (0 mm, 300 mm, and 600 mm) delamination bandwidth. The width of 0 mm corresponds to concrete slabs fully bonded to the RHMA-G base.
    - The slab-RHMA-G interaction at the delamination band is modeled as a rigid contact with no bonding. Consequently, the two materials separate from each other when the slabs curl/warp.

- Depending on the width of the delamination band, the slab curvature, and the FWD loading level, the slab corner may come in contact with the base when the FWD loading is applied (Figure 6.3, right). The slab and the base remain in contact at all times when full bonding is assumed.

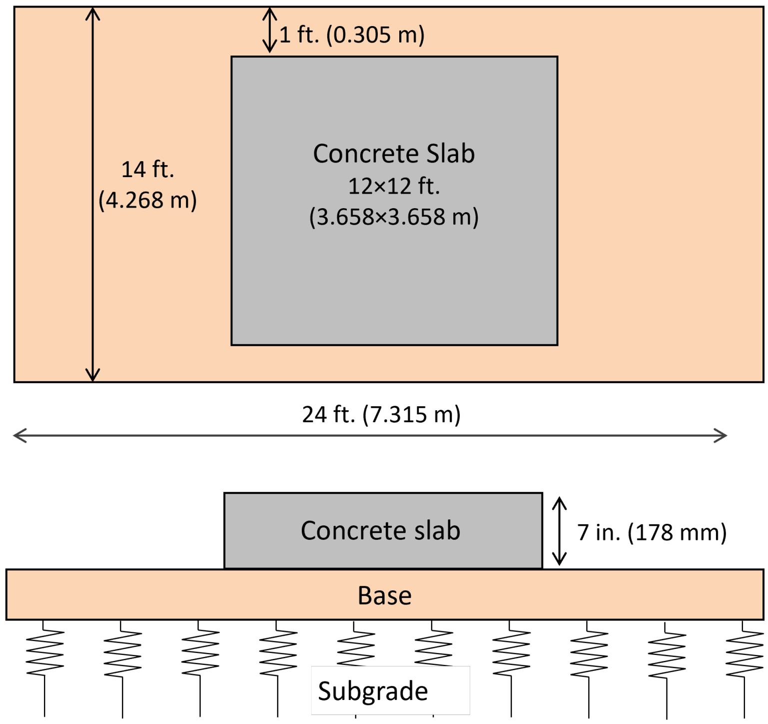

Figure 6.1: FEM model layout (top) and cross-section (bottom).

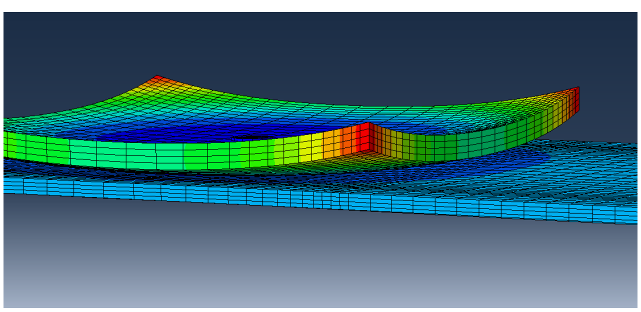

Slab subjected to night-time curvature before the FWD loading; the slab corners deflect upwards and separate from the base.

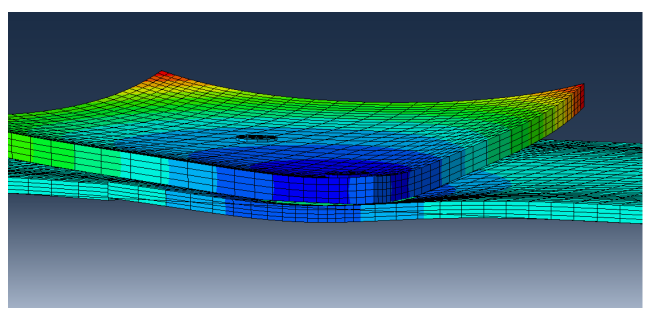

The loaded corner deflects downwards due to the FWD loading; the corner gets back in contact with the base.

Note: ε_{diff} = -150 με; FWD load = 15.7 kips (70 kN).

Figure 6.2: FEM modeling of FWD loading on CC section.

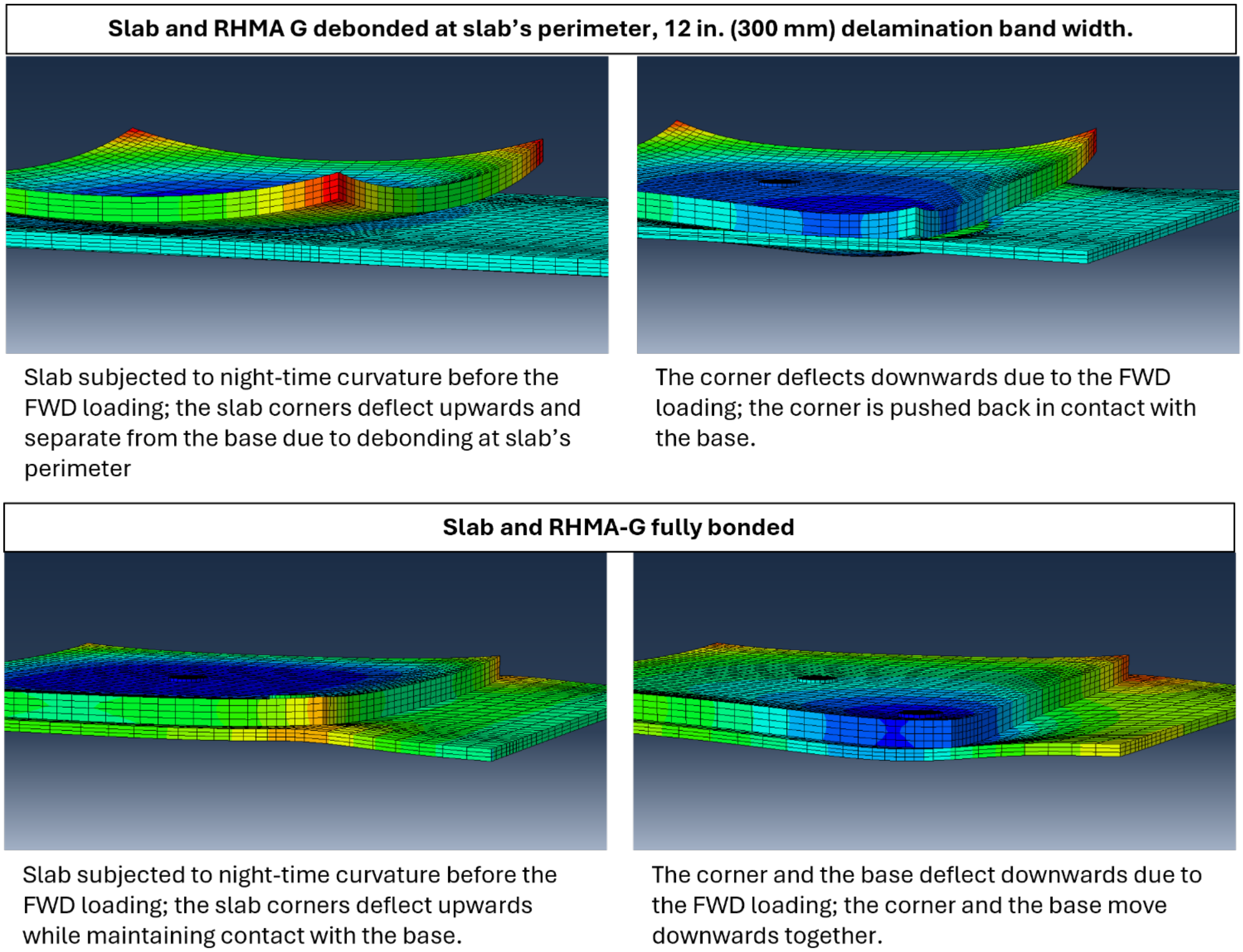

Note: ε_{diff} = -150 με; FWD load = 15.7 kips (70 kN).

Figure 6.3: FEM modeling of FWD loading on RHMA-G section.

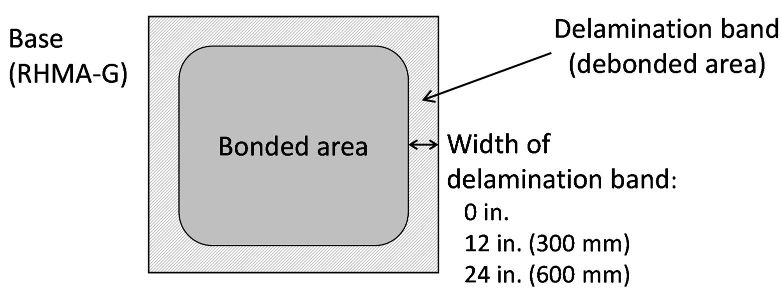

Figure 6.4: Delamination band at slab's perimeter.

6.1.2 Model Results

6.1.2.1 Section CC (Curing Compound and LCB)

The comparison between the CC section (curing compound and LCB) FEM model predicted deflection versus the measured deflection under the FWD loading is shown in Figure 6.5. For low slab curvature ($\varepsilon_{diff} \approx 0$), the model provides a reasonable prediction of the measured deflection. For high curvature ($\varepsilon_{diff} << 0$), the model overpredicts the deflection measured at the corner. In other words, the model overestimates the impact that slab curling/warping has on the corner deflection. This outcome is not surprising as past research shows that the actual (geometric, as measured with VWSG) curvature of the slabs may be higher than the effective curvature, with effective curvature defined as the apparent curvature based on slab structural response to traffic or FWD loading *(17)*. Based on the Figure 6.5 results, the effective curvature of the slabs is around half the actual curvature. In other words, a differential strain of -250 με in *Abaqus* results in the corner deflection measured when the actual curvature of the slab (measured with VWSG) is -500 με.

The curvature was modeled in *Abaqus* by applying a temperature difference ($\Delta T_{EQ} = \varepsilon_{diff}/CTE$) between the top and bottom of the slab. The temperature difference is applied to the complete slab, the same at the center as at the edges, shown by the "constant ΔT" series in Figure 6.6. The constant ΔT approach is the one typically used for concrete pavement mechanistic-empirical modeling, including the *AASHTOWare Pavement ME Design* model *(10)*. A second approach for applying the curvature action in *Abaqus* was tried. In the second approach, referred to as variable linearly ΔT, the temperature difference for modeling (ΔT) varies linearly between the center of the slab, where it is assumed to be zero, and the corner, where it is assumed to be ΔT_{EQ} (ε_{diff}/CTE), as shown in Figure 6.6. The second approach can be regarded as a simplified way to consider concrete creep.

The model provided a very good prediction of the measured deflection at the center and corners across the whole curvature range (ε_{DIFF} 0 to -500 με) when the curvature action was introduced following the variable linearly ΔT approach. See model predictions versus measured deflection in Figure 6.7.

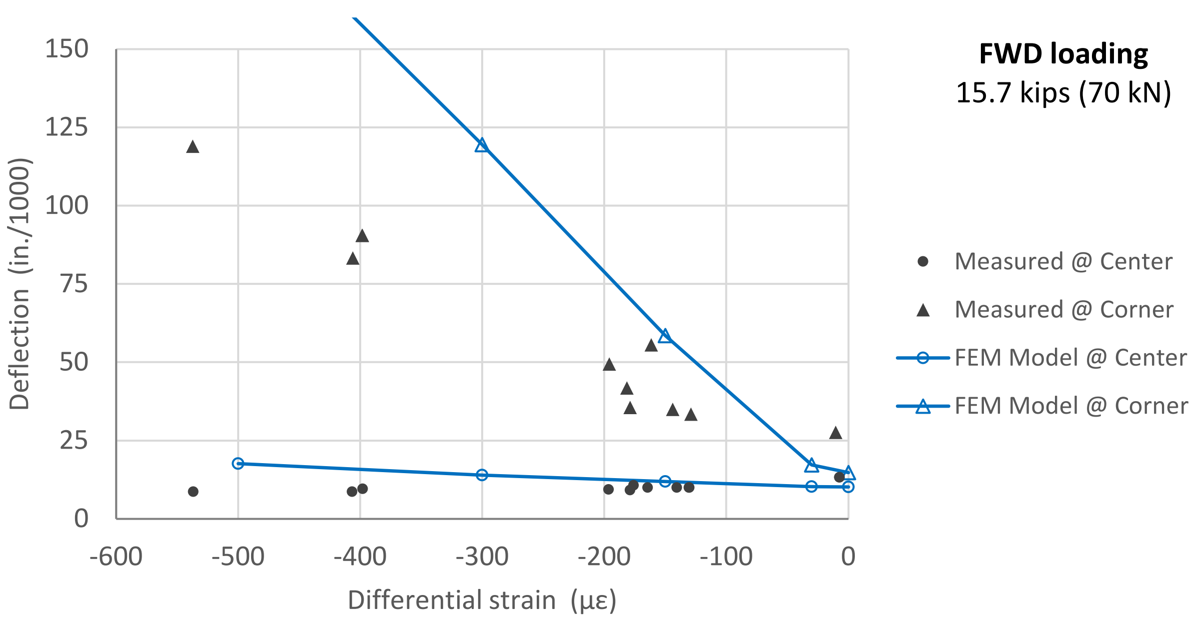

Figure 6.5: FEM modeling results versus measured deflection, FWD loading, CC section.

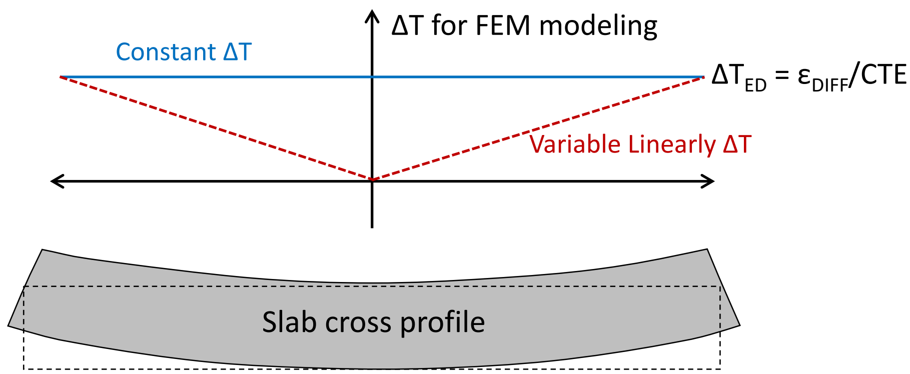

Figure 6.6: Applying the slab curvature action in *Abaqus*.

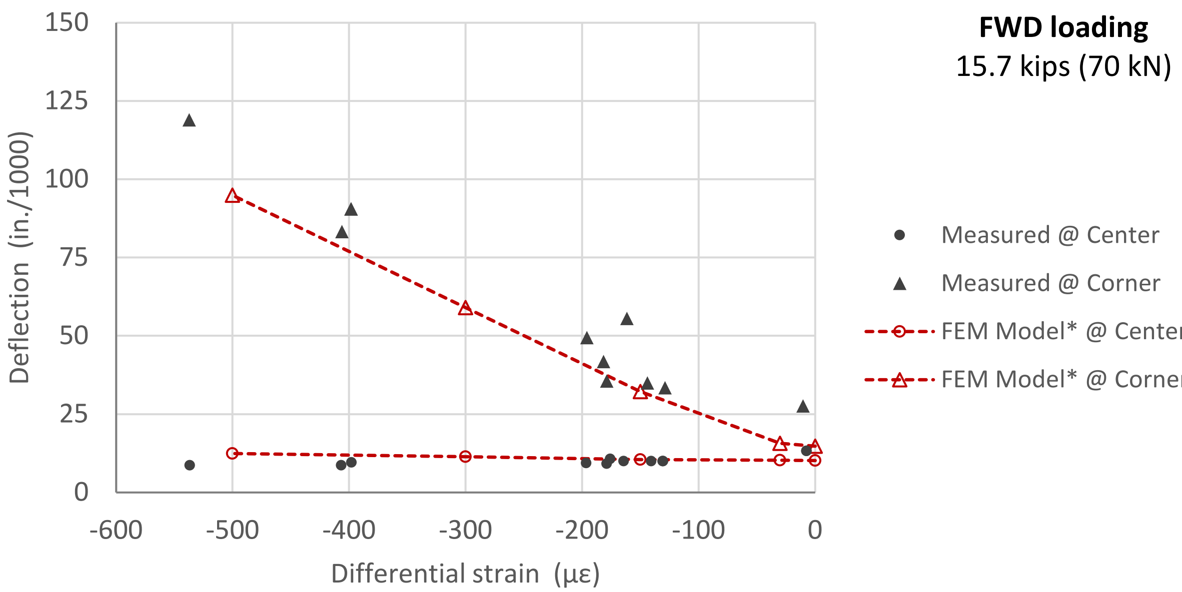

Figure 6.7: FEM modeling results versus measured deflection, FWD loading, CC section; slab curvature modeled following variable linearly ΔT approach.

6.1.2.2 Section RHMA (RHMA-G Base)

The comparison between section RHMA (RHMA-G base) FEM model predicted deflection versus the measured deflection under the FWD loading (15.7 kips, 70 kN) is shown in Figure 6.8. The following should be considered when interpreting the figure:

- Different levels of slab-base debonding (DB) have been modeled: DB = 0 in., 12 in., and 24 in. (0 mm, 300 mm, and 600 mm), where DB is the width of the delamination band at the slab perimeter (Figure 6.4).
- The RHMA-G elastic modulus and the PLCC elastic modulus, to a lesser extent, varied between FWD evaluations (Table 6.1). The RHMA-G elastic modulus varied because of the temperature differences between evaluations. The y-axis bars in the figure expand between the predicted deflection for the highest and lowest modulus of the RHMA-G and the PLCC. The practical

totality of the variation is due to the RHMA-G stiffness changes rather than the PLCC stiffness changes.

As shown in Figure 6.8, the corner deflection increases as the slab curvature increases (ε_{DIFF} becomes more negative). This pattern of variation indicates some nonlinearity, most likely due to debonding between the slab and the RHMA-G base. Based on the FEM modeling, the debonding would affect the area from 12 to 24 in. (300 to 600 mm) from the slab perimeter. Modeling following the variable linearly ΔT approach indicates similar debonding (Figure 6.9).

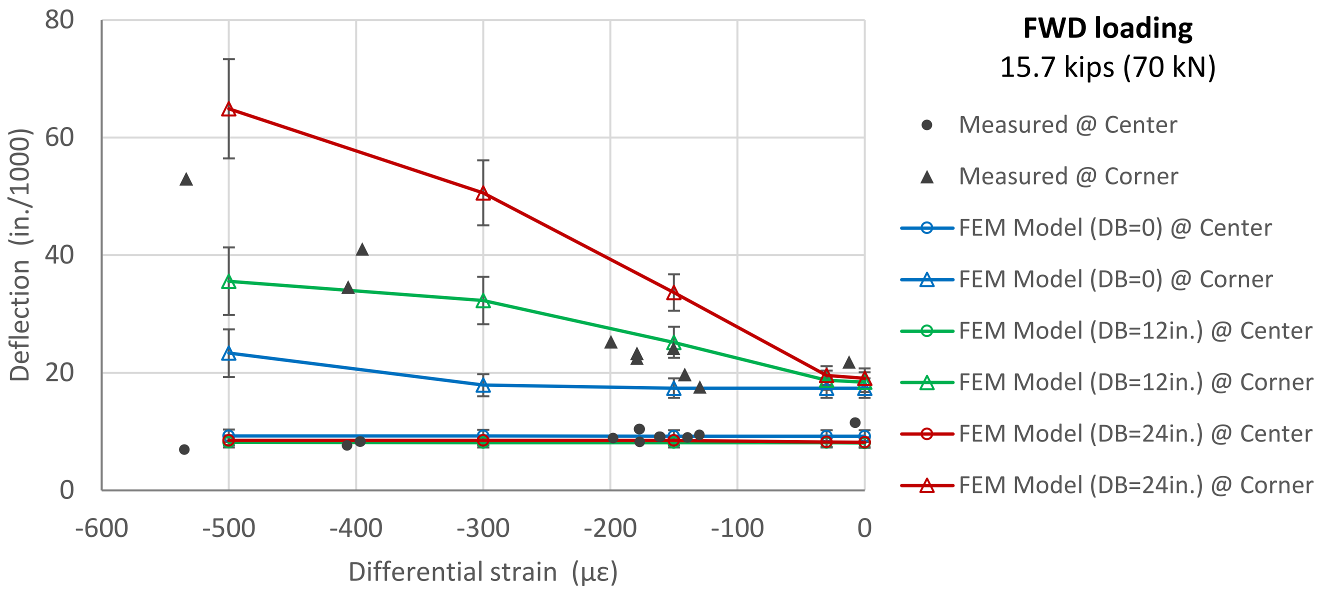

Figure 6.8: FEM modeling results versus measured deflection, FWD loading, RHMA section.

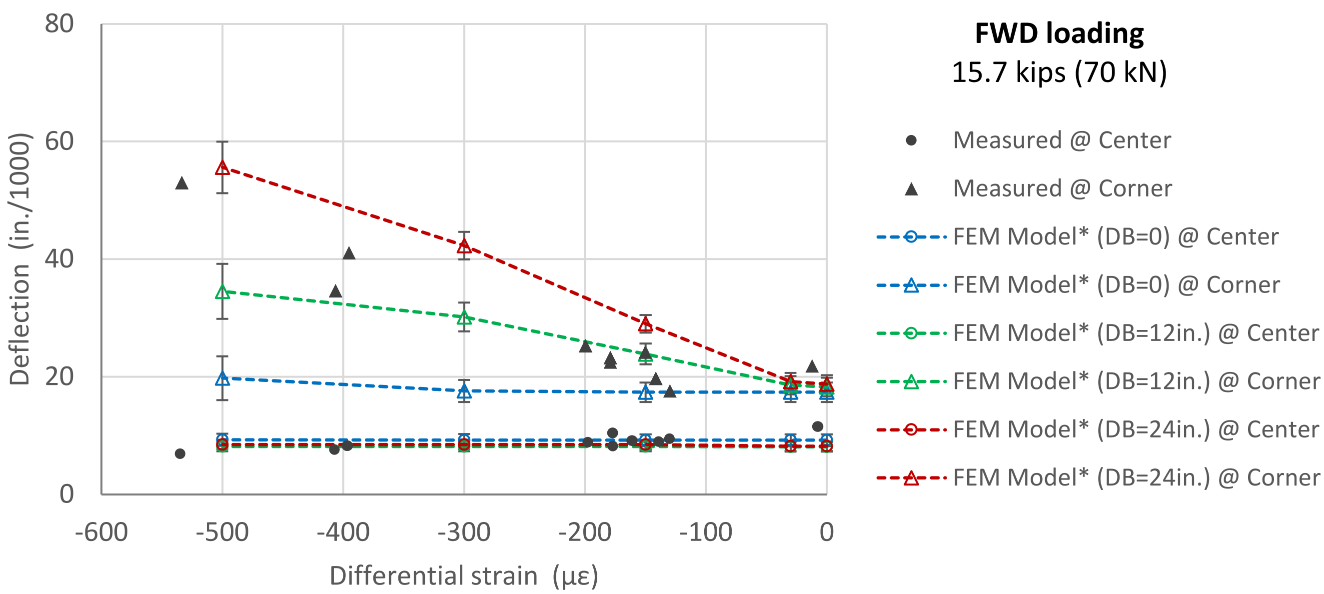

Figure 6.9: FEM modeling results versus measured deflection, FWD loading, RHMA section; slab curvature modeled following variable linearly ΔT approach (explained in 6.1.2.1).

6.2 Modeling Slab-Base Debonding

6.2.1 Model Definition

The goal of the modeling is to predict the debonding that takes place between the concrete slabs and the base due to the slab curling/warping created by the hygrothermal actions. The following are details of the FEM modeling conducted in this research:

- Analysis type: Dynamic
- Slab and base finite element type: eight-node linear brick element with incompatible modes and second-order accuracy (this element is referred to as C3D8I in Abaqus)
- Geometry (Figure 6.1):
  - Number of slabs: 1
  - Slab thickness: 7.0 in. (178 mm)
  - Base thickness: RHMA-G is 3.0 in. (76 mm)
- Subgrade: Tensionless Winkler foundation; k = 368 psi/in. (0.10 MPa/mm), based on FWD backcalculation. The finite element is a four-node doubly curved shell, with negligible thickness and reduced integration (this element is referred to as S4R in Abaqus).
- PLCC stiffness (linear elastic material): The PLCC elastic modulus was assumed to be 5.0 million psi (35,000 MPa), which is an average value across the time period modeled in this research (June 2022 to September 2023), based on the laboratory-measured modulus of elasticity (ASTM C469) of the PLCC sampled during construction (Section 5.3).
- RHMA-G (linear viscoelastic material): The generalized Maxwell model was used for modeling the RHMA-G material. This model, implemented in the *Abaqus* FEM software, consists of a series of Maxwell models arranged in parallel, shown in Figure 6.10. The model parameters were determined based on the results of the dynamic modulus testing (Figure 5.1) and hanging test (Figure 5.2) following the methodology described and used in previous UCPRC research *(18)*. A constant temperature of 77°F (25°C) was assumed in the FEM modeling.
- Slab curvature:
  - The curvature was modeled by introducing a temperature difference (ΔT_{EQ}) between the top and bottom of the slabs: $\Delta T_{EQ} = \varepsilon_{DIFF}/CTE$. A negative ε_{DIFF} indicates the slab top is cooler than the bottom.
  - A curvature (ε_{DIFF}) of -500 με was modeled. The curvature is the "action" that produces the debonding. The -500 με corresponds to the maximum curvature measured in slabs, shown in Figure 4.2.
  - The -500 με were applied as -300 με drying shrinkage taking place over four months plus -200 με due to thermal gradients taking place over 12 hours (Figure 6.11).
- Loading steps:
  - The problem was modeled in three steps (Figure 6.11):

- Step 1: Self weight of the slabs and base.
- Step 2: Slab warping (drying shrinkage).
- Step 3: Slab curling (thermal gradient).

  - As previously explained, the three steps are assumed to be dynamic.

- Slab-RHMA-G interaction:
  - The interaction between the slab and the RHMA-G is modeled with an interlayer of cohesive elements (referred to as COH3D8 in Abaqus) of 0.4 in. (10 mm) thickness (Figure 6.12). The cohesive elements are assigned the same material model (viscoelastic) and model parameters as the RHMA-G. The cohesive elements interlayer represents the top part of the RHMA-G base. The rest of the RHMA-G base, modeled with brick elements, is reduced by 0.4 in. (10 mm) in thickness to discount the interlayer thickness. The cohesive elements can undergo damage, a feature that is used for modeling the debonding.
  - The slab and RHMA-G are assumed to be fully bonded before the hygrothermal action begins (before slab curvature is imposed), meaning that the damage in the cohesive elements is null at the beginning of step 2.
  - As the slab curls/warps, the cohesive elements (top part of the RHMA-G base) and the brick elements (rest of the RHMA-G base) experience deformation (Figure 6.13). As the deformation increases, the cohesive elements experience damage, while the brick elements do not. This means that damage is assumed to take place at the top of the RHMA-G base, which agrees with experimental evidence *(3,4)*. The consequence of the damage is that the stiffness of the cohesive elements decreases. The relationship between cohesive element deformation and damage is determined by a traction-separation law that must be defined in the FEM modeling.
  - The traction-separation law defines the strains at the damage initiation and the damage evolution law until failure. The type and parameters of the traction-separation law were determined using inverse engineering to match the results of the RHMA-G testing in the UTM-ramp test (Figure 6.14). Overall, the cohesive elements and the selected traction-separation law accurately reproduced the specimen failures in the UTM-ramp tests, shown in the Figure 6.15 example.

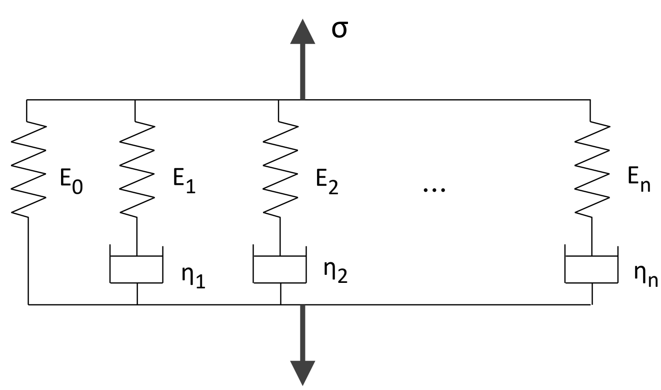

Figure 6.10: Viscoelastic model used for RHMA-G (generalized Maxwell model).

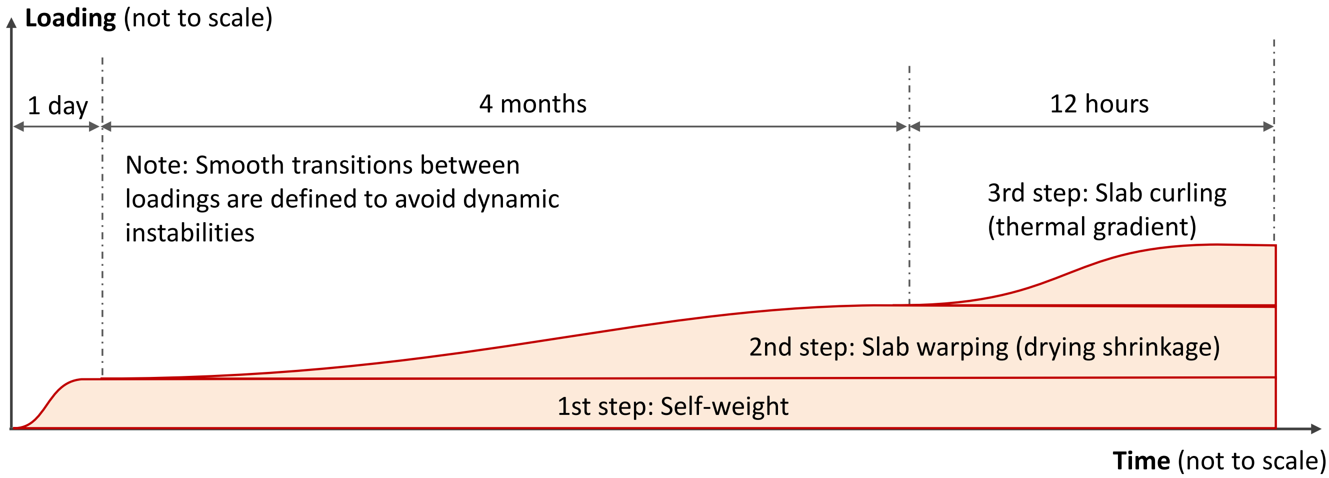

Figure 6.11: Representation of the time variation of the curvature action applied in the FEM modeling.

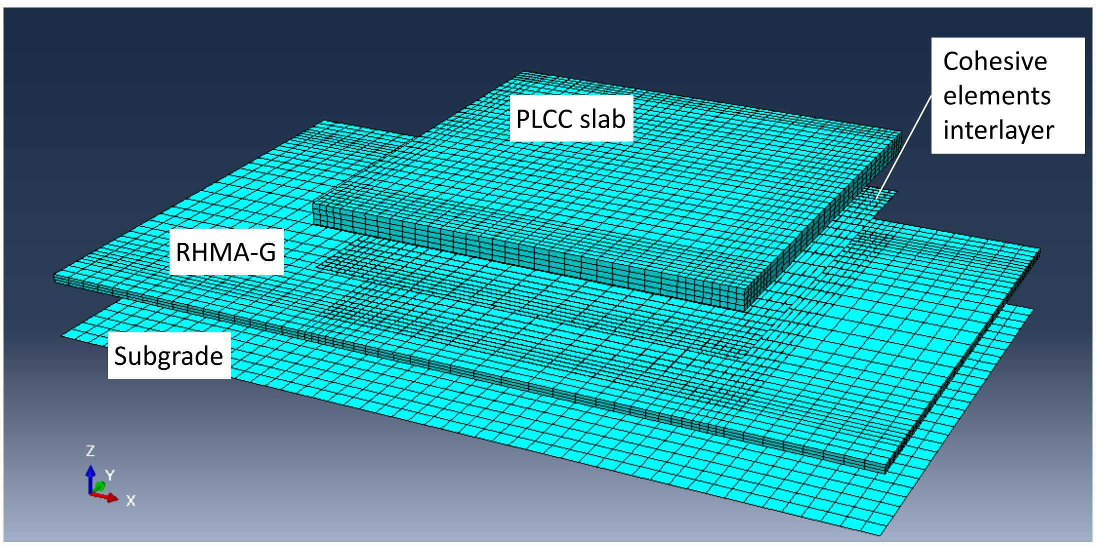

Figure 6.12: Disassembled representation of the FEM model with RHMA-G base.

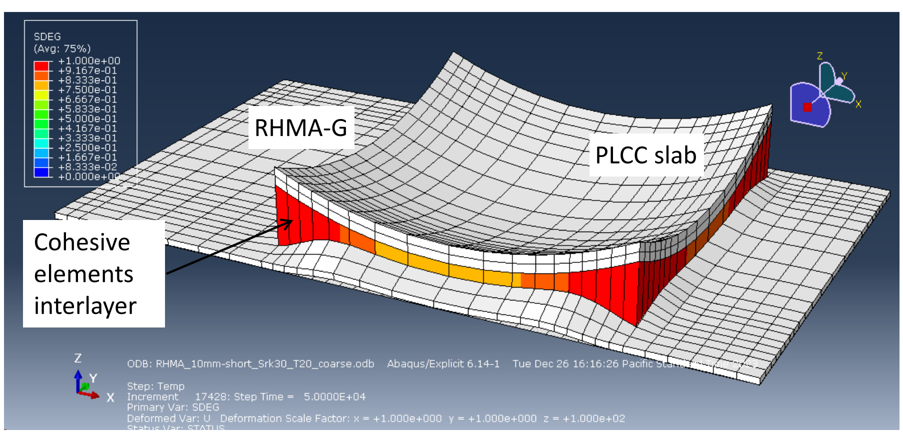

Note: SDEG is stiffness degradation; a value of 1 indicates complete degradation.

Figure 6.13: Cohesive element deformations as the slab curls/warps.

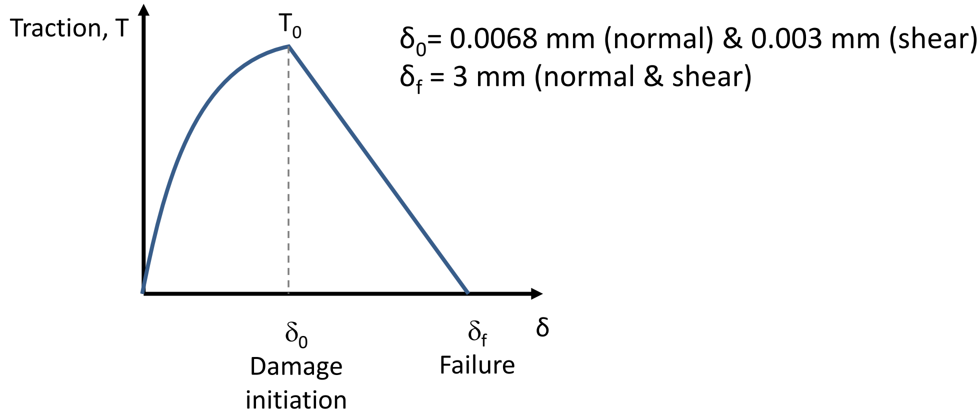

Figure 6.14: Cohesive elements traction-separation law.

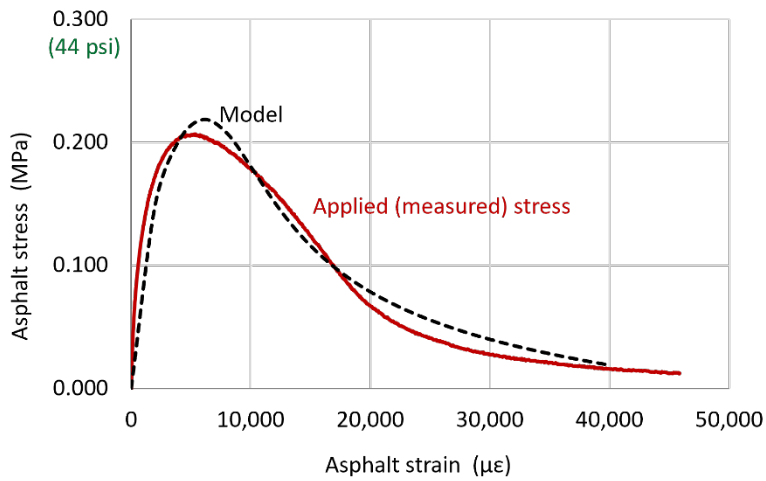

Figure 6.15: Example of RHMA-G damage modeling in the UTM-ramp test.

6.2.2 Model Results

6.2.2.1 Section CC (Curing Compound and LCB)

The debonding was not modeled in this section, as the slabs and the LCB have been debonded since construction due to the curing compound interlayer.

6.2.2.2 Section RHMA (RHMA-G Base)

The FEM model predicts the damage that the RHMA-G interlayer cohesive elements experience as the slab curls/warps due to the drying shrinkage and thermal gradients. The damage predicted at the end of step 3, due to the application of -500 με curvature, is shown in Figure 6.16. The damage, referred to in *Abaqus* as stiffness degradation (SDEG), is defined as a number between 0 and 1, where 0 corresponds to no damage and 1 corresponds to complete failure where the finite element loses 100% of its structural capacity. In Figure 6.14, SDEG is 0 when deformation is less than or equal to δ0. SDEG then increases linearly versus deformation up to δ_f, where SDEG reaches 1.

As shown in Figure 6.16, the interlayer stiffness degrades up to 75% (0.75 damage) along an 18 in. (450 mm) wide band around the slab perimeter, while it maintains more than 50% of its structural capacity (less than 0.5 damage) in the inner zone. This outcome agrees with the debonding that was estimated from FWD deflection. As shown in Section 6.1.2.2, the pattern of variation of FWD corner deflection versus slab curvature (ε_{DIFF}) was compatible with 12 to 24 in. (300 to 600 mm) debonding areas at the slab perimeter.

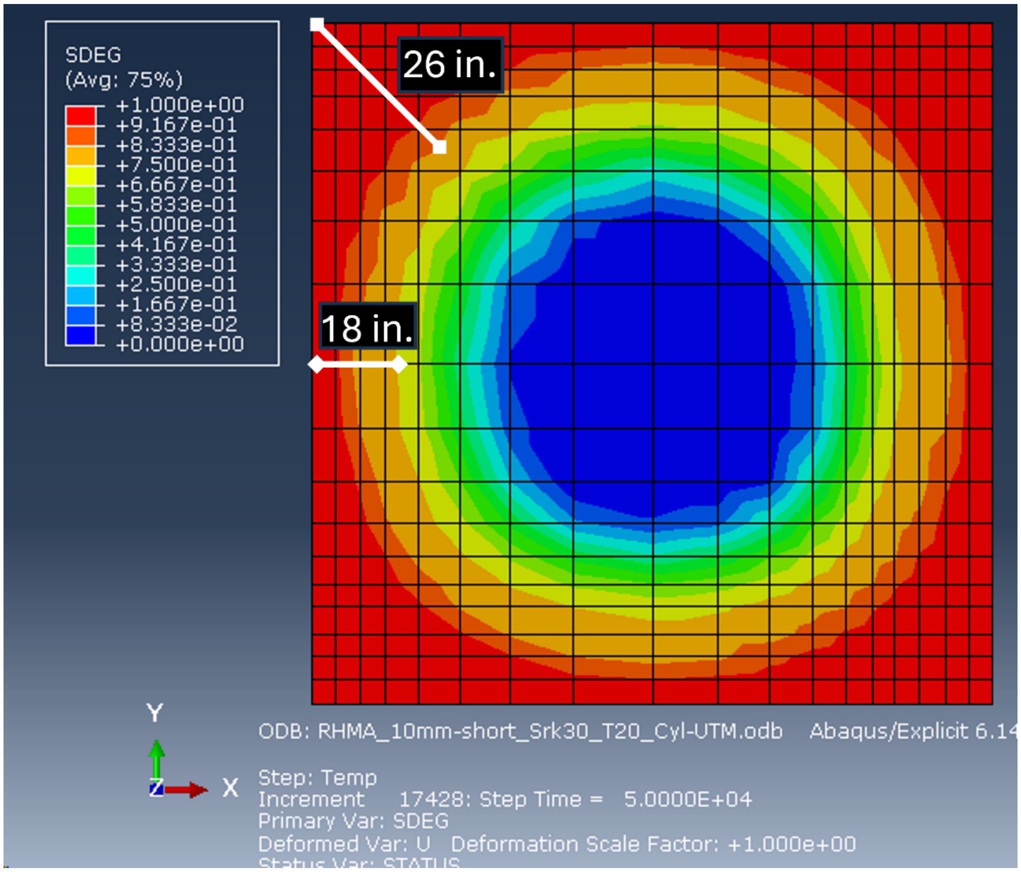

Figure 6.16: RHMA-G cohesive element damage due to slab curvature; end of step 3 (ε_{DIFF} = -600 µε).

7 RESULTS AND DISCUSSION

The results of the testing of the asphalt concrete mixes and interlayers and the monitoring of the test track are discussed below. The discussion is organized around the different questions that this research study was expected to answer (Section 1.3).

7.1 How Should Asphalt Concrete Design Be Adapted to Optimize Its Performance as a Base for Rigid Pavement?

The experimental data collected in this research—and in particular, the corner deflection versus the slab curvature (ε_{DIFF}) data shown in Figure 4.8—indicate that the RHMA-G provides much better slab support than the LCB. Nonetheless, the corner deflections in the slab with the RHMA-G base still show some sensitivity versus ε_{DIFF}. This outcome indicates that there is debonding between the slab and the RHMA-G. The modeling with FEM, shown in Section 6.1.2.2, estimates that the pattern of variation of corner deflection versus ε_{DIFF} in the section with the RHMA-G base is compatible with a debonding of 12 to 24 in. (300 to 600 mm) around the slab perimeter. Such debonding agrees with the results of the laboratory testing of the RHMA-G under tension (UTM-ramp test) together with the FEM modeling, shown in Section 6.2.2.2. This outcome indicates that there is room for improving the performance of the RHMA-G as a JPCP base. The improvement should be in the direction of enhancing the material's capacity to deform without cracking under slow loading.

There are different ways to enhance the RHMA-G (and asphalt mixes in general) capacity to deform under slow loading without cracking. One is to increase the asphalt binder content; another is to soften the binder by selecting a lower PG grade base binder (e.g., PG 58-16 instead of PG 64-10). Most likely, enhancing the capacity to deform under slow loading will result in softer asphalt mixes and increased susceptibility to rutting. While the increased susceptibility to rutting is not an issue (as the base will be protected by the JPCP slabs), the softening of the asphalt mix may go against one of the goals identified in Section 2.4.1: help JPCP slabs to resist traffic loading (Goal 1). The impact of the asphalt mix softening on JPCP performance is analyzed in the following discussion.

A limited sensitivity analysis with the FEM software *ISlab2005* was conducted to assess the impact of a potential reduction of the stiffness of the asphalt concrete base. *ISlab2005* is the FEM software behind *AASHTOWare Pavement ME Design*. A three-slab JPCP structure was analyzed (Figure 7.1). Some features of the JPCP are the following:

- Slab size: 12 × 14 ft. (3.6 × 4.2 m), width × length
- Transverse joint load transfer efficiency (LTE): 90%
- Slab thickness: 8 in. (200 mm)
- Base thickness: 3 in. (76 mm)
- Slab (concrete) stiffness: $5 \cdot 10^6$ psi (35,000 MPa)
- Base (asphalt mix) stiffness: 300,000 to 1,200,000 psi (2,100 to 8,300 MPa)
- Subgrade: tensionless Winkler foundation, k = 250 psi/in. (0.068 MPa/mm)
- Shoulder: none

- Slab-base bonding, two scenarios:
    - Bonded (bonded in the horizontal and vertical directions)
    - Unbonded (unbonded in the horizontal direction while bonded in the vertical direction; debonding in the vertical direction cannot be modeled with *ISlab2005*)
- Traffic loading, two scenarios:
    - Edge loading (Figure 7.1): 20 kips (90 kN) single axle. This loading scenario may result in bottom-up transverse cracking.
    - Corner loading, consisting of truck head loading at opposite sides of the slab (Figure 7.2): 12 kips (50 kN) steering axle and 34 kips (150 kN) tandem drive axle; 15 ft. (4.5 m) wheelbase (distance between steering axle and center of drive axle). This loading scenario may result in top-down transverse cracking and top-down longitudinal cracking. See the model result example in Figure 7.3

The maximum tensile stress at the bottom of the concrete slab under the edge loading scenario is plotted versus the stiffness of the asphalt base in Figure 7.4. As shown in the figure, the bonding condition has a much larger impact on the concrete tensile stress than does the stiffness of the asphalt base. In fact, a soft asphalt base bonded to the slab results in lower tensile stress in the concrete (better slab support) than a stiff asphalt base that is unbonded to the slab. This outcome indicates that the softening of the asphalt mix should not be a concern if it helps to improve slab-base bonding.

The corner loading FEM modeling results are presented in Figure 7.5. In this figure, the "Bonded" series corresponds to a scenario where the slabs can curl/warp without losing the support from the base, while the "Debonded" series corresponds to a scenario where the slabs separate from the base as they curl/warp. In such a scenario, the slabs lose the base support at the corner and edges, and, consequently, the truck loading produces high tensile stresses at the top of the slab. The tensile stresses are highly dependent on the curling/warping level (ΔT in the figure). In fact, for ΔT equals -40°F (-22°C), which corresponds to ε_{DIFF} equals -200 με, the tensile stresses at the top of the slab exceed by far the tensile stresses at the bottom of the slab under the edge loading scenario. As shown in the figure, the stiffness of the asphalt base has a minor impact, essentially negligible, on the tensile stresses at the top of the slab.

In summary, based on the two traffic loading scenarios, the FEM modeling indicates that the softening of the asphalt base is not a concern for JPCP performance.

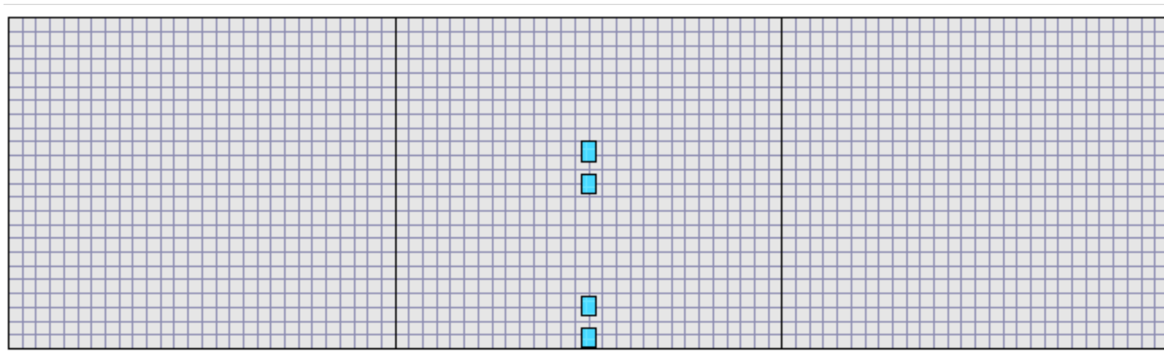

Figure 7.1: FEM model layout, single-axle loading at slab edge (*ISlab2005*).

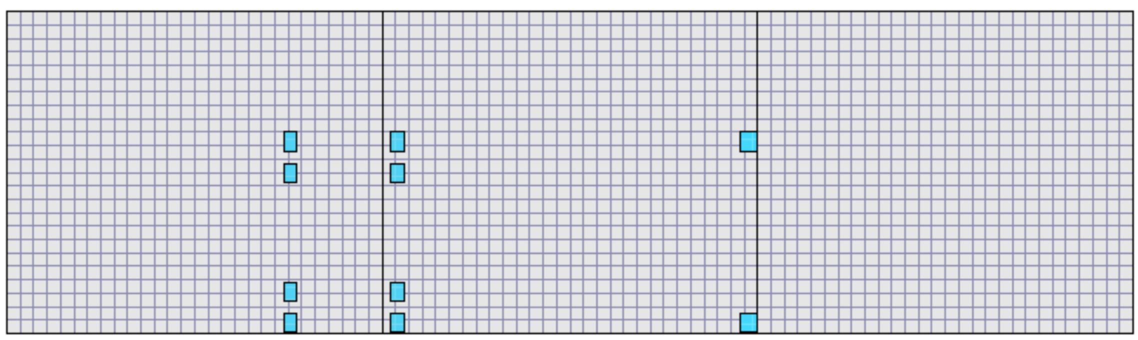

Figure 7.2: FEM model layout, truck head loading at opposite sides of the slab (*ISlab2005*).

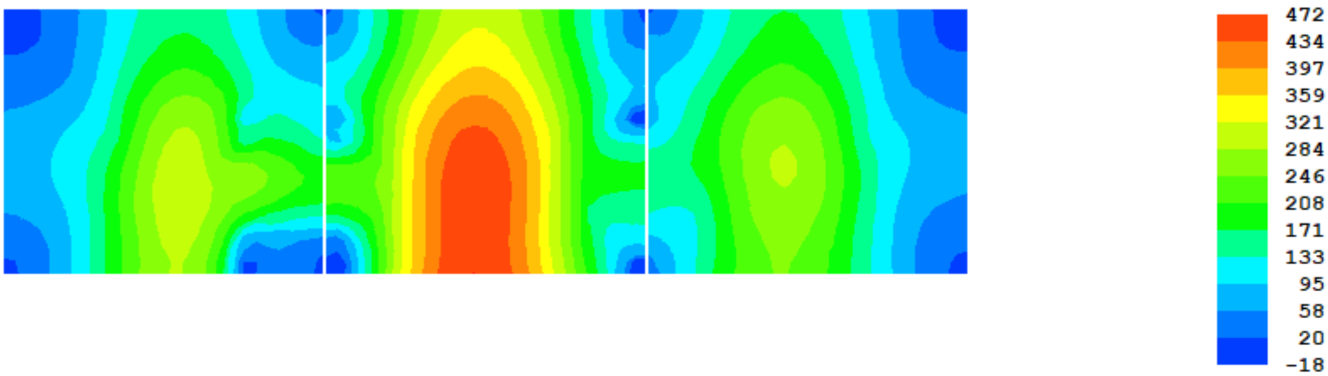

Figure 7.3: Example of tensile stress at slab top under 46 kips (200 kN) truck head loading at opposite sides of the slab (*ISlab2005*).

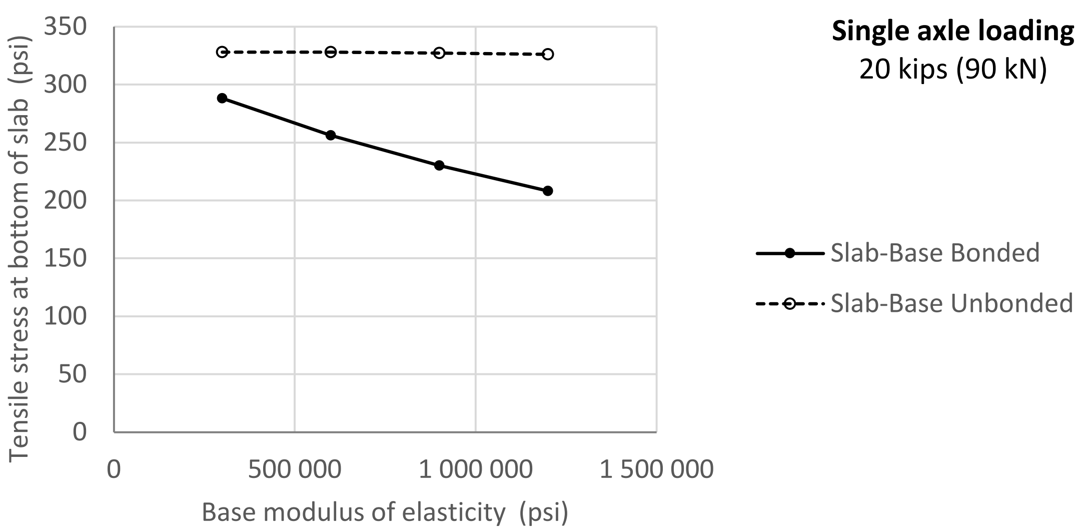

Figure 7.4: Tensile stress at slab bottom under 20 kips (90 kN) single-axle loading at slab edge.

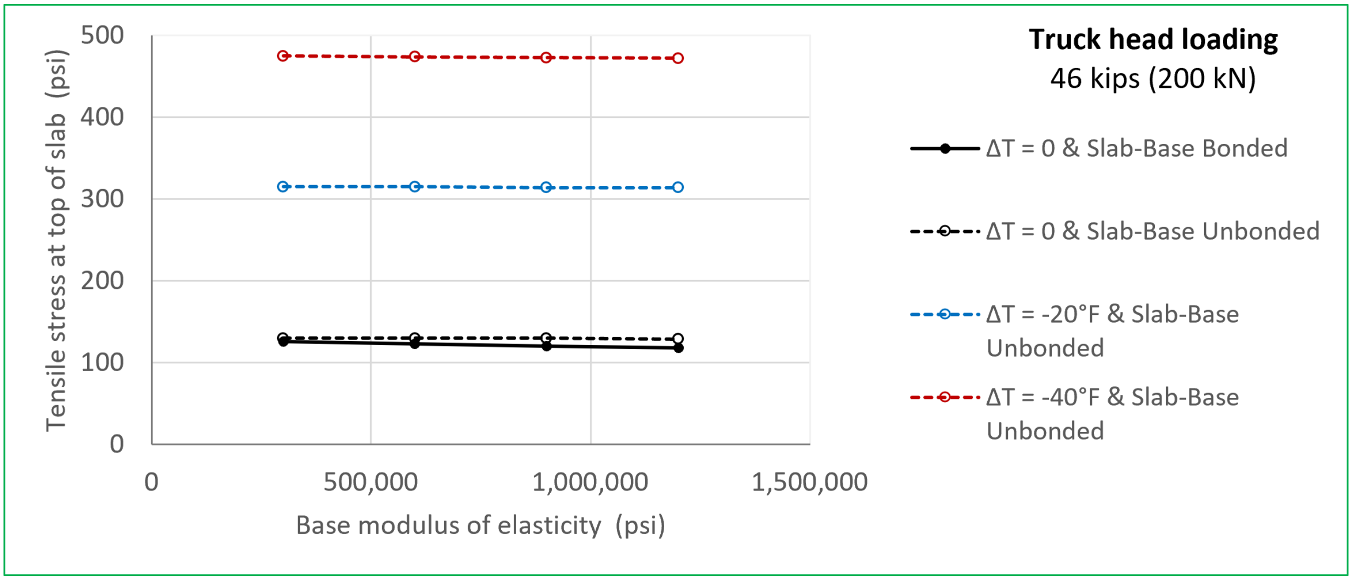

Figure 7.5: Tensile stress at slab top under 46 kips (200 kN) truck head loading at opposite sides of the slab.

Another direction for improving the design of asphalt concrete for rigid pavement bases is enhancing moisture resistance. Rigid pavements are typically designed for a 40-year life (around 60 years before major reconstruction). The asphalt base is expected to perform properly for much longer than in conventional asphalt pavements, though similar to the expectation for the life of asphalt base layers in a 40-year design life asphalt pavements.

There are different ways to enhance the asphalt mix moisture resistance. One approach is to increase the asphalt binder content. A second approach is to use anti-stripping additives. A third approach is to use the increased binder content to also increase the compaction requirements to produce a mix with less than 3% air-voids, making it essentially impermeable to water. Some of these additives may soften the mix, which should not be a concern regarding JPCP performance. As previously discussed, FEM modeling indicates that the softening of the asphalt concrete base is not a concern for JPCP performance.

7.2 Can RHMA-G Be Used as a Rigid Pavement Base Instead of HMA?

The answer to the question of whether RHMA-G can be used as a rigid pavement base instead of HMA requires consideration of the required properties of the JPCP base, which were identified and discussed in Section 2.4.1 and listed in Table 2.3. The required properties are included in Table 7.1, together with a comparison of RHMA-G versus HMA expected performance. In the "Comments" column of the table, a brief discussion is included regarding whether the experimental data agree with the expected performance.

As shown in Table 7.1, the RHMA-G is expected to match or improve HMA for most properties, and this expectation is confirmed by experimental data collected in numerous studies (fatigue resistance, rutting/raveling resistance, and resistance to water-induced damage) *(19)* or by limited experimental results from this research (capacity to remain bonded to the concrete slab and erosion resistance).

Table 7.1: RHMA-G Versus HMA Comparison

Property	Goals[a]	Expected	Comments
High stiffness under rapid loading (~10 Hz)	1	RHMA-G worse than HMA	Expectation confirmed by past experimental data and agrees with limited experimental results from this research
Capacity to remain bonded to the concrete slab	1, 2, 3	RHMA-G similar to HMA	Expectation agrees with limited experimental results from this research
Low stiffness under slow loading (<0.001 Hz)	2	RHMA-G similar to HMA	Expectation does NOT agree with limited experimental results from this research
Capacity to deform under slow loading (<0.001 Hz)	2, 5	RHMA-G better than HMA	Expectation does NOT agree with limited experimental results from this research
Erosion resistance	3, 5	RHMA-G similar to HMA	Expectation agrees with limited experimental results from this research
Fatigue resistance (relevant to thin slabs with undoweled joints)	3, 5	RHMA-G better than HMA	Expectation confirmed by past experimental data
Early-age rutting/raveling resistance	4, 5	RHMA-G similar to HMA	Expectation confirmed by past experimental data
Resistance to water-induced damage	5	RHMA-G similar to HMA	Expectation confirmed by past experimental data
Resistance to material-related distresses	5	RHMA-G similar to HMA	Not relevant to asphalt bases

[a] The following are the details of each JPCP base goal: (1) Goal 1: Help JPCP slabs to resist traffic loading, (2) Goal 2: Absorb hygrothermal movements of the concrete slabs while imposing minimum slab restraint and preventing slab-base separation, the "cushion effect," (3) Goal 3: Help traffic load transfer between slabs, (4) Goal 4: Resist construction traffic without raveling or rutting, and (5) Goal 5: Long-term structural and material integrity.

For one of the required properties, high stiffness under rapid loading, the RHMA-G is expected to perform worse than the HMA, and this expectation agrees with past experimental data *(19)* and with limited experimental results from this research. Nonetheless, the reduced stiffness of the RHMA-G compared with the HMA is expected to have a minor effect on the JPCP cracking performance, shown in Section 7.1.

For two of the required properties, low stiffness under slow loading and capacity to deform under slow loading, the RHMA-G was expected to perform similarly to or better than the HMA. Nonetheless, this expectation does not agree with the limited experimental results of this research. As shown in Figure 5.2, the creep compliance (flow under constant stress) was much higher for the HMA than for the RHMA-G, while the capacity to deform under slow loading was slightly better for the HMA than for the RHMA-G (shown in Figure 5.3).

Because this outcome might be related to the particular mixes selected for this research, two additional mixes were tested. The additional mixes were an HMA and an RHMA-G, and they were referred to as HMA2 and RHMA-G2, respectively. They differ from the original mixes in terms of the binder source and the aggregate size. The HMA2 binder source is Pacific Northwest, while the original HMA binder source is Valero Benicia. The RHMA-G binder source is San Joaquin Refinery, while the original RHMA-G binder source is Valero Benicia. Its nominal maximum aggregate size (NMAS) is 1/2”, while the original RHMA-G NMAS is 3/4”. The testing results for the additional mixes are presented in Figure 7.6 (creep compliance) and Figure 7.7 (strain capacity).

The testing results for the additional mixes (HMA2 and RHMA-G2) support the expectation that the RHMA-G performs similarly to or better than the HMA, which was the opposite of what was found for the first HMA and RHMA-G. This indicates that mix specification properties for both materials should be set to maximize performance as an asphalt base.

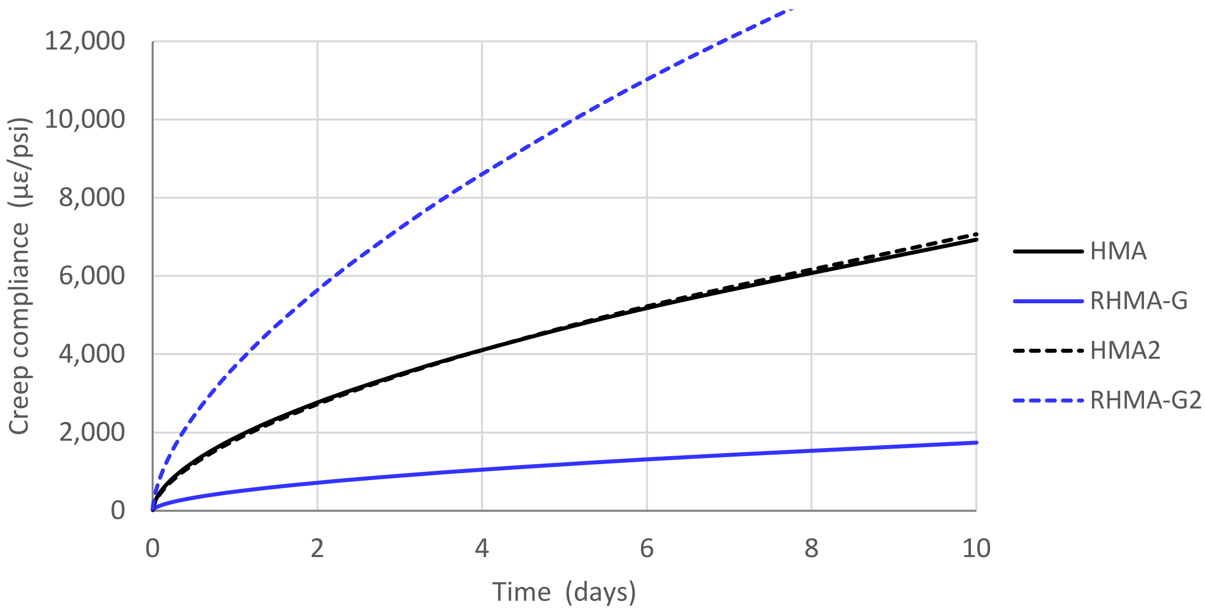

Figure 7.6: Creep compliance of the asphalt concrete mixes at 77°F (25°C), from hanging test.

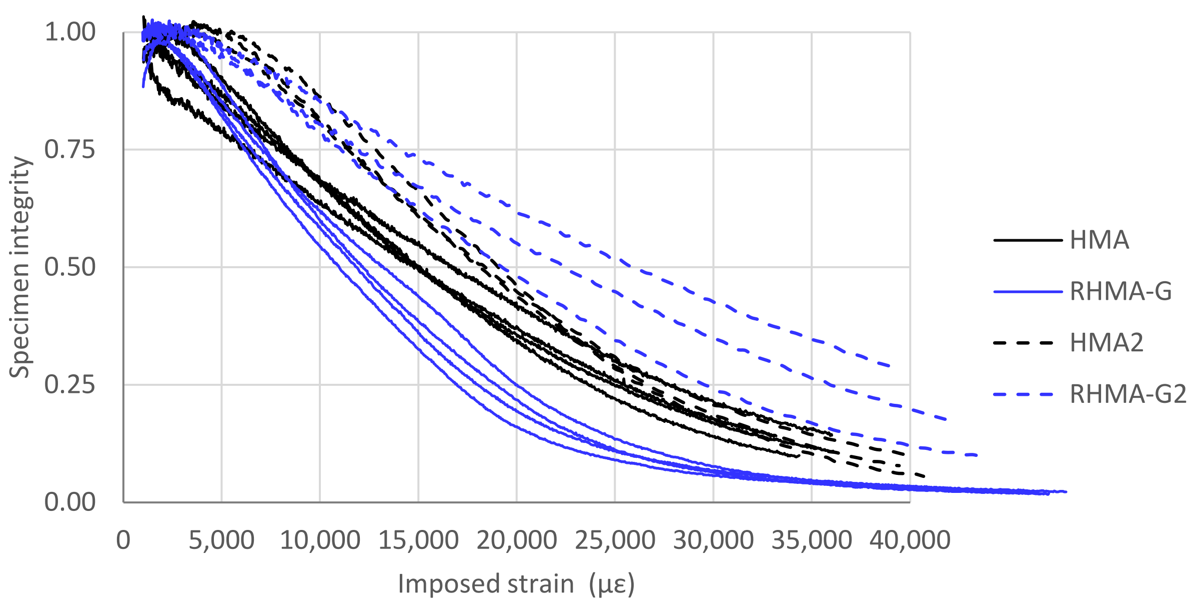

Figure 7.7: Strain capacity of the asphalt concrete mixes at 77°F (25°C).

7.3 Why Does JPCP Perform Considerably Worse, in Terms of Cracking, With LCB Than With HMA Base?

The experimental data collected in this study indicate that the JPCP slabs are seldom flat; they curl and warp due to temperature changes and drying shrinkage (Figure 4.2).

For the section with LCB, the experimental data and FEM modeling indicate the following:

- As the slab curls/warps, it loses support from the base, as lean concrete is a rigid material with little capacity to flow/adapt.
- Because of the lack of support from the base, the slab functions as a cantilever beam rather than as a slab supported by a multilayer structure.

The experimental data collected from the section with the RHMA-G base indicate that the RHMA-G base provided much better support to the slab than the LCB. When the slab curvature was very high during the summer evaluations, the corner deflection in the section with LCB and curing compound was up to three times the corner deflection in the section with RHMA-G base. These outcomes validate the hypothesis regarding JPCP-base interaction that was formulated in Section 1.1 and depicted in Figure 1.2.

In summary, the experimental data collected from the sections and the FEM modeling confirm that the use of an LCB, together with the curing compound interlayer, results in rigid contact between the slabs and the base that is not desirable. This rigid contact causes the slabs to lose support from the base as they curl/warp due to temperature changes and drying shrinkage. Because of this loss of support, the traffic loading applied close to or at the joints produces considerable tensile stresses at the top of the slabs, which may result in top-down cracking. This conclusion is particularly relevant to dry and warm climates, such as those present in most regions of California.

7.4 Can the Performance of JPCP with LCB Be Improved by Using an Engineered Interlayer?

The slab corner deflection under the FWD loading increased considerably as the slab curvature (ε_{DIFF}) increased (Figure 4.8), and the rate of increase strongly depended on the type of base and interlayer. The rate of increase was much higher in the slab with LCB and curing compound than in the slab with RHMA-G base. This outcome is attributed to the low capacity of the lean concrete to flow and adapt to the movements of the slab.

The geotextile diminished the performance of the curing compound interlayer, as the corner deflection slightly increased. This outcome confirms the initial expectation that the geotextile would not be able to provide the “cushion effect” required to prevent the rigid contact between the slabs and the LCB.

The microsurfacing interlayer (used instead of the curing compound) considerably improved the performance of the curing compound interlayer. In fact, the corner deflection in the section with LCB and microsurfacing interlayer was similar to the corner deflection in the section with RHMA-G base. This outcome indicates that a relatively thin interlayer, 0.2 in. (5 mm), is capable of providing the “cushion effect” required to prevent the rigid contact between the slabs and the LCB.

8 CONCLUSIONS AND RECOMMENDATIONS

The goal of the research presented in this report was to develop recommendations for improving the design of asphalt concrete for use as a base for rigid pavements and engineered interlayers (typically referred to as "bond breakers") placed between the JPCP slabs and the LCB. The research is based on three main pillars: full-scale test track monitoring, laboratory testing, and FEM modeling. This research project included the following sampling and testing activities:

- A full-scale test track was built and monitored to study JPCP slab-base interaction mechanisms. The test track includes four independent slabs—one slab with an RHMA-G base and three slabs with an LCB and one interlayer (curing compound, geotextile, or microsurfacing). The curing compound interlayer represents the current practice of JPCP construction in California. The geotextile is a nonwoven polypropylene geosynthetic, 14.7 oz./yd^2 (500 g/m^2), meeting AASHTO M288 specifications. The microsurfacing is a Type II gradation meeting Caltrans Std. Specs. Section 37-3, "Slurry Seals and Micro-Surfacings," with a thickness around 0.2 in. (5 mm). PLCC was used for building the slabs, which measure 12 × 12 ft. (3.6 × 3.6 m) and are 7 in. (178 mm) thick. The slabs were instrumented with thermocouples and VWSG to measure concrete strain due to the hygrothermal actions (drying shrinkage and thermal actions). The measured strains were used to calculate the curling/warping (curvature) of the slabs.

- In addition to monitoring the concrete hygrothermal strains, the test track was periodically evaluated using the FWD. In each of the evaluations, each slab was tested at the center and corners twice a day (morning and afternoon). The goal of the FWD evaluations was to determine how the corner deflection changes versus the curvature of the slab and how this change varies from section to section. The monitoring period presented in this report was from the construction of the test track in June 2022 to September 2023.

- The different materials—RHMA-G, LCB, and PLCC—were sampled during the test track construction and used for specimen preparation and laboratory testing.

- In addition to the RHMA-G, a standard HMA was sampled and tested in the laboratory. The HMA represents current practice for JPCP and CRCP base construction in California. The two asphalt concrete mixes (RHMA-G and HMA) were tested following a protocol that was developed in this research project for the evaluation of asphalt concrete mixes for use as JPCP bases. The testing protocol includes standardized asphalt concrete tests as well as new tests that were developed as part of this research project, the hanging test and the UTM-ramp test. These two tests measure the capacity of the asphalt concrete to absorb hygrothermal movements of the concrete slabs while imposing minimum slab restraint and preventing slab-base separation, a capacity referred to in this report as the "cushion effect."

- The interlayers were not tested in the laboratory.

- Two FEM models were developed and used in this research, both employing *Abaqus* software. The first models the structural response of the slabs under FWD. The second models the slab-base debonding that occurs due to the slab curling/warping created by the hygrothermal actions.

8.1 Conclusions

The conclusions are summarized in the following discussion and grouped to address the main questions this research intended to answer.

(1) How should asphalt concrete design be adapted to optimize its performance as a rigid pavement base?

- The experimental data collected in this research indicate that there is room for improving the performance of asphalt concrete as a JPCP base. Enhancements should focus on increasing the capacity to deform under slow loading and resisting long-term moisture damage.
- Most likely, increasing the capacity to deform under slow loading and enhancing long-term moisture resistance will result in softer asphalt concrete, which increases susceptibility to rutting. However, rutting is not an issue as the base will be protected by the JPCP slabs. Additionally, FEM modeling indicates that the softening of the asphalt concrete base is not a concern for JPCP performance.
- The directions for improving asphalt concrete for JPCP bases are also applicable to CRCP bases.

(2) Can RHMA-G be used as a rigid pavement base instead of HMA?

- No reason was found not to use RHMA-G instead of HMA as a rigid pavement base, indicated by the two mixtures tested in this project. The lower stiffness of the RHMA-G compared with the HMA is expected to have a minor effect on the rigid pavement performance.
- The results of the laboratory testing of two HMA and two RHMA-G mixes used regularly in Caltrans projects indicate that RHMA-G should perform similarly to HMA as a rigid pavement base.

(3) Why does JPCP perform considerably worse, in terms of cracking, with LCB than with HMA base?

- The experimental data collected in this research indicate that the RHMA-G base provides much better support to the slab than the LCB with the typical curing compound interlayer when the slab curvature is high. In the summer evaluations, when slab curvature was particularly high, the corner deflection in the section with LCB and curing compound was up to three times the corner deflection in the section with the RHMA-G base.
- The experimental data collected from the sections and the FEM modeling confirm that the use of an LCB, together with the curing compound interlayer, results in a rigid contact between the slabs and base that is not desirable. Because of the rigid contact, the slabs lose support from the base as they curl/warp due to temperature changes and drying shrinkage. Because of this loss of support, the traffic loading applied close to or at the joints produces considerable tensile stresses at the top of the slabs, which may result in top-down cracking.

(4) Can the performance of JPCP with LCB be improved by using an engineered interlayer? If yes, which interlayer?

   - Yes. Despite its small thickness of 0.2 in. (5 mm), the microsurfacing interlayer (used instead of the curing compound) considerably improved the performance of the curing compound interlayer. In fact, the corner deflection in the section with the LCB and the microsurfacing interlayer was similar to the corner deflection in the section with the RHMA-G base.
   - The geotextile diminished the performance of the curing compound interlayer. This outcome confirms the initial expectation that the geotextile would not be able to provide the "cushion effect" required to prevent the rigid contact between the slabs and the LCB.

8.2 Recommendations

The following are recommendations based on the findings of this research:

- It is recommended that RHMA-G be allowed as the base layer of rigid pavements in addition to HMA. The same thickness should be prescribed for both materials. Caltrans may consider extending the rubber use mandate to the base layer of rigid pavements.
- It is also recommended that the use of a slab-LCB microsurfacing interlayer be evaluated in a pilot project before including microsurfacing as an alternative in Caltrans Std. Specs. Section 36-2, "Base Bond Breaker." On the other hand, it is recommended that Caltrans Std. Specs. Section 36-2 be updated to not allow the use of geotextile as a slab-LCB bond breaker.
- Further research is needed to improve the design of asphalt concrete mixes, including HMA and RHMA-G, for optimizing their performance as a rigid pavement base. This research and optimization will be conducted in ongoing Caltrans PPRC Project 4.99, "Piloting New Asphalt Base Designs and Interlayers for Concrete Pavements." The same applies to optimizing cold recycling materials for use as a rigid pavement base, which is the focus of ongoing Caltrans PPRC Project 4.98, "Use of Cold Recycling as Base for Concrete Pavements."

REFERENCES

1. Mateos, A., Saboori, A., Lea, J., and Harvey, J.T. 2022. *Development of Caltrans Jointed Plain Concrete Pavement Design Catalog Tables Using Pavement ME* (Research Report: UCPRC-TM-2021-03). Davis and Berkeley, CA: University of California Pavement Research Center. https://doi.org/10.7922/G2Z31WZQ.

2. California Department of Transportation. 2024. *Standard Specifications: 2024 Edition*. Sacramento, CA: California Department of Transportation. https://dot.ca.gov/-/media/dot-media/programs/design/documents/2024_stdspecs-a11y.pdf.

3. Mateos, A., Harvey, J. T., Wu, R., Paniagua, F., and Paniagua, J. 2019. *Development of Improved Guidelines and Designs for Thin BCOA: Summary, Conclusions and Recommendations* (Summary Report: UCPRC-SR-2018-01). Davis and Berkeley, CA: University of California Pavement Research Center. https://escholarship.org/uc/item/5g04q2mb.

4. Mateos, A., Harvey, J. T., Millan, M. A., Wu, R., Paniagua, F., and Yang, S. 2023. *Thin Concrete Overlay on Asphalt Pilot Project at Woodland SR 113: Initial Performance* (Technical Memorandum: UCPRC-TM-2023-01). Davis and Berkeley, CA: University of California Pavement Research Center. https://doi.org/10.7922/G26D5R9B.

5. Lee, E. B., Choi, K., and Harvey, J. T. 2005. *Pre- and Postconstruction Analysis of the Interstate 15 (Devore) Concrete Pavement Reconstruction Project* (Research Report: UCPRC-RR-2005-14). Davis and Berkeley, CA: University of California Pavement Research Center. https://escholarship.org/uc/item/4588h3jp.

6. Xu, C. and Cebon, D. 2017. *Analysis of Cracking in Jointed Plain Concrete Pavements* (FHWA-HRT-16-073). Washington, DC: Federal Highway Administration. https://www.fhwa.dot.gov/publications/research/infrastructure/pavements/ltpp/16073/16073.pdf.

7. Saboori, A., Lea, J., Harvey, J. T., Lea, J., Mateos, A., and Wu, R. 2021. *Pavement ME JPCP Transverse Cracking Model Calibration and Design Catalog Framework (Version 2.5.5)* (Research Report: UCPRC-RR-2020-02). Davis and Berkeley, CA: University of California Pavement Research Center. https://doi.org/10.7922/G26D5R8W.

8. Kim, C., Lea, J., Kannekanti, V., and Harvey, J.T. 2022. *Updating Weigh-in-Motion (WIM) Spectra in PaveM* (Research Report: UCPRC-TM-2018-01). Davis and Berkeley, CA: University of California Pavement Research Center. https://doi.org/10.7922/G2JD4V3M.

9. Jones, D., Harvey, J. T., and Kohler, E. R. 2008. *Summary Report on the Evaluation of Rigid Pavement Long-life Strategies.* Davis and Berkeley, CA: University of California Pavement Research Center. https://escholarship.org/uc/item/5r24b3dg.

10. National Cooperative Highway Research Program. 2003. *Guide for Mechanistic-Empirical Pavement Design of New and Rehabilitated Pavement Structures*. Washington, DC: National Cooperative Highway Research Program. https://trid.trb.org/view/703699.

11. Cackler, T. 2017. *Performance Assessment of Nonwoven Geotextile Materials Used as Separation Layer for Unbonded Concrete Overlay of Existing Concrete Pavement Applications in the U.S*. Ames, IA:

National Concrete Pavement Technology Center. https://www.cptechcenter.org/wp-content/uploads/2018/10/MAPbriefDec2017.pdf.

12. Pavement Interactive. n.d. "Slurry Seals." Maintenance. Accessed September 22, 2023. https://pavementinteractive.org/reference-desk/maintenance-and-rehabilitation/maintenance/slurry-seals/.
13. Rao, S., and Roesler, J. R. 2005. *Characterization of Effective Built-in Curling and Concrete Pavement Cracking on the Palmdale Test Sections* (Research Report: UCPRC-RR-2005-09). Davis and Berkeley, CA: University of California Pavement Research Center. https://escholarship.org/uc/item/5477s826.
14. King, D., and Roesler, J. R. 2014. "Backcalculation Procedure for Bonded Concrete Overlays of Asphalt Pavement." *Transportation Research Record* 2457, no. 1: 72–79. https://doi.org/10.3141/2457-08.
15. California Department of Transportation. 2023. Highway Design Manual, Seventh Edition. Sacramento, CA: California Department of Transportation. https://dot.ca.gov/programs/design/manual-highway-design-manual-hdm.
16. Tayebali, A. A., Guddati, P. M., Yadav, S., and LaCroix, A. 2017. *Use of Moisture Induced Stress Tester (MiST) to Determine Moisture Sensitivity of Asphalt Mixtures* (NCDOT Project 2017-01). Raleigh, NC: North Carolina State University. https://connect.ncdot.gov/projects/research/RNAProjDocs/2017-01Final%20Report.pdf.
17. Yu, H., and Khazanovich, L. 2001. "Effects of Construction Curling on Concrete Pavement Behavior." In *Seventh International Conference on Concrete Pavements: The Use of Concrete in Developing Long-Lasting Pavement Solutions for the 21st Century, Volume 1*. Orlando, FL, September 9–13, 2001.
18. Mateos, A., Harvey, J., Paniagua, F., Paniagua, J., and Wu, R. 2023. *Drying Shrinkage Response of Full-Scale Thin Concrete Overlay on Asphalt Sections* (Research Report: UCPRC-RR-2023-01). Davis and Berkeley, CA: University of California Pavement Research Center. https://doi.org/10.7922/G2FQ9TZG.
19. Wu, R., Harvey, J., Lea, J., Mateos, A., Yang, S., and Hernandez, N. 2021. *Updates to CalME and Calibration of Cracking Models* (Research Report: UCPRC-RR-2021-01). Davis and Berkeley, CA: University of California Pavement Research Center. https://doi.org/10.7922/G2CR5RNT.

Caltrans

UCPRC
UNIVERSITY of CALIFORNIA PAVEMENT RESEARCH CENTER | Davis Berkeley